NORTHWESTERN UNIVERSITY

Non-covalent and Ion-specific Interactions in Charged Macromolecules

A DISSERTATION

SUBMITTED TO THE GRADUATE SCHOOL IN PARTIAL FULFILLMENT OF THE REQUIREMENTS

for the degree of

DOCTOR OF PHILOSOPHY

Field of Materials Science and Engineering

by

Kazi Sadman

Evanston, Illinois

June 2019

© Copyright by Kazi Sadman, 2019

All Rights Reserved

Abstract

Non-covalent and ion-specific interactions in the context of charged polymers are ubiquitous in nature and in synthetic applications. For example, mussels utilize metal-coordinate bonds to form tough underwater adhesion to a wide range of substrates. The sandcastle worm uses coacervation of oppositely charged polymers to build robust structures for self-defense. In new antimicrobial macromolecule design, the balance of cationic charge and hydrophobicity can allow broad spectrum specificity to bacteria while preserving non-toxicity to mammalian cells. These biological inspirations motivate a deeper understanding of non-covalent interactions between charged polymers, or polyelectrolytes, such that these interactions may be carefully engineered for synthetic applications such as surfactants, electro-deposited coatings, and fouling-resistant surfaces. This thesis will explore a number of non-covalent interactions in model systems of polyelectrolyte complexes (PECs), which are materials composed of oppositely charged polyelectrolytes. PECs were deemed as intractable materials from a processing standpoint since they cannot be melt processed like traditional thermoplastics, and are not soluble in any organic solvents. To overcome these significant limitations, the layer-by-layer assembly technique was developed where alternating monolayers of polycations and polyanions were deposited sequentially on a substrate. A further advancement came with the discovery that PECs can be dissolved into associating polymer solutions using concentrated salt solutions, which permits traditional polymer casting techniques to be used. The associative behavior of PECs are affected by hydrophobicity, ion-pairing affinity, molecular weight, topology, and hydrogen bonding interactions among other factors, making these materials an excellent test case to assess the role of individual non-covalent interactions. Furthermore, since PECs respond to the solution ionic strength, they are also a great platform to test the interaction of different salts with charged macromolecules.

This thesis will focus on strategies to control the deposition of PECs into thin-films, quantifying their mechanical behavior, and elucidating the role of salt identity in modulating their response.

Chapter 2 will introduce a one-step electrochemical approach for depositing PEC films which overcomes the low-throughput nature of the commonly used layer-by-layer technique. Chapter 3 will focus on the role of hydrophobic effects in dictating the mechanical behavior of PECs, and Chapter 4 will focus on the response of very strongly associating complexes that are nearly insoluble in any context. Together, Chapter 3 and 4 will build a comprehensive picture of hydrophobic and ion-specific interactions in PEC materials, and will emphasize the importance of the complex's water fraction for governing the rheological properties.

To achieve these goals, the quartz crystal microbalance (QCM) will be developed and utilized as an advanced rheometer to simultaneously measure the areal mass and viscoelastic properties of PECs. This approach will provide deep physical insights into the behavior of these materials because the QCM is ideally suited to quantifying the response of materials where a change in mass is associated with a change in the mechanical properties. In the case of PECs, rheological properties are primarily governed by the water content of the materials, which can be measured accurately on the QCM in response to added salt which swells the complex. Since this technique operates at a single high frequency, it also allows exquisite resolution of time-dependent changes in properties. However, using the QCM is often a challenge for casual users since it requires an understanding of thickness limits for sample preparation, and requires one to use the correct viscoelastic analysis. This work will provide the reader with a guideline for best practices to use the QCM as a rheometer, outline the thickness limitations for accurate viscoelastic analysis, and provide a MATLAB data analysis GUI (found here) that can directly analyze data from the popularly used QCM-D instrument. Therefore, another aim of this work is to provide any users of the QCM with intuition and framework behind how to design, perform, execute experiments, and finally analyze the obtained results.

Lastly, this work will investigate the adsorption of highly charged polyelectrolytes to oil/water interfaces. The behavior of charged molecules at interfaces is of significant technological impor-

tance due to its relevance in surfactant science. While the behavior of amphiphiles at interfaces has been well-studied, that of highly charged macromolecules has not. Yet quantifying the behavior of highly charged molecules near hydrophobic interfaces is of paramount importance for many chemical and biological contexts, for example, to inform the design of new antibiotics for drug-resistant bacteria. The significant role of ion solvation in mediating the adsorption of charged macromolecules will be quantified and discussed.

Acknowledgements

One could say I have had the privilege of living two very distinct lives– one in Bangladesh and one in the United States. Inevitably, there have been people in each of these lives– and those who have linked the two– who have contributed significantly to making this thesis possible. I am grateful beyond words to many of these individuals, but I will attempt to articulate what I can here.

I will start with my advisor, **Prof. Kenneth Shull**. People can look to the scientific literature to appreciate the quality of your work, or they can seek inspiration from the amazing individuals who have graduated under your supervision. They will not be surprised by what they find. However, to me your kindness, humility, and ability to listen has been as exemplary as your scientific tutelage. I will forever value these qualities. I am so grateful for the wisdom you conferred, in ways both said and unsaid, and for the freedom you gave me to explore my own ideas. It is needless to say that joining your group was a privilege for me, especially because you helped me be bold enough to always think big, but never to lose sight of the more important things in life. I hope we have many opportunities to work together in the future.

A special thanks to my committee members, **Prof. Monica Olvera de la Cruz**, **Prof. John Torkelson**, and **Zhang Jiang**. I also deeply thank the many collaborators over the years, especially, **Clinton Weiner**, **Bavand Keshavarz**, **Yechan Won**, **Jeff Ting**, **Jyotirmoy Mandal**, **Felipe Jiménez-Ángeles**, and **Profs. Kimberly Gray**, **Bryan Vogt**, and **Mark Schlossman**.

To **James Howell**, my high school English teacher– I learned so much from you, both in and out of the classroom, that has become an integral part of who I am. Your dedication is an absolute gift to those around you.

To **Prof. Michael Dickey**, my REU advisor at N. C. State University– I would not have chosen to go to graduate school had it not been for the invaluable experience in your lab. Your kindness, creativity, and openness has continued to inspire me since the day I met you. A special thanks goes to **Dr. Ying Liu**, my graduate mentor, whose hard work showed me the calibre necessary to

succeed in graduate school.

To **Prof. Jan Genzer**, my "adopted" REU mentor. Your humor and positive outlook inspired me to go to graduate school. Thank you!

To **Elizabeth**, thank you for teaching me the QCM. It set me down the right path, and I have never looked back.

To **Josh** and **Lauren**, thank you for your guidance with the QCM. So much of my work was made easier due to your contributions!

To **Qifeng**, I have been so incredibly lucky to have overlapped with you during my PhD. Your work ethic and intelligence are truly inspirational.

To **Ha-Kyung**, it was so awesome having you around in the office and in the lab. You should have started experimenting earlier!

To **Yaoyao**, your positivity, intelligence, and work ethic pushed me to do better nearly every day of my graduate work. It was so much fun being officemates with you, because you know, it's "Friday inside when the door is closed."

To **Matt**, I'm so glad you joined our group. We definitely dialed up the fun meter in the office!

To **David**, thanks for all the memories. Akron, San Fransisco, and Boston was so much fun!

To **Tom, Gwen**, **Qihua**, and **Anthony**– good luck on your journey ahead. I'm excited to see where you guys take the group!

To **Ryan**, **Sheel**, **Anthony**, **Michelle**, **Meghan**, **Emma**, and **Nick**– You are some of my best friends. So many memories made that I will always cherish. Two of the most memorable days are **Anthony** and **Meghan's** and **Jack** and **Allie's** weddings. Nights I wish I could relive!

To my friend **Ian Roberts**– your friendship and loyalty are invaluable to me. I am so glad you are my friend, and I have no doubt we will be friends for a long, long time.

To my BD colleagues- **Richard**, **Sajiv**, **Christine** and **Nicole**- thank you for making my time at BD memorable. One can only hope to always find coworkers as kind and generous as you guys.

Thank you!

To **Katie**– thank you for making me a part of Numix. It was so much fun applying to CRI and getting a taste of the crazy start-up world! I learned so much from you.

To **Tom Wu** and **Richard Saballos**, I was so lucky to have mentored you both!

To my friends **Dewan (Asif) Sayeed** and **Amitabh Syed**. Your friendship has defined who I am. It was the privilege of a lifetime growing up with you two– and I look forward to growing old knowing you guys. We've come such a long way.

To my **Aunt Parul**, who gave me one of the most incredible gifts I will ever receive– the opportunity to move to the United States. Thank you. I've worked very hard to make you proud.

To my cousin, **Rusho**– thanks for making me laugh, and for always reminding me what is most important.

To **Babu Uncle**, **Lily Aunty**, **Afzal Uncle**, **Moon Aunty**, thank you for what you've done for me and my family. Returning the favor would be impossible, and so I will strive to pay it forward instead.

To my **parents**– I know the sacrifices you guys have had to make to give me and my sisters the life we have. I hope this thesis is one step toward reaping the fruits of your labor.

To **Yasmin**– your intelligence, sincerity, and hard work has continued to inspire me. We've made it a long way so far.

Lastly, this work was supported by the U.S. Department of Energy Office of Science under Contract DE-AC02-06CH11357, by the National Institute of Standards and Technology (NIST) as part of the Center for Hierarchical Materials Design (CHiMaD), and by the National Science Foundation (NSF DMR-1410968 and DMR-1710491). Additional funding from Argonne National Laboratory is acknowledged. Partial support was also received from the Dow Chemicals through the Sustainability Innovation Student Challenge Award (SISCA). This work made use of the MatCI Facility which receives support from the MRSEC Program (NSF DMR-1121262) of the Materi-

als Research Center at Northwestern University. Also, this work made use of the IMSERC at Northwestern University, which has received support from the Soft and Hybrid Nanotechnology Experimental (SHyNE) Resource (NSF NNCI-1542205); the State of Illinois and the International Institute for Nanotechnology (IIN).

"Life is a storm, my young friend. You will bask in the sunlight one moment, be shattered on the rocks the next. What makes you a man is what you do when that storm comes. You must look into that storm and shout as you did in Rome. Do your worst, for I will do mine! Then the fates will know you as we know you."- Edmond Dantès, The Count of Monte Cristo

Contents

List of Figures

List of Tables

Chapter 1

Quantitative Rheometry of Thin Soft Materials Using the Quartz Crystal Microbalance (QCM)

Abstract: The quartz crystal microbalance (QCM) is a powerful fixed-frequency rheometer that allows one to correlate mass transfer from an adhered film with changes in its shear modulus and viscoelastic phase angle. In the thin-film limit, the resonance frequency of the QCM is related to the coupled mass on the quartz sensor through the Sauerbrey expression that relates the mass to the change in resonance frequency. However, when the thickness of the film is sufficiently large, the relationship becomes more complicated and both the frequency and damping of the crystal resonance must be considered. In this regime, a rheological model of the material must be used to accurately extract the adhered film's thickness, shear modulus, and viscoelastic phase angle from the data. In the present work we examine the suitability of two viscoelastic models, the "Voigt" model (***Physica Scripta*** 1999, 59, 391-396) and a more realistic power-law model (***Langmuir*** 2015, 31, 4008), to extract the rheological properties of a thermo-responsive hydrogel film. By

changing temperature and initial dry film thickness of the gel, the operation of QCM was traversed from the Sauerbrey limit, where viscous losses do not impact the frequency, through the regime where the QCM response is sensitive to viscoelastic properties. The density-shear modulus and the viscoelastic phase angle from the two models are in good agreement when the shear wavelength ratio, d/λ_n, is in the range of 0.05-0.20, where d is the film thickness and λ_n is the wavelength of the mechanical shear wave at the n^{th} harmonic. A framework is provided for estimating the physical properties of soft materials in the megahertz regime by using the physical behavior of polyelectrolyte complexes. This provides the user with an approximate range of allowable film thicknesses for accurate viscoelastic analysis with either model, thus enabling better use of the QCM-D in soft materials research. This work appears in *Anal. Chem.* 2018, 90, 6, 4079-4088.

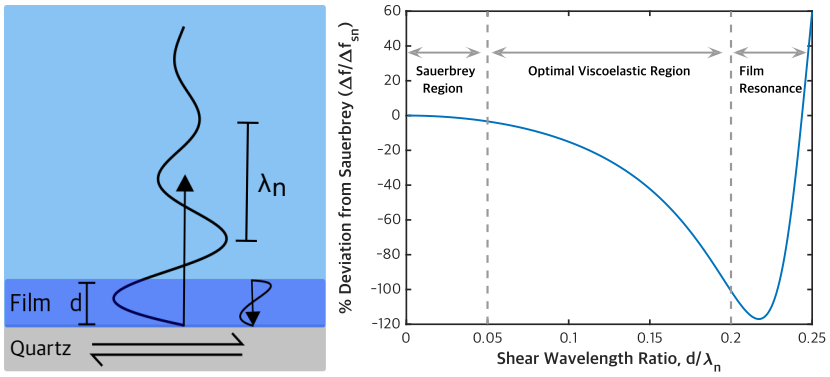

1.1 Introduction

For nearly 70 years the piezoelectric oscillation of a quartz resonator has been used as an ultra sensitive mass sensor, utilizing the Sauerbrey relationship between the resonant frequency and the mass per unit area deposited on the crystal.[9] This relationship has enabled the quartz crystal microbalance (QCM) to be a mainstay of vacuum science.[10, 11] In the 1980's Kanazawa and co-

workers demonstrated that QCM operation in liquids was possible,[12] opening opportunities for QCM to contribute to many electrochemical[13, 14, 15] and biological[16, 17, 18] investigations. However, the frequency change due to coupled mass at the crystal surface only provides a partial description of the adhered layer, especially if it is viscoelastic in nature. Viscous losses associated with the material lead to energy dissipation of the crystal, providing additional information regarding the adhered film. The dissipation is obtained from the half width at half maximum (Γ) of the conductance peak at the resonance condition, which is proportional to the energy transfer from the resonator to the medium with which it is in contact.[19, 20] Therefore, measuring Γ offers access to rheological information of the system.[21, 22, 23, 24] The QCM's high sensitivity has already enabled a breadth of informative work on characterizing soft materials[14, 25, 26, 27, 28, 29, 30], yet many QCM investigations would benefit further if its capabilities as a high-frequency rheometer were made clearer.

Commercialization of instrumentation developed by Kasemo and co-workers has enabled the proliferation of rheological characterization of thin soft materials based on the measurement of the resonant frequency and dissipation of the QCM at multiple harmonics.[31] Values of the dissipation obtained with the QCM-D (Quartz Crystal Microbalance with Dissipation) instrument are generally reported in terms of a dissipation factor, D, which is directly proportional to Γ at each harmonic, n, via Eq. 1.1. [22] In the present work we use D and Γ interchangeably as they are the same parameter.

$$D_n = 2\Gamma_n / f_n \tag{1.1}$$

The viscoelastic nature of many biological[32, 33] and polymeric[24, 34, 35, 36] materials at surfaces has been determined with the QCM-D, but these results are tied to the model used to describe the viscoelastic properties of the film.[16, 37] A viscoelastic model is needed because the QCM response for a thin film at a given resonant harmonic depends on three quantities (the

film's mass per area, and the real and imaginary parts of the complex modulus at the resonant frequency), but only two quantities are measured at each harmonic (the resonant frequency and dissipation). As a result, information needs to be obtained at multiple harmonics, with some assumption made regarding the frequency dependence of the viscoelastic properties of the film. A commonly employed model is the Voigt model, where the storage modulus is assumed to be frequency independent, whereas the loss modulus is assumed to scale linearly with the frequency.[37] Data are typically reported at a reference harmonic, n_{ref}, which is generally either 1 (corresponding to a frequency of 5 MHz for the commonly used quartz crystals with a fundamental resonance frequency of 5 MHz) or 3 (a frequency of 15 MHz for a 5 MHz crystal). In the original Voigt model, the properties at different resonant harmonics are therefore related as follows:

$$G'_n = G'_{n_{ref}} = |G^*_{n_{ref}}| \cos(\phi_{n_{ref}})$$

$$G''_n = \frac{n}{n_{ref}} G''_{n_{ref}} = \frac{n}{n_{ref}} |G^*_{n_{ref}}| \sin(\phi_{n_{ref}})$$

Here $|G^*_n|$ is the magnitude of the complex modulus and ϕ is the viscoelastic phase angle, which is defined to be 0^o for perfectly elastic materials and 90^o for Newtonian fluids. As pointed out by Reviakine *et al.,* these assumptions are not rheologically consistent, and only observed in real materials in some specific and highly unusual situations.[23] A more robust assumption about the frequency response of materials in the megahertz regime is a power-law assumption. Noting this, a correction to the original Voigt assumption was made, and was termed as the Extended Voigt Model. Here the mechanical response is assumed to be:

$$G'_n = |G^*_{n_{ref}}| n^{\alpha} \cos(\phi_{n_{ref}}), 0 \leq \alpha \leq 2$$

$$G_n'' = |G_{n_{ref}}^*| n^b \cos(\phi_{n_{ref}}), -2 \leq b \leq 0$$

While the Extended Voigt Model is an improvement on the original assumptions of the Voigt model, it is still not an accurate description of the frequency response of soft materials, because α and b appear to be independent fit parameters, which can violate the Kramers-Kronig relation for linear viscoelasticity (Eq. 1.2).[38]

$$\frac{G'(\omega)}{\omega^2} = \frac{2}{\omega} \int_0^\infty \frac{G''(x)/x}{\omega^2 - x^2} dx \tag{1.2}$$

For the Kramers-Kronig relation to be obeyed the following must be true: $\alpha = b + 1$ for $0 \leq \alpha \leq 1$. Therefore, the more realistic and generally useful model is a power-law model where the storage and loss moduli are both assumed to be power-law functions of the frequency, with the phase angle related directly to the value of the power-law exponent. This power-law model is simpler to apply, and introduces very little error into the physical properties extracted from an appropriately designed QCM experiment.[39] It has been applied to investigations of polyelectrolyte complexation[13, 24, 40], curing of thermosets[36], and kinetics of click-reactions.[41] Mathematically, the power-law model assumes:

$$|G_n^*| = |G_{n_{ref}}^*| n^{\phi/90}$$

This approach minimizes fit parameters while also being a more realistic assumption. In the present work, we illustrate the use of this approach to swelling measurements of thin layers of a crosslinked gel, comparing results obtained with the Voigt (V) and the power-law (R) models. In the process of this comparison, we delineate regimes of QCM operation where the Sauerbrey relationship applies and where deviation from Sauerbrey is significant enough to allow viscoelastic characterization of thin films.

1.2 Experimental Methods

Materials and sample preparation: A random copolymer of N-isopropylacrylamide (NIPAAm) and 2-(N-ethylperfluorooctane sulfonamido)ethyl acrylate (FOSA) with 5 mol % FOSA as reported previously[42, 43] was used as the hydrogel with hydrophobic associations of FOSA producing nano-aggregates that provided physical crosslinks when hydrated.[43] These hydrogels exhibit volume phase transition of an LCST-type with a midpoint of 17 °C in the bulk[43] and 20 °C in thin films.[44] Changing the temperature from 35 °C to 5 °C increased the swelling % (Eq. 1.10) of the films from 50 and 350 %. This large change in the water content of the hydrogel significantly impacted its rheological properties. The dried copolymer was dissolved in dioxane at 1.0 and 1.75 wt% for spin coating on the silica-coated quartz sensors (QSX-335, Q-Sense). These sensors had a diameter of 14 mm, thickness of 0.37 mm, and fundamental resonant frequency of 5 MHz. The sensors were cleaned by sonication in toluene, isopropanol, and DI water. Immediately prior to film casting, the sensors were further cleaned by ultraviolet-ozone (UVO CLEANER®, Model 42, Jelight Company Inc.) for 90 s. The copolymer-dioxane solutions were spun coat at 2500 rpm for 30 s onto the quartz sensors. After 1 h at ambient conditions, the films on the sensors were annealed for 18 h at 150 °C and 27 torr vacuum.

The hydrogel films on the quartz sensor were characterized using QCM-D (Q-Sense E1) and SE (J.A. Woollam, M-2000UI) at the same time using the ellipsometry module (Q-Sense, Biolin Scientific). The thickness of the dry copolymer was determined using Δf relative to the uncoated sensor in air with an assumed density of 1000 kg/m^3. Simultaneous measurement with SE provided an optical route to also determine the copolymer film thickness using an optical stack for the sensors consisting of gold (optically opaque), titanium, TiO_2, and silica from bottom to top. The ellipsometric angles of the sensors were fit using the protocol described previously for these QCM-D sensors.[45] These thicknesses were then fixed to fit for the thickness of the copolymer or hydrogel that was coated on the sensor with the optical properties of the copolymer and hydro-

gel, which were both well described by the Cauchy model. The thickness determined from the Sauerbrey expression based on the frequency shift from the blank crystal agreed within 3% of the thickness obtained from ellipsometry for the dry copolymer film.

For the swelling measurements, the coated sensor was first exposed to liquid water at 25 °C and allowed to equilibrate. The temperature was subsequently raised to 35 °C and allowed to equilibrate for 1 h. Then the temperature was decreased in 1-2 °C increments each hour until 5 °C was reached, with a total of 24 temperature steps. The frequency and dissipation of the bare sensor in water at each temperature was used as the reference for calculating Δf_n and ΔD_n. This reference state allowed for the viscosity and density changes in the water with temperature as well as the effect of temperature itself to be removed from the data.

The QCM-D data were fit using two different protocols that relate the viscoelastic properties of the film to the oscillator response. The Voigt Extended Viscoelastic model was used in conjunction with the standard Q-Tools software (Q-Sense), which is based on the model refined by Voinova and co-workers.[37] The frequency and dissipation changes were recursively fit to this model to minimize the mean square error between the prediction and measured values. The same input parameters/assumptions were used with a different viscoelastic model that is based on a self-consistent description of the complex modulus as developed by Shull and co-workers.[24, 39] The power-law model developed by Shull and co-workers can be utilized to directly solve the data obtained by the QCM-D instrument using the MATLAB code found here. The fits from both models can be used to determine the shear modulus, phase angle and thickness of the hydrogel. Additional details about these two models are further explained in the subsequent Theory section.

Polyelectrolyte complexes were synthesized as reported previously.[1] Briefly, 10 wt% of poly(4-vinylpyridine) was quaternized with iodomethane at 10 % excess in DMSO. This cationic polymer was precipitated with equimolar poly(styrenesulfonate) in excess deionized water. The precipitates were washed with deionized water until the solution conductivity reached $\approx 50\ \mu S/cm$,

followed by overnight drying at 60 ^{o}C. 1.5 g of the dried complex was dissolved in 15 ml of 1.7 M KBr to form the coacervate phase. The coacervate was directly spin coated onto the QCM crystal before swelling measurements in KBr solutions up to 1.0 M at 0.1 M increments.

1.3 Theory & Modeling of QCM Operation

For sufficiently rigid and/or thin adhered layers, the frequency will be directly related to mass through the Sauerbrey expression (Eq. 1.3), such that details of the viscoelasticity of the material are not relevant to describe QCM operation.[46] The point for quantitative failure of the Sauerbrey expression can be described in terms of the ratio d/λ_n, which is the film thickness (d) normalized by the shear wavelength of the mechanical oscillation (λ_n) in the medium at the n^{th} overtone or harmonic, occurring roughly for $d/\lambda_n \approx 0.05$.[39] For sufficiently thick viscoelastic films, d/λ_n can approach 0.25, leading to an increase in frequency with increasing mass[46], counter to the directionality of the Sauerbrey expression. This film resonance effect also leads to a very large increase in Γ (equivalently D), making the parameter difficult to measure accurately. Film resonance is most pronounced at $d/\lambda_n = 0.25$, but its effects become significant from $d/\lambda_n = 0.20$.[39] Therefore the regime where viscoelastic details can be measured accurately should be in the range of $d/\lambda_n = 0.05 - 0.20$. Film resonance effects are less pronounced for more dissipative (less elastic, $\phi > 45^{\circ}$) films, such that viscoelastic properties can be measured for $d/\lambda_n = 0.25$ or even larger.

$$\Delta f_{sn} = \frac{-2nf_1^2}{Z_q}\rho d = \frac{-2nf_1^2}{Z_q}\Delta M_A \tag{1.3}$$

where f_1 is the fundamental resonance frequency of quartz (5 MHz in our case), n is the order of the measured harmonic (n=1, 3 or 5), Z_q is the acoustic impedance of quartz (8.84×10^6 kgm^{-2}s^{-1} for AT-cut quartz), d is the film thickness, and ρ is its density.

In order to understand the challenges with analyzing the behavior of a viscoelastic film on the QCM, it is first necessary to understand the effect of viscoelasticity on the QCM response. As mentioned earlier, the presence of viscoelastic character in the film results in an increased Γ; however, measuring a change in Γ does not necessarily mean that the viscoelastic properties have changed. This is simply due to the fact that changes in areal density (i.e., thickness) also changes Γ, and therefore, a rheological model must be used which takes into account both frequency and dissipation shifts to paint an accurate picture. The sensitivity of the QCM to viscoelasticity arises from deviations to the Sauerbrey expression, the magnitude of which depends on the quantities d/λ_n and ϕ. The shear wavelength of a mechanical oscillation in a medium further depends on the following expression:

$$\lambda_n = \frac{1}{f_n}\left[\frac{|G_n^*|}{\rho}\right]^{1/2}\frac{1}{cos(\phi/2)} \tag{1.4}$$

where ρ is the density, $|G_n^*|$ is the magnitude of the complex shear modulus, ϕ is the viscoelastic phase angle of the medium and n is the order of the overtone. Since viscoelastic information can only be calculated in a limited range of d/λ_n, typically 0.05-0.20, Eq. 1.4 presents a challenge since $|G_n^*|$ and ϕ are material parameters of interest to begin with. This issue is addressed later in this chapter.

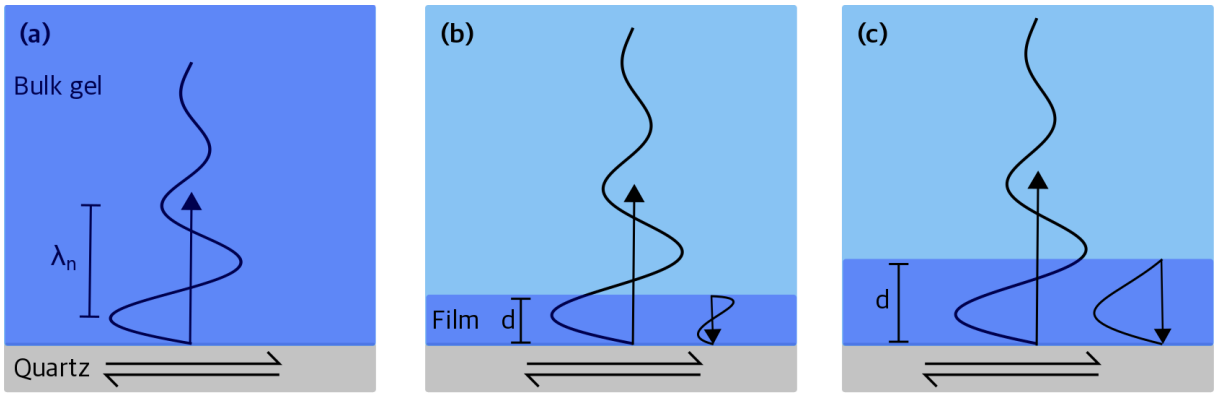

Figure 1.1: Propagation of the shear wave generated from AC driven quartz-sensor surface into a sample consisting of a hydrogel film immersed in water. For sufficiently thick films, (a) the wave decays through the hydrogel (or any viscous medium) without encountering an interface for reflection, which probes the "bulk" properties. For thinner films, the hydrogel-water interface is encountered by the shear wave, which can result in (b) partial wave reflection from the interface to slightly decrease the crystal frequency ($0.05 < d/\lambda_n < 0.25$) or (c) coupling of the reflected wave with the propagating wave that effectively increases the crystal frequency (film resonance, $d/\lambda_n \approx 0.25$). Note that this figure is not drawn to scale, and the shear wave is exaggerated.

The description of the shear wave propagation can be expressed in three limiting cases as pictorially illustrated in Figure 1.1. If the hydrogel/medium is sufficiently thick, the shear wave decays completely within the adhered layer of the material (Figure 1.1a). This case can be considered equivalent to bulk measurement of the medium (the hydrogel in this case) where the response does not depend upon the fluid in contact with the hydrogel.[22, 24] In this limit the QCM response is described simply by the following two equations:

$$\Delta f_n = \frac{-f_1}{\pi Z_q}(\rho|G_n^*|)^{1/2}\sin(\phi/2) \tag{1.5}$$

$$\Delta \Gamma_n = \frac{f_1}{\pi Z_q}(\rho|G_n^*|)^{1/2}\cos(\phi/2) \tag{1.6}$$

Note that the change in the QCM-D dissipation factor is related to $\Delta\Gamma$ as $\Delta D_n = 2\Delta\Gamma_n/f_n$. Therefore, bulk materials are described by two equations with two unknowns, and this scenario

works very well for viscous liquids ($\phi > 60^o$) in which the quartz crystal can simply be exposed to or immersed in. Note also that in this case the wave is eventually completely damped in the bulk medium and thus no thickness information exists.

A more common case is when the shear wave propagates through the adhered layer and then fully decays in the bulk solvent; thus, both the film and the aqueous phase contribute to the crystal response. A shear wave encountering the hydrogel-water interface splits into a transmitted wave and a reflected wave (Figure 1.1b). The reflected wave generally slightly decreases the oscillation frequency at the sensor.[47] However, it is possible for the reflected shear wave to couple with the outbound shear wave to effectively increase the oscillation frequency at the sensor surface from the addition of these two transverse waves (Figure 1.1c). The condition under which the shear wave is coupled to the reflected wave is known as film resonance and is a result of approaching the quarter wave condition ($d/\lambda_n = 0.25$).

For a film of thickness d and density ρ deposited on the crystal, deviation from Sauerbrey can be quantified in terms of two quantities: $\Delta f_n/\Delta f_{sn}$ and $\Delta\Gamma_n/\Delta f_{sn}$. Here, Δf_{sn} is the expected Sauerbrey shift, $\Delta f_{sn} = (2nf_1^2\rho d)/Z_q$, and Δf_n and $\Delta\Gamma_n$are the experimentally measured shifts at the n^{th} harmonic with respect to the bare crystal. If the film is sufficiently thin, i.e., in the Sauerbrey limit, then $\Delta\Gamma_n \approx 0$ and $\Delta\Gamma_n/\Delta f_{sn} \approx 0$. Similarly, no deviation from Sauerbrey is expected here, so $\Delta f_n/\Delta f_{sn} \approx -1$. If the film swells, d increases and viscoelastic properties begin to take effect, resulting in $\Delta\Gamma_n/\Delta f_{sn} > 0$ and $\Delta f_n/\Delta f_{sn} < -1$. This behavior is described fully by the QCM master equation (Eq. 1.9). Figure 1.2 plots the deviation from Sauerbrey for materials with differing viscoelastic character ($\phi = 15^o, 30^o, 45^o$), and identifies the different regimes of QCM operation.

We now define two quantities, r^* and D_n^*, which will be prove to be insightful for understanding the QCM response. We will refer to the properties of the film and the liquid with the subscripts f and l, respectively. An asterisk denotes a complex quantity and the subscript n denotes the harmonic order, as usual.

$$r^* = \left(\frac{\rho_\ell G^*_{n\ell}}{\rho_f G^*_{nf}} \right)^{1/2} \tag{1.7}$$

$$D^*_n = \frac{2\pi d}{\lambda_n} \left(1 - i \tan\left(\phi_n/2\right)\right) \tag{1.8}$$

Here, r^* is the ratio of the film properties relative to the properties of the overlaying liquid medium, and D^*_n is a complex quantity whose value depends on d/λ_n and ϕ. With these two quantities, the entire QCM response can be described by the following equation:

$$\frac{\Delta f_n + i\Delta\Gamma_n}{\Delta f_{sn}} = -\frac{\tan(D^*_{nf})}{D^*_{nf}} \left[\frac{1 - (r^*)^2}{1 + ir^* \tan(D^*_{nf})} \right] \tag{1.9}$$

Written in this form it is more appreciable that there is no net response for the case where the film and liquid medium have identical properties ($r^* = 1$), and that the QCM response for a film in air is recovered for $r^* = 0$ (see DeNolf *et al.*).[39] The method of solving Eq. 1.9, and all related nuances have been reported elsewhere for films in air[39] and for films in a liquid environment.[24] The MATLAB code to solve Eq. 1.9 (or equivalent expressions of it) using the power-law assumption for experimentally determined frequency and dissipation shifts can be found here.

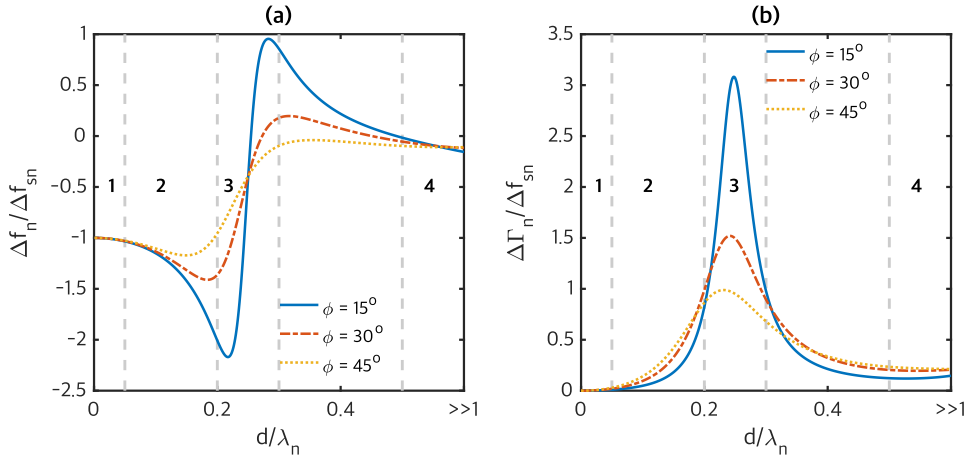

Figure 1.2: Impact of d/λ_n on the deviation from the Sauerbrey limit for primarily elastic films ($\phi = 15^o$) to viscoelastic films ($\phi = 45^o$). Four regimes of operation are delineated: (1) Sauerbrey, (2) viscoelastic, (3) near film resonance, and (4) bulk-like (Eq. 1.5 and 1.6 apply). These plots are obtained from Eq. 1.9 with $r^* = 0$, that is, a film in air.

1.4 Results & Discussion

Measuring the swelling ratio of stimulus responsive soft materials is usually a simple yet insightful experiment. The swelling behavior can be modulated using pH[48], temperature[44], light[49] or electrochemical[50] stimuli, and these approaches have been exploited to construct soft materials for a variety of coating and biomedical applications.[51] Typically, a change in the swelling ratio results from the ingress or egress of water from the material, corresponding with a change in the mechanical properties due to the increase or decrease in crosslink density. Measuring these changes for thin soft materials is challenging since the traditional tensile tests or dynamic mechanical analysis cannot be performed. A further complication is that often the *in-situ* behavior of responsive coatings or gels are of interest, which is where the utility of QCM becomes invaluable since it is capable of monitoring subtle viscoelastic changes with a fine time resolution. Furthermore, few other mechanical testing methods can adequately characterize materials ranging in properties from Newtonian liquids to glassy solids. Given these advantages, the QCM is an attractive material char-

acterization platform. Since films utilized in QCM experiments can have a range of thicknesses, especially if the material is responsive, it is most convenient to define a swelling % for comparison across samples and materials. We define the swelling % of a film with thickness d and density ρ using Eq. 1.10:

$$Swelling\,\% = \frac{d\rho - (d\rho)_{dry}}{(d\rho)_{dry}} \times 100 \tag{1.10}$$

Here, $(d\rho)_{dry}$ is the areal mass of the film after removal of all water.

In the present work, a thermo-responsive hydrogel based on a random amphiphilic copolymer enables change in the swelling % with temperature. Such a large change in the swelling % is expected to span orders of magnitude in modulus, which coupled with the change in thickness, traverses d/λ_n from the Sauerbrey limit to the viscoelastically sensitive regime. Our aim is to quantify the value of d/λ_n beyond which the Sauerbrey relationship starts to deviate, and from which point on viscoelastic information can be obtained.

1.4.1 Characterization of PNIPAAm-FOSA Hydrogels

One challenge with experimentally exploring predictions associated with the shear wavelength is the wide parameter space in d/λ_n that requires widely varying thickness and/or rheological properties, which is difficult to obtain without a multitude of samples. Here a thermo-responsive hydrogel based on a random amphiphilic copolymer enables large changes in the swelling and mechanical behavior with temperature. As the film swells, it traverses from the Sauerbrey limit to the viscoelastically sensitive regime, and ultimately into film resonance conditions as d/λ_n approaches 0.25. To systematically elucidate this d/λ_n landscape, we begin with two films of initial areal densities of 52 and 100 mg/m^2. For simplicity we assume that the film density is $1 g/cm^3$, and thus simply refer to the two films as 52 and 100 nm. Probing the properties of these two films, which are a factor of two in thickness apart, across a large temperature range allows us

to systematically observe the QCM response. We are interested in learning how well the swelling behavior of these gels compare to the behavior of PECs, and comparing results from the Voigt model (V) and the power-law model (R). We now make a note about the nomenclature to be used in the remainder of this chapter. Since obtaining mechanical properties from QCM experiments require data from two harmonics, we refer to the V model solutions as $n/n+2$, with n being the harmonic order. For example, we primarily focus on the $3^{rd}/5^{th}$ harmonic combinations in this section. The R model uses the frequency shifts of two harmonics and the dissipation shift of another harmonic to solve for material properties. This is denoted as, for example, a 3:5,5 calculation which uses Δf_3, Δf_5 and $\Delta\Gamma_5$.

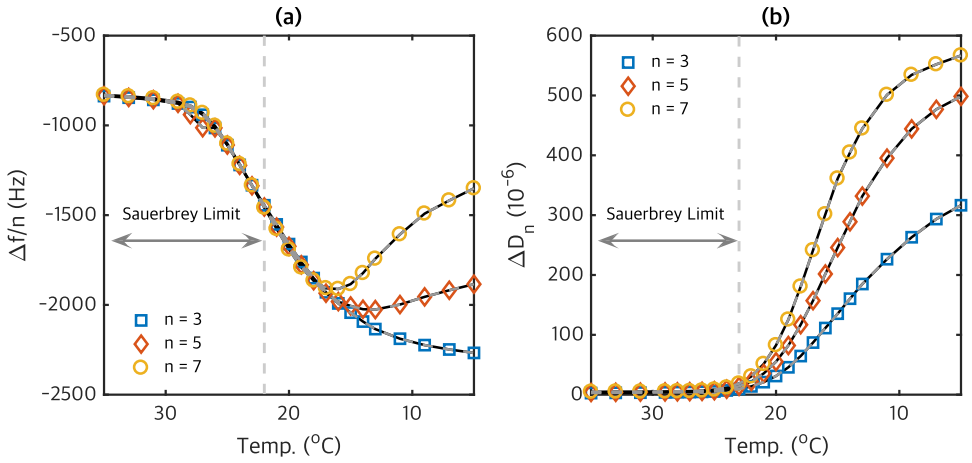

Figure 1.3: Δf_n and ΔD_n in water for the 100 nm initial dry film. The x-axis is reversed to highlight that the hydrogel was cooled incrementally starting from 35 °C. The solid black lines are fits using the Voigt model and the gray dashed lines are predictions using the power-law model. The Sauerbrey limit applies to the left of the gray dashed lines, where the dissipation is too small. Note that for both the models examined there is no significant difference in the goodness of the fit for Δf_n and ΔD_n.

Figure 1.3 plots the frequency and dissipation shifts for the 100 nm dry film. At high temperatures, the dissipation is small and the frequency shifts obey the Sauerbrey relationship. At lower temperatures, the film swells and d/λ_n increases until film resonance effects cause an uptick in the frequency shift with increasing mass. It is important to note that the effect of temperature on the

resonance of the crystal can introduce some error in Δf_n for very thin films, so it is important to use a reference (blank) crystal to subtract these effects from the measured signal as described in the Experimental Section. Figure 1.4 plots the mechanical behavior of the two films as a function of temperature using both the V and R models. At cooler temperatures, there is a good agreement between the two models for the modulus and phase angle for both films. However, as the temperature increases and the film becomes stiffer as a consequence of deswelling, the QCM response approaches the Sauerbrey limit where no viscoelastic information can be obtained. The temperature above which the Sauerbrey limit applies in this case is above 22^o C for the 100 nm film and 19^o C for the 52 nm film. Interestingly, Figure 1.4 shows that the Voigt model attempts to fit the frequency and dissipation shifts even in the Sauerbrey regime, and provides quite reasonable answers for the 52 nm film– by chance. While it is tempting to believe the Voigt solutions in the Sauerbrey regime for the 52 nm film, by considering the 100 nm film response one should quickly dismiss it. This thicker film remains in the viscoelastically sensitive regime over a larger range of temperature, where again we find good agreement between the two models, but its response becomes non-physical at high temperatures where an increasing modulus and a decreasing phase angle is expected. This simple comparison between films of two thicknesses highlights the danger of attempting to model QCM data in the Sauerbrey limit where only the frequency shift can be used to calculate the areal mass. Both models are in good agreement for the swelling behavior.

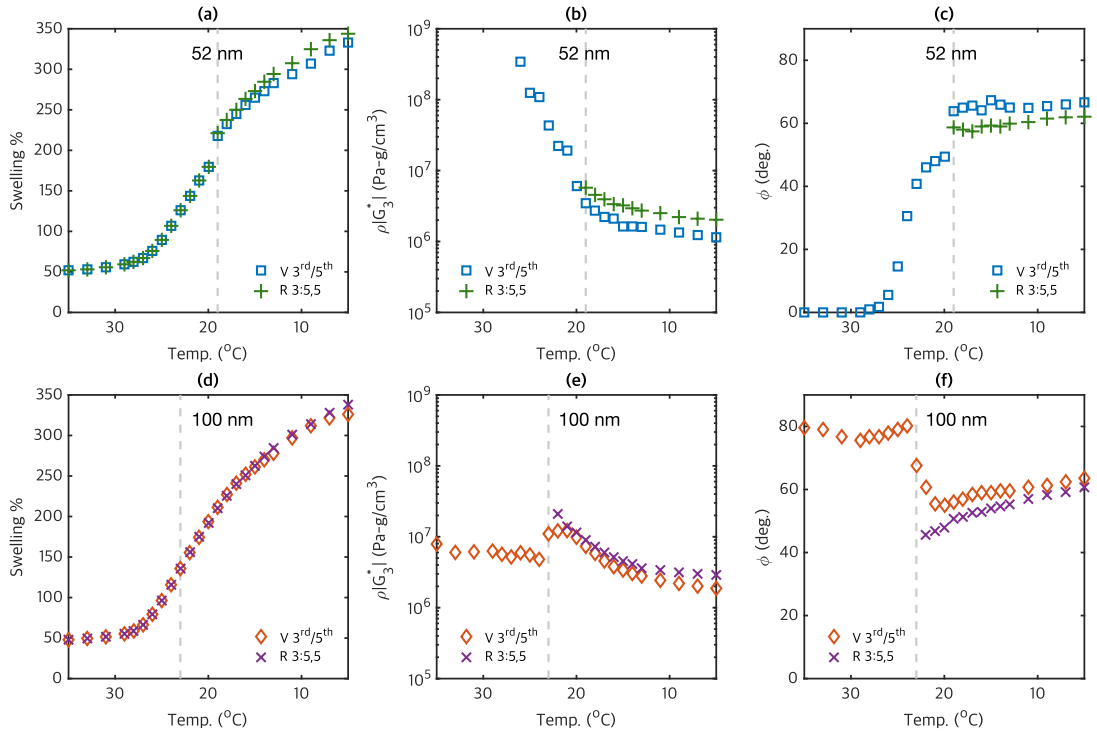

Figure 1.4: Comparison of the Voigt (V) and power-law (R) models for (a) swelling, (b) modulus and (c) phase angle of the 52 nm dry film. (d) Swelling, (e) modulus and (f) phase angle of the 100 nm dry film. The Sauerbrey limit applies to the left of the gray dashed lines. For the 100 nm film, the viscoelastic properties from the Voigt model are non-physical at higher temperatures, highlighting the danger of fitting the shifts in the Sauerbrey limit. Note that the moduli calculated correspond to 15 MHz (n=3).

We have described that d/λ_n must be in the 0.05-0.20 range for optimal viscoelastic data. This illustrated in Figure 1.5 where d/λ_n remains below 0.05 for a significant portion of the temperature range, and as expected, it remains in the Sauerbrey regime for a slightly larger temperature window for the thinner film. The results of this section highlight the need to be in the correct thickness regime for a film such that $0.05 < d/\lambda_n < 0.2$. Since the Voigt model aways provides excellent fits to the measured frequency and dissipation shifts, it is up to the experimentalist to determine whether the solved modulus and phase angle make physical sense in light of d/λ_n and in the context of the material being investigated. This assessment is a challenge without a robust framework to provide guidance on when to trust the modulus determined from the Voigt model.

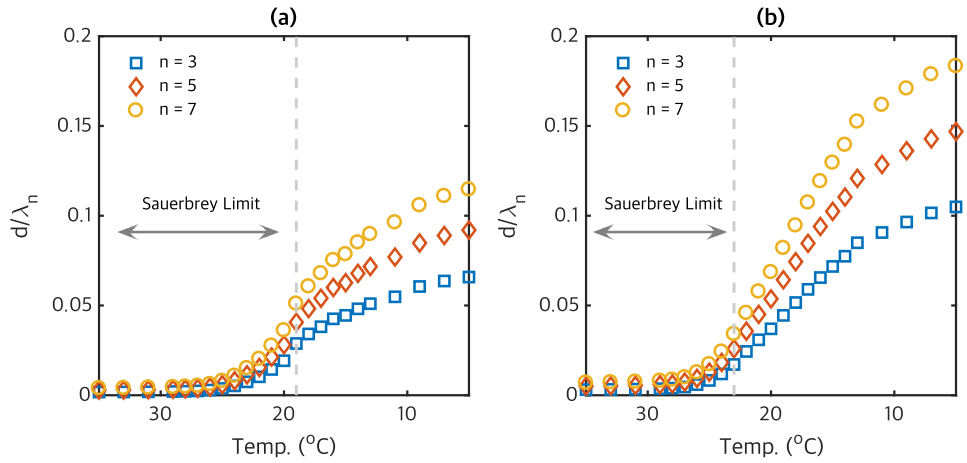

Figure 1.5: Changes in d/λ_n for hydrogels of (a) 52 nm and (b) 100 nm initial dry thickness. The rough temperature range over which the Sauerbrey limit applies is highlighted.

1.4.2 PECs as Model Systems

Polyelectrolyte complexes (PECs) consist of oppositely charged macromolecules that associate due to the large entropy gain from counter ion release. In the dry state these complexes form glassy solids, but when immersed in salt solutions, the ion pairs formed between the polycation and polyanion can be broken causing water ingress into the complex.[1] Thus, the swelling ratio of the complex can be controlled by choosing the solution ionic strength. At even higher salt concentrations, the solid complexes form a viscous coacervate phase. Addition of more salt leads to dissolution of the coacervate phase into a single phase solution with properties very close to that of water. This salt responsive behavior of PECs falls on a continuum of mechanical properties from glassy solids to Newtonian liquids, where the physical properties are primarily dependent on the amount of water in the material– a phenomenon that is reminiscent of many soft materials.[1] However, in most cases the entire range of mechanical properties are not accessible on the same materials system. For example, gels with well defined hydrophobic domains similar to the copolymer being investigated in this work, or covalently crosslinked systems, typically have an upper limit to the swelling ratio. Our recent work quantified the entire mechanical spectrum associated

with polyelectrolyte complexation using the QCM, such that the whole range of physical properties were comparable on a single mechanical testing platform.[1] This allowed data from from the liquid-like coacervates to be directly comparable to those from glassy complexes without any caveats. Since PECs span the entire mechanical spectrum, they are an excellent model system to elucidate how the physical properties of soft matter are related.

$$\phi = -9.5 \times ln(\rho|G_3^*|) + 200 \tag{1.11}$$

Figure 1.6a illustrates the mechanical spectrum associated with PECs, providing an empirical relationship (Eq. 1.11) between the shear modulus and the viscoelastic phase angle. Importantly, Eq. 1.11 illustrates that a simple log-linear expression describes soft materials that is swollen by water at this high frequency. This expression is also followed by polyethylene oxide solutions[52], protein-oxometalate complexes[24], and polyelectrolyte complexes,[1, 13] demonstrating the approximate generality of this relationship for a broad variety of soft matter at the megahertz frequency.

Eq. 1.11 displays how the physical behavior of soft materials are coupled in terms of the modulus and the phase angle. The question now becomes how to identify *where* on the mechanical spectrum a given material lies. Since the swelling behavior of a coating or a film is quite simple to measure accurately using ellipsometry or the QCM via the Sauerbrey relationship, we speculate it could serve as a basis of comparison. Again, we turn to the behavior of a model PEC. Figure 1.6b plots the shear modulus versus swelling of poly(styrene sulfonate) complexed with methyl quaternized poly(4-vinylpyridine), which varies log-linearly with swelling. We assume that the fit to the data would follow an expression of the form:

$$\rho|G_3^*| = \rho_o|G_3^*|_o e^{-S \times Swelling\%} \tag{1.12}$$

where $\rho_o|G_3^*|_o$ is the density-shear modulus of the dry glassy material at the third crystal harmonic (15 MHz), and S is a sensitivity factor. $\rho_o|G_3^*|_o$ is typically $\approx 2 \times 10^9$ Pa-g/cm^{3}for glassy polymers. The value of S determines how sensitive the modulus is to changes in swelling, and is ≈ 0.03 for polyelectrolyte complexes swollen by water. Note that between Eq. 1.11 and 1.12, S is the single parameter whose value quantifies changes in physical properties over the entire swelling range. If the swelling % of a soft material is now known, Eq. 1.11 and 1.12 provide an estimation of the material's properties at $n = 3$ (15 MHz). We speculate that Eq. 1.11 is quite general and describes a wide variety of soft materials– an assumption we seek to investigate in the context of the physically crosslinked gel in this chapter. While we expect that Eq 1.12 is more material specific, we nevertheless suspect that it is a smart approximation for films swollen in water from an initially glass-like state. Note that in Eq. 1.11 and 1.12 we have used mechanical properties at $n = 3$ (15 MHz).

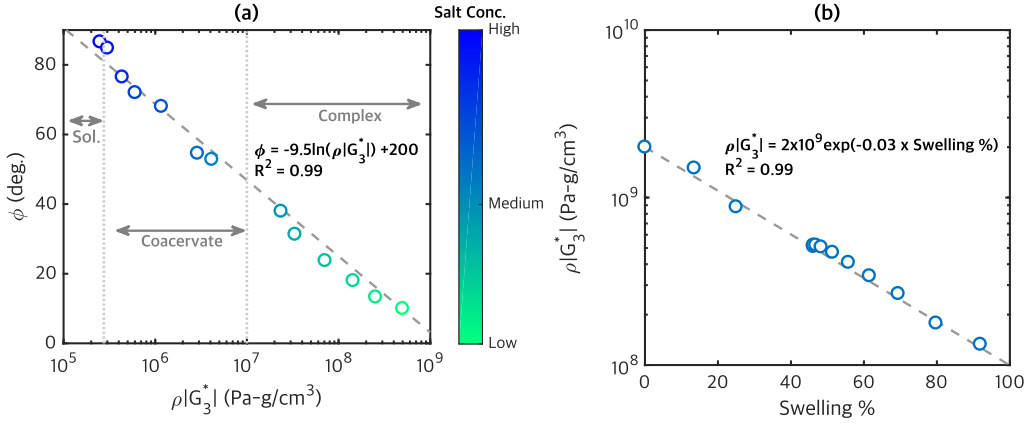

Figure 1.6: (a) Influence of salt concentration on the mechanical spectrum of polyelectrolyte complexation. The QCM was used to elucidate the continuous transition from solid complex to coacervate to a single phase solution.[1] Note that in this MHz regime, water has a $\rho|G^*|$ of 10^5 Pa-g/cm^3 and ϕ of 90^o. Glassy films have $\rho|G^*| \approx 10^9$ and $\phi < 10^o$. (b) The effect of swelling on the density shear-modulus of poly(styrene sulfonate) and methyl quaternized poly(4-vinylpyridine) polyelectrolyte complex. Dashed lines are Eq. 1.11 and 1.12. More details about polyelectrolyte complex's physical behavior are explored in Chapter 3.

We now proceed to comparing the behavior of the physically crosslinked gels of the present

work to the behavior of PECs. Figure 1.7a plots the properties of PNIPAAm-FOSA gels on the spectrum of mechanical properties which may be assumed by soft materials at the megahertz frequency. We find that Eq. 1.11 excellently describes the relationship between ϕ and $\rho|G_3^*|$. Just as salt allowed movement along Eq. 1.11 for PECs, temperature allows the same movement for the PNIPAAm-FOSA gels. A high temperature results in a high modulus and a low ϕ, while a low temperature results in a low modulus and a high ϕ. Next, Figure 1.7b plots the swelling-modulus behavior of the 52 nm and 100 nm films. At lower swelling ratios (< 200 %) the PNIPAAm-FOSA films begin to be described by Eq. 1.12. Figure 1.7 leads us to several important conclusions about the high frequency responsive behavior of soft materials. The relationship between ϕ and modulus is not arbitrary, i.e., a material cannot have a high modulus and a very large ϕ simultaneously. In this respect, Figure 1.7a is quite general. However, the relationship between the swelling ratio and the modulus is more material specific. In this particular case, we find that the swelling ratio and the modulus starts to deviate from Eq. 1.12 as the temperature is decreased. Yet, since polymer glasses have a modulus of around $\approx 2 \times 10^9$ Pa at 15 MHz, it is reasonable to expect that such a material would approximately follow Eq. 1.12, at least initially. Indeed we find that at lower swelling ratios PNIPAAm-FOSA gels approach the behavior of PECs, while at large swelling ratios there is significant deviation, where $|G^*|$ must necessarily plateau at a value at least as large as the value for pure solvent ($\approx 10^5$ Pa for water at 15 MHz). Nevertheless, PECs provide a guide for approximating materials properties at a specific swelling % up to 175 % nearly quantitatively. More importantly, by generalizing soft materials properties using Figure 1.7a we have now enabled one to calculate the parameter d/λ_n using Eq. 1.4 for a film of thickness d if the approximate swelling % (Eq. 1.10) is known. Therefore, a more guided and quantitative approach may now be taken to aim for $0.05 < d/\lambda_n < 0.20$. While the QCM measures mechanical properties in the MHz regime, these mechanical data are consistent with those measured at lower frequencies.[53]

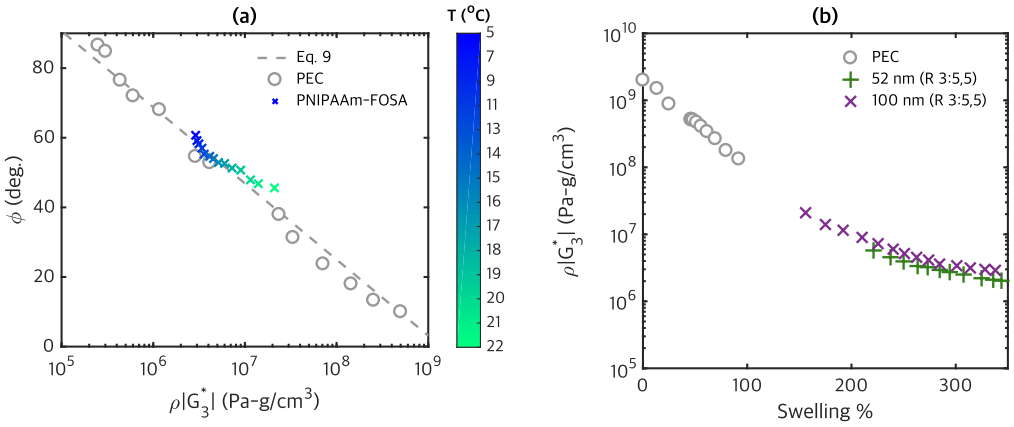

Figure 1.7: (a) Movement of the 100 nm film properties on the mechanical spectrum (Eq. 1.11) as a function of temperature, and (b) the swelling-modulus behavior of the 100 nm and 52 nm film in comparison to Eq. 1.12. Gray data points were reproduced from Figure 1.7 and ref. 1.

1.4.3 Optimal Film Thickness for QCM-D Rheology

The QCM is a highly versatile and inexpensive fixed frequency rheometer which can be used to probe thin soft materials *in-situ*. In this context, the QCM has tremendous potential to elucidate the responsive behavior of advanced coatings and soft materials. While the simplicity of experiments and the quality of data are advantageous, the correct analysis of those data requires a good understanding of QCM response in terms of d/λ_n. Recall that λ_n requires knowledge of the material properties to which the crystal is in contact (Eq. 1.4). This is challenging for casual QCM users since it in not immediately intuitive what the appropriate thickness must be for a material with a particular modulus and phase angle. A typical consequence of this in literature is that users often attempt to fit data for films that are too thin, and where the QCM is not sensitive to viscoelasticity. However, there are quantitative thickness limits to QCM operation which must be met in order to obtain meaningful data. Recall that modeling QCM data requires the frequency and dissipation shifts from two harmonics, and let us then consider the case of $n = 3,5$. The optimal thickness window in this scenario would be where both the harmonics deviate from the Sauerbrey limit, yet the Γ of the higher harmonic remains low enough such that it is still measurable. The maximum Γ

that is accurately measurable is about 10 kHz. Thus, to obtain data that is sensitive to viscoelasticity and can be solved by either the V model or the R model, d/λ_3 must be at least around 0.05 and Γ_5 must be less than 10 kHz. Figure 1.8 lists the range of thickness which satisfy both of these requirements for the $n = 3,5$ and $n = 5,7$ harmonic combinations at all relevant mechanical properties. Note that no thickness range is provided for $\phi > 70^o$ since it is recommended that the bulk limit (1.5 and 1.6) be used here, if possible. For the reader interested in exploring QCM experiments in more detail we point to a breadth of work[1, 13, 17, 24, 29, 36, 40, 41, 53, 54], and the excellent book by Johannsmann.[55]

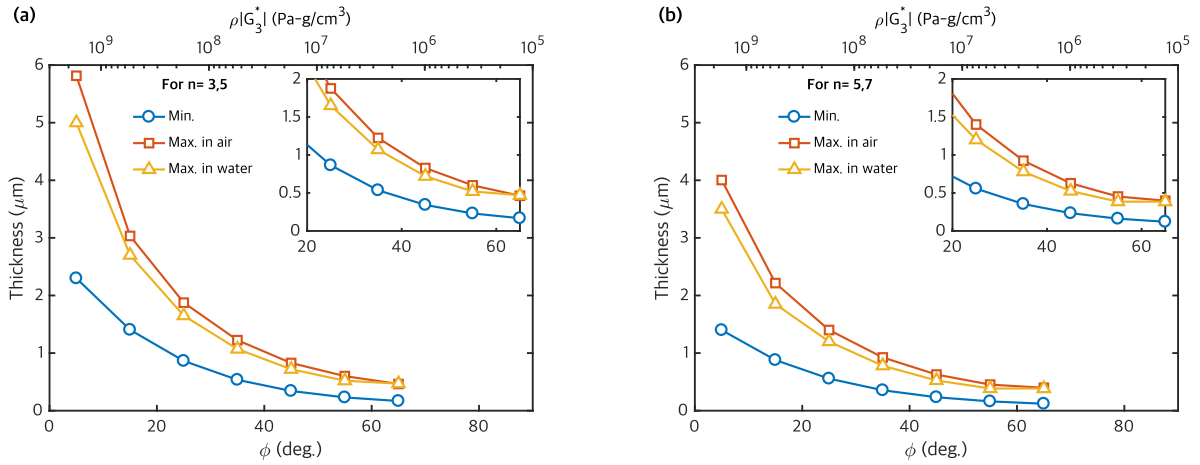

Figure 1.8: Recommended thickness ranges for accurate QCM rheology for films with a particular modulus and/or phase angle in air or water using (a) $3^{rd}/5^{th}$ and (b) $5^{th}/7^{th}$ harmonic combinations. The insets show zoom-ins of the thickness for ϕ between 20^o and 65^o. Thickness upper bounds are calculated by limiting the dissipation of the higher harmonic in each case to 10 kHz. Thickness lower bounds are calculated by setting the minimum deviation from Sauerbrey limit of the lower harmonic in each case to be 2% ($d/\lambda_n \approx 0.05$). The density is assumed to be 1 g/cm^3 here, therefore these thickness ranges are approximate.

1.4.4 Recommendations for Accurate Viscoelastic Analysis using the QCM

Based on the results of this work, some general recommendations are made for taking a more guided approach to QCM-D rheology:

- If the swelling % of a film in water is known relative to its dry thickness, then Eq. 1.11 and Eq. 1.12 can be used to approximate the mechanical properties, which can subsequently be used to identify the optimal thickness range using Figure 1.8. While Eq. 1.11 appears to be quite general in describing the fixed frequency response of soft materials, we find that Eq. 1.12 is more material specific (as it is expected to be). However, Eq. 1.12 still provides a good approximation for mechanical properties at lower swelling ratios for initially glass-like films.

- Figure 1.8 is agnostic of materials chemistry and/or mechanism of responsiveness (pH, ionic strength, temperature, etc.). It only requires the user to have an approximate knowledge of the modulus and/or phase angle of their material in the megahertz regime. For reference, at this frequency water has $\rho|G_3^*| = 10^5$ Pa-g/cm^3 and $\phi = 90^o$, gels (or hydrated soft materials) typically have $\rho|G_3^*| \approx 10^8 - 10^6$ Pa-g/cm^3 and $\phi = 20 - 70^o$, and glassy materials have $\rho|G_3^*| \approx 10^9$ Pa-g/cm^3 and $\phi < 1 - 5^o$.

- For glassy films (e.g. polystyrene, $\phi \approx 1^o$), 4-6 μm thick films provide enough dissipation change to be modeled accurately. For soft viscoelastic films (e.g. gels, $\phi \approx 45^o$), 0.6-1.2 μm films are a good start. For viscous liquids (e.g. polymer solutions) Eqs. 1.5 and 1.6 can be solved simultaneously at a single harmonic, n, to obtain $\rho|G_n^*|$ and ϕ by exposing the crystal to the semi-infinite liquid-like medium.

- For best results, harmonics $n = 3, 5, 7$ are recommended for modeling. Higher order harmonics should be used with caution since coupling of anharmonic resonances with the main resonance peak may lead to erroneous observation of Δf and $\Delta\Gamma$. Modeling with $n = 1$ is discouraged due to insufficient energy trapping.[55]

- Films should be as smooth and homogeneous as possible.

- For viscous liquids, the bulk limit should be used.

1.5 Conclusion

In the present work a thermo-responsive hydrogel undergoing large swelling changes was used to probe the three distinct regimes of QCM operation. At high temperatures the film was stiff and deswollen and the Sauerbrey limit applied. As the film was cooled, it swelled significantly and the film thickness, modulus and phase angle could be calculated using the Voigt (V) and the power-law (R) model. At even higher swelling ratios, the film neared resonance conditions where an uptick in the frequency could be observed with increasing mass, contrary to the Sauerbrey relationship. Both models accurately predicted this behavior and were able to calculate the film properties with good agreement. However, the Voigt model was found to provide modulus and phase angles even in the Sauerbrey limit where no viscoelastic information exists in the QCM response. While in the case of the 52 nm dry film the Voigt model appeared to provide reasonable values even in the Sauerbrey limit, it failed to replicate those values for the 100 nm film. Therefore, it is imperative for QCM users to avoid fitting frequency and dissipation shifts in the Sauerbrey limit. To that end, we demonstrated that a minimum value of $\approx$0.05 is needed for the film thickness normalized by the shear wavelength (d/λ_n) for the QCM to be sensitive to viscoelastic properties. However, often some prior knowledge about the material being investigated is required to accurately calculate d/λ_n, since the shear wavelength depends upon the film's modulus and phase angle. We provided a quantitative relationship between the modulus and the phase angle (Eq. 1.11) and the swelling % and modulus (Eq. 1.12) which could be used to approximate material properties at a specific swelling ratio, ultimately allowing one to approximate d/λ_n. These relationships were enabled by quantifying the mechanical behavior of polyelectrolyte complexes, whose properties span the entire mechanical spectrum from low viscosity fluids to glassy solids. While dependence between swelling and modulus can be material specific, the behavior of polyelectrolyte complexes serves as a good approximation nonetheless, especially at lower swelling ratios. Finally, we provided thickness ranges as a function of the mechanical properties of materials being investigated where

the QCM response would be sensitive to viscoelasticity. This should provide QCM users an initial guess as to what thickness regime to aim for to obtain meaningful viscoelastic data.

Chapter 2

pH Controlled Electrodeposition of Polyelectrolyte Complex Films

Abstract: Polyelectrolyte complex (PEC) films made from oppositely charged polymer chains have applications as drug delivery vehicles, separation membranes, and biocompatible coatings. Conventional layer-by-layer (LbL) techniques for polyelectrolyte coatings are low-throughput and multistep processes that are quite slow for building films on the order of micrometers. In this work, PEC films are electrochemically deposited using a rapid one-pot method yielding thick (1 μm) films within short experimental time scales (5 min). This rapid electrodeposition is achieved by exploiting the reduction of hydrogen peroxide at mild electrode potentials that avoid water electrolysis, yet trigger the pH responsive self-assembly of a PEC film of poly(acrylic acid) and poly(allylamine). *In-situ* rheology using an electrochemical quartz crystal microbalance (EQCM) quantified the shear modulus-density product of the deposited layer to be on the order of 10^7 Pa-g/cm^3 at a frequency of 15 MHz, with a viscoelastic phase angle at this frequency of approximately 50^o. This electrodeposition scheme furthers the development of PEC coatings for more high-throughput applications where a fast and efficient single step approach would be desirable for obtaining coatings. This work appears in *Langmuir* 2017, 33, 8, 1834-1844.

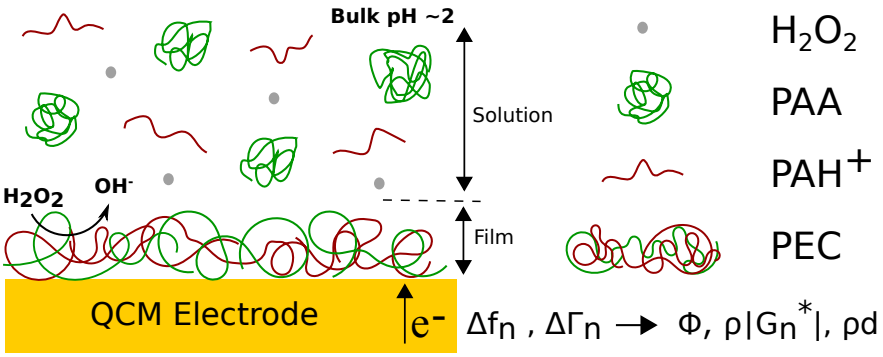

2.1 Introduction

Polyelectrolyte complexation is an interesting self-assembly phenomenon because it yields stimulus responsive soft matter spanning a broad range of physical properties. This versatility stems from the ionic interactions that allow oppositely charged polyelectrolytes to form either solid-like precipitates (complexes) or fluid-like dense phases (coacervates).[1, 3, 6] The dynamic nature of electrostatic bonds characteristic of polyelectrolytes promises advancements in a range of technological applications such as drug delivery[56, 57], coatings[58], membranes[4, 59] and adhesives.[60, 61] To date, the layer-by-layer (LbL) deposition process employing the sequential assembly of oppositely charged macromolecules onto a substrate has been the most common method for controllably making tunable polyelectrolyte complex (PEC) coatings. This facile approach, coupled with the rich chemistry of polyelectrolytes, has led to many advances in developing surface treatments and stimulus-responsive materials.[59, 62, 63] Additionally, the physical behavior of polyelectrolyte coacervates and multilayers has now become well documented.[1, 6, 64, 65, 66, 67, 68]

Polyelectrolyte multilayering yields smooth and conformal coatings with nanometer scale control using a simple aqueous processing method. However, a significant shortcoming of this method

is its inherently low-throughput nature due to the multiple alternating steps involved.[2, 69] Several improvements upon the LbL technique, such as spin, spray, potential and exponential growth-assisted assembly, have significantly improved the rate of PEC film growth, but these approaches do not fundamentally overcome limitations associated with the sequential assembly process.[70, 71, 72, 73] Many commercial applications where polyelectrolytes are of relevance, such as electrodeposited paints[74], require an efficient one step process. For PEC coatings to be applicable in such high-throughput contexts it is necessary to consider alternative single step deposition schemes. Kelly *et al.* recently spin-coated a polyelectrolyte coacervate and achieved uniform films on the order of microns.[2] This approach preserves the simplicity of the LbL process, but it is restricted to planar surfaces. Krogman *et al.* have reported a fast and novel spray assembly of conformal PECs on fibers. This approach, however, typically requires a direct line of sight to the substrate [75]. Garnier and Dochter *et al.* reported the electrochemical codeposition of polyelectrolytes by masking the true charge on one of the chains and subsequently deprotecting it via a pH stimulus generated by an applied potential.[76, 77] While this approach permits high-throughput conformal coatings of large arbitrary shapes- as exemplified by pH controlled paint electrodepositions- it involves a synthesis step to chemically modify either the cationic or anionic polyelectrolyte.

Electrochemical approaches to codeposition of polyelectrolytes are particularly appealing because the substrate potential can be adjusted to realize a desired deposition rate, film thickness and mechanical response of the deposited film. Indeed, polyelectrolyte adsorption and LbL assembly under electrochemical potential biases have been shown to improve the rate of deposition[78, 79, 80], but this approach often suffers from the high electrode potentials used where water electrolysis can be an issue, while only marginally overcoming the limitations of LbL assembly.[81] Nilsson *et al.* recently studied the anodic electrodeposition of a cationic polyelectrolyte using QCM-D (quartz crystal microbalance with dissipation monitoring), but they noted that the evolution of O_2 bubbles

from water electrolysis during the deposition process only allows one to calculate estimates for film mass and viscosity from the QCM response.[82] In its simplest application, the QCM is a very sensitive mass balance for sufficiently rigid films, as quantified by the Sauerbrey equation.[22] If a viscoelastic film is applied at the quartz crystal surface, there is a deviation of QCM response from the Sauerbrey limit that depends on the thickness and viscoelastic character of the film. By quantifying this deviation it is possible to use the QCM as a fixed-frequency rheometer, obtaining the high frequency (typically 5 or 15 MHz) mechanical properties of the film deposited at the crystal surface.[24] Although the QCM has been used extensively in polyelectrolyte research, it is almost exclusively employed to gain qualitative insights in terms of frequency and dissipation shifts. The viscoelastic information contained in those shifts is rarely quantified, usually due to difficulties in modeling with the widely used Q-sense instrument.

In this study, we develop a rapid one-pot electrochemical deposition scheme that uses a pH stimulus to trigger the self-assembly of a PEC film of poly(acrylic) acid and poly(allylamine) HCl at moderate cathodic potentials, circumventing the electrolysis of water and thereby the evolution of H_2 gas. The pH stimulus is generated by exploiting the reduction of H_2O_2 at the working electrode of a custom electrochemical quartz crystal microbalance (EQCM), achieving $\approx 1\ \mu m$ films within short time scales (≈ 5 min). We demonstrate that H_2O_2 is an ideal molecule for generating a pH gradient that can induce the self-assembly of a PEC film at the electrode surface, and perform *in-situ* rheology of the film using the EQCM, monitoring the evolution of its viscoelastic phase angle (ϕ) and density- shear modulus product ($\rho|G^*|$). Our results suggest that the mechanical properties of the deposited PEC film are dependent on the bulk solution pH, working electrode potential and the initial salt, H_2O_2 and polymer concentrations. Finally, we present Finite Element Modeling (FEM) results to guide intuition behind the deposition mechanism during the initial stage of film growth.

2.2 Experimental Methods

2.2.1 Materials

Poly(acrylic) acid (PAA, molar mass 250,000 g mol^{-1}) and poly(allylamine) HCl (PAH, molar mass 60,000 g mol^{-1}) were purchased from Polysciences Inc. (Warrington, PA). Sodium chloride, sodium sulfate, hydrogen peroxide (35 wt%) and hydrochloric acid (37 wt%) were purchased from Sigma-Aldrich. Deionized water (conductivity ~ 5 $\mu S/cm$) was used for making all solutions.

2.2.2 Electrochemical Quartz Crystal Microbalance

A custom three-electrode electrochemical quartz crystal microbalance (Advanced Wave Sensors, Valencia, Spain) was used to deposit polyelectrolyte complex films. The EQCM holder was connected to both an N2PK impedance analyzer (Thornhill, ON, Canada) and a potentiostat (BioLogic SP-150, Grenoble, France). Electrodepostion was conducted using a silver chloride reference electrode (Ag/AgCl) and a platinum counter electrode. All potentials reported in this paper are referenced to the Ag/AgCl electrode. AT-cut, 1 inch, 5 MHz quartz crystals with an 1.27 cm^2 working Au electrode (Stanford Research Systems, Sunnyvale, CA) were used as manufactured.

We have previously detailed the mathematical approach for obtaining viscoelastic information from QCM experiments, an analysis that can be extended to data obtained from the Q-sense instrument.[24, 39] The values of interest obtained from the QCM portion of the experiment are the the resonant frequency, f_n, and the bandwidth, Γ_n. Here f_n is the frequency corresponding to the maximum conductance measured across the electrodes on either side of the quartz crystal at the n^{th} harmonic. We measure the resonances at the first harmonic ($n = 1$, f_n =5 MHz) and at the third harmonic ($n = 3$, $f_n = 15$ MHz). The bandwidth is the half-width of the conductance peak, measured at half its height. The bandwidth is a measure of the energy dissipation in the system, and we often refer to Γ_n simply as the "dissipation". When a film is deposited onto the electrode

surface of the QCM, the frequency and dissipation values shift relative to the bare crystal, allowing one to define a complex frequency shift, Δf_n^*[22]:

$$\Delta f_n^* = \Delta f_n + i\Delta\Gamma_n \tag{2.1}$$

If the film at the electrode surface is submerged in a liquid, as in our experiments, then Δf_n^* includes shifts from both the film and liquid loads at the quartz surface. If frequency and dissipation shifts from the liquid load are subtracted from Δf_n^*, and the film is sufficiently thin and rigid, then $\Delta\Gamma_n$ becomes negligible and the frequency shift becomes proportional to the areal mass of the film (ΔM_A) through the well-known Sauerbrey relation (eq. 1.3)[22]. In our experiments, we reference Δf_n and $\Delta\Gamma_n$ to the resonance frequency of the crystal submerged in solution.

When QCM measurements are combined with electrochemical tests, the QCM electrode in contact with the aqueous medium serves as the working electrode in a three-electrode electrochemical cell. Current or potential can be controlled and measured by a potentiostat, while the QCM simultaneously measures changes in mass (eq 1.3) at the electrode surface due to the electrochemical process. If a viscoelastic film is applied at the quartz surface (i.e., $\Delta\Gamma > 0$) then the QCM response deviates from the Sauerbrey limit of eq. 1.3, and the magnitude of the deviation allows calculating the viscoelastic parameters of the layer. Mathematically this deviation is represented by the following QCM master equation[24]:

$$\frac{\Delta f_n^*}{\Delta f_{sn}} = \frac{\Delta f_n + i\Delta\Gamma_n}{\Delta f_{sn}} = -\frac{D_{nf}^{*-2} + R_{n\ell}^{*2}}{\cot(D_{nf}^*)/D_{nf}^* + R_{n\ell}^*} \tag{2.2}$$

where $R_{n\ell}^*$ and $D_{n\ell}^*$ are defined as follows:

$$R_{n\ell}^* = \frac{\Delta f_{n\ell} + i\Delta\Gamma_{n\ell}}{\Delta f_{sn}} \tag{2.3}$$

$$D_{nf}^{*} = \frac{2\pi d}{\lambda_n}\left(1 - i\tan\left(\phi_n/2\right)\right) \tag{2.4}$$

with:

$$\lambda_n = \frac{1}{f_n}\left[\frac{|G_n^{*}|}{\rho}\right]^{1/2}\frac{1}{\cos(\phi_n/2)} \tag{2.5}$$

In the above equations, λ_n is the wavelength of the shear wave within the film, G_n^{*} is the complex modulus of the film, ϕ_n is its phase angle, and the subscripts f and ℓ refer to the film and liquid, respectively. Eq 2.2 provides the divergence from the Sauerbrey limit for a viscoelastic material, allowing one to calculate its areal mass (ρd), density-modulus product (ρG_n^{*}) and phase angle (ϕ_n). For the experiments reported here, Δf_n and $\Delta\Gamma_n$ were recorded at the first and third harmonics (n = 1, 3), yielding four experimental parameters ($\Delta f_{1,3}$ and $\Delta\Gamma_{1,3}$). Since $\Delta f_n^{*}/\Delta f_{sn}$ is a function of ρd, d/λ_n and ϕ_n, three parameters are needed to numerically solve for the three variables. In the work described here, we use the frequency shift of the first and third harmonics and the dissipation shift of the third harmonic (a 1,3:3 calculation in our nomenclature). For a film in air, $R_{n\ell}^{*} = 0$, which reduces eq 2.2 to our previously reported one-layer in air model [39]. One final relation is needed to convert d/λ_3 to $\rho|G_3^{*}|$:

$$\rho|G_3^{*}| = 9(\rho d)^2 f_1^2 \cos(\phi/2)\left(\frac{d}{\lambda_3}\right) \tag{2.6}$$

Equations 2.1-2.6 provide all the necessary relations needed to estimate the viscoelastic parameters of the deposited film. Note that we are only sensitive to the mass of the thin film when its thickness is not too large, with a cutoff thickness determined by the decay length, δ_n, of the shear wave in the film, with δ_n given by the following expression:

$$\delta_n = \frac{\lambda_n}{2\pi}\cot\left(\phi_n/2\right) \tag{2.7}$$

2.2.3 Electrodeposition

Deposition was carried out in solutions containing 0.250% PAH and 0.192% (w/v) PAA (26.7 mM repeat units each). The pH was adjusted to the desired experimental value using HCl and then sodium chloride and hydrogen peroxide were added. For each experiment, the resonance frequencies of the bare crystal in air at the first and third harmonics were recorded. Next, the resonance frequencies of the crystal immersed in the prepared polymer solution were recorded with reference to the bare crystal in air. The open circuit potential of the electrochemical cell was monitored for 30 seconds before electrodeposition was carried out at -0.5V vs. Ag/AgCl while the QCM measured shifts in frequency (Δf_n) and dissipation ($\Delta\Gamma_n$) at the 1st and 3rd harmonics were recorded in solution. All experiments were conducted at room temperature.

2.2.4 Dynamic Light Scattering

Dynamic light scattering was performed using a Malvern Zetasizer Nano S (Worcestershire, UK) system at 25^{o}C using a 173^{o} backscatter angle. The refractive index (1.330) and viscosity ($8.87 * 10^{-4}$ Pa$*$s) of water at 25^{o}C were used as the dispersant properties; the refractive index and attenuation coefficient of the polymer were estimated at 1.45 and 0.001, respectively. We report the average $\pm$ one standard deviation of four measurements at each condition.

2.2.5 Finite Element Modeling

Finite element modeling was performed using COMSOL Multiphysics 5.2 with a Corrosion Module using our previously reported approach to calculate the proton and peroxide depletion rates at the electrode surface during the initial period of film growth.[83] A time-dependent, tertiary current distribution with a reduced 1-D interval was used. The left boundary of the 1-D interval was defined to be the working electrode, and the right boundary was defined to be the bulk solution.

The dependent variables were the electrolyte potential and the concentration of all chemical species in space and time. Table 2.1 presents all the diffusion coefficients and initial concentrations used as model inputs. Current and potential were defined at the working electrode as measured from EQCM tests.

Four boundary conditions were specified in this model:

1) A "no flux" condition was set at each electrode boundary.

2) The potential and current at the electrode boundary was defined as a function of time as measured from the experimental data.

3) The electrolyte potential at the bulk electrolyte boundary was set equal to the experimentally measured open circuit potential.

4) The initial concentrations of H^+, OH^-, PAH^+, PAA, H_2O_2, and Cl^- were set as their bulk concentrations at the bulk electrolyte boundary.

Species	**Diffusion Coefficient (m^2/s) [84]**	**Initial Concentration (mM)**
H^+	9.331×10^{-9}	11.2
OH^-	5.273×10^{-9}	8.91×10^{-10}
H_2O_2	1.71×10^{-9}	120
Na^+	1.334×10^{-9}	-
Cl^-	2.03×10^{-9}	30 + 26.7
PAH^+	8×10^{-12} (DLS)	26.7 (0.250% (w/v))
PAA	6×10^{-12} (DLS)	26.7 (0.192% (w/v))

Table 2.1: Diffusion coefficients and initial concentrations of all dependent variables in numerical modeling. Na^+ concentration was used to maintain electroneutrality internally in the simulation. Diffusion coefficient for H_2O_2 was used as determined by Kern [8], while PAH^+ and PAA were measured experimentally by dynamic light scattering.

Flux of individual species were related to the experimentally measured current to calculate species concentrations at the electrode. The flux of a component i (N_i) is related to its contribution to the current, j_i, by Faraday's Law written in the following form [85]:

$$N_i = \frac{\nu_i j_i}{n_i F} \tag{2.8}$$

where ν_i is the stoichiometric coefficient of the component, n_i is the number of electrons involved in the reaction, and F is Faraday's constant. Component fluxes are driven by three processes - diffusion, electromigration, and convection - according to the Nernst-Planck equation [85]:

$$N_i = -D_i \bigtriangledown c_i - z_i u_{m,i} F c_i \bigtriangledown \phi_l + c_i u \tag{2.9}$$

where c_i is the component concentration, D_i is the diffusion coefficient, z_i is the charge, $u_{m,i}$ is its ionic mobility, ϕ_l is the electrolyte potential, and u is the convection velocity vector. The three terms on the right hand side of eq 2.9 correspond, from left to right, to diffusion, electromigration, and convection. Ionic mobility is related to the diffusion coefficient through the Nernst-Einstein relation [85]:

$$u_{m,i} = \frac{D_i}{RT} \tag{2.10}$$

where R is the molar gas constant and T is temperature.

The total transport rate of component i through the electrolyte, $R_{i,tot}$, is given by the mass balance eq [85]:

$$\frac{\partial c_i}{\partial t} + \bigtriangledown N_i = R_{i,tot} \tag{2.11}$$

Equation 2.11 can be solved numerically for the concentrations of the i components as a function of time using experimental parameters such as the electrode potential, measured current, and species concentrations.

2.2.6 Atomic Force Microscopy

The morphological features of electrodeposited PEC films were examined using tapping mode on a Dimension FastScan AFM with ScanAsyst (Bruker Co., Billerica, MA). AFM images were obtained in air at rate of 0.50 Hz with scan sizes of 25×25 μm. Films for AFM imaging were

obtained after approximately 6 minutes of deposition by removing the electrode from solution *while* maintaining the potential to limit film dissolution. Films were then dried in air.

2.3 Results & Discussion

Electrodeposition of polyelectrolytes has been studied in great detail in the context of a weak polyelectrolyte becoming insoluble at an electrode surface by losing its charge due to a pH gradient. For example, the cathodic neutralization of the aminopolysaccharide chitosan causes it to precipitate out of solution in response to an applied potential.[86] Electrodepostion schemes can also be easily extended to polyelectrolyte-inorganic particle composites to obtain a variety of functional coatings.[87, 88] An analogous approach to PEC film deposition is desirable as it allows spatiotemporal control over the film growth process in a potentially high-throughput and versatile way. However, in addition to the issue of establishing a pH gradient at moderate potentials (to avoid water electrolysis), it is necessary to exclusively initiate the electrostatic complexation of the polyelectrolytes at the electrode surface such that a coating can be obtained. This is challenging under low salt conditions (<1.0 M salt) because polyanions and polycations immediately form precipitates upon mixing. Our approach utilizes the cathodic reduction of H_2O_2 at a moderate potential (-0.5 V) in an acidic solution (pH ~ 2) to alkalize the vicinity of the electrode and prompt the electrostatic self-assembly a PEC film composed of the weak polyelectrolytes PAA (pK_a ~5.5) and PAH (pK_a ~8.5). The acidic conditions fully protonate PAA, thereby precluding premature complexation of PAA and PAH in the bulk. The reduction of H_2O_2 at the cathode initiates the local electrostatic complexation of the polyelectrolytes by slowly deprotonating PAA (PAH remains in its cationic form). Water reduction does not proceed at this potential, thus facilitating the formation of a homogeneous film. Furthermore, we probed the *in-situ* mechanical response of the PEC film by performing its electrodeposition using an EQCM as schematically outlined in Figure 1.1. We present the results of our investigations in the following sections, beginning with

the electrochemical behavior of H_2O_2.

2.3.1 Electrochemical Behavior of H_2O_2

Figure 2.1 shows the cyclic voltammograms for water and hydrogen peroxide obtained in a pH 2 solution with an Au working electrode. Without peroxide, the current remains close to zero, indicating that no water reduction is occurring at these potentials. When 10 mM of peroxide is added to the solution, a significant increase in the reduction current is observed, with the current commencing around -0.1 V and peaking around -0.45 V. Comparing the voltammograms of water and peroxide, it is evident that the large reduction current is solely due to peroxide reduction. Gerlache *et al.* and Stewart *et al.* have previously reported similar reduction behavior of peroxide, and have offered some mechanistic insights for the chemical steps involved.[89, 90] Gerlache *et al.* studied the effect of pH and peroxide concentration on the voltammogram, while Stewart *et al.* concluded that the peroxide reduction in an acidic environment involves the dissociative adsorption of peroxide molecules on to a metal surface via the formation of metal-OH species. These metal-OH species are subsequently reduced at cathodic potentials, forming OH^- that can neutralize H^+ ions in solution via the following overall mechanism:

$$H_2O_2 + 2H^+ + 2e^- \rightarrow 2H_2O \tag{2.12}$$

Exploiting the reduction of H_2O_2 to generate a pH gradient has the following advantages:

1. H_2O_2 reduces at moderate potentials
2. No H_2 gas is generated since water electrolysis is avoided
3. The reaction product is simply water- the original solvent

Circumventing the electrolysis of water to generate a pH gradient is essential for achieving uniform films. Furthermore, it enables our mathematical approach- which assumes uniform contact at the film-electrode interface- for extracting viscoelastic parameters from a film deposited on a

QCM. The *in-situ* rheology of the deposited PEC film is discussed in the next section.

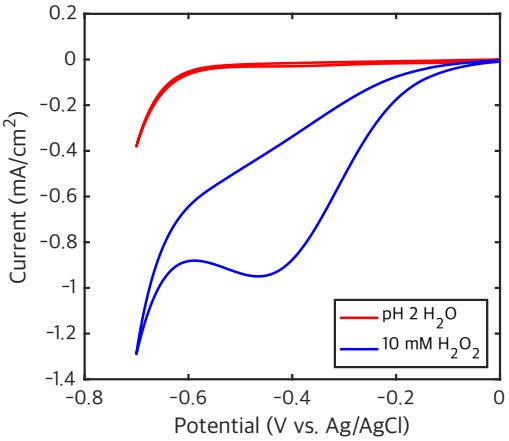

Figure 2.1: Cyclic voltammograms of water and 10 mM H_2O_2 obtained in a pH 2 solution with 1 M Na_2SO_4 acting as the supporting electrolyte. The scan rate was 20 mV/s vs. a Ag/AgCl reference electrode.

2.3.2 Rheology of the Electrodeposited PEC Film

Under acidic conditions, PAH and PAA form weak complexes, but if the pH is raised to the vicinity of 5.5 (pK_a of PAA), an insoluble polyelectrolyte complex precipitates from solution.[91] This phenomenon presents the opportunity to controllably induce the self-assembly of a PEC film at an electrode by providing an appropriate local pH stimulus. At a cursory glance, the electroreduction of water could induce a pH gradient, but this approach has several drawbacks, most notably the very low potentials (<-1.0V) necessary to reduce water, and the formation of H_2 gas which would interfere with the film deposition process. In the previous section it was demonstrated that hydrogen peroxide reduces at intermediate potentials and that the reduction reaction consumes protons locally at working electrode surface, raising the pH. Figure 2.2 presents the evolution of mechanical properties of PEC film deposited from a pH of 1.95 and 26.7 mM PAH and PAA by setting the electrode potential to -0.5 V.

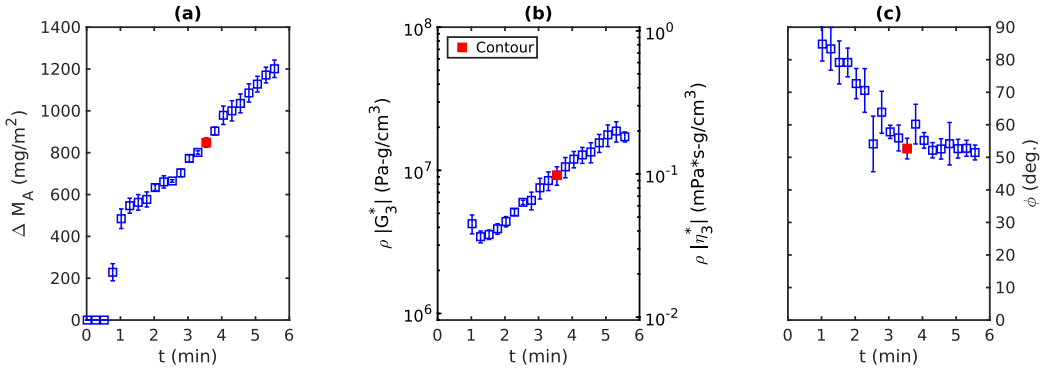

Figure 2.2: Electrodeposition of a PEC film from a solution of pH 1.95, 120 mM H_2O_2, 30 mM NaCl, and 26.7 mM PAH and PAA, respectively. (a) and (b) show the increase in the areal mass and density-shear modulus product and (c) shows the decrease in the viscoelastic phase angle. The working electrode potential was set to -0.5 V vs. Ag/AgCl. Mechanical properties were calculated using the 1:3,3 calculation and the viscosity in (b) was calculated by noting that $|\eta_3^*| = |G_3^*|/2\pi f$, where f is the experimental frequency (15 MHz). Error bars presented are the standard errors of three trials. The filled time point in red was used to calculate the error contour plots in Figure 2.5.

At a pH of 1.95 the mixture was clear, indicating that the polyacid and the polybase were very weakly complexed. We observed the turbidity of the solution increase when the pH exceeded 2. According to Figure 2.2, rapid film deposition began about 30 s after the potential at the working electrode was set, followed by a linear increase in the areal mass, an increase in the density-modulus product, and a decrease in the phase angle. Assuming that the density of the deposited PEC layer in Figure 2.2 is about 1 g/cm^3 (a reasonable approximation for a highly hydrated film), an areal mass of 1200 mg/m^2 corresponds to a 1.2 μm thick film- a significant improvement over conventional layer-by-layer techniques considering the short time scale of this experiment.[70, 79, 92, 93] Polyelectrolyte multilayers typically grow via a slow initial "linear" regime followed by a faster "exponential" regime, and in certain cases can yield micron thick films within ~15 bilayers.[70, 79, 93] Each bilayer addition can take ~ 20 min when adsorption times and washing steps are considered. In our case, the multiple-step LbL process is simplified to a single continuous process with a faster and linear control over the thickness. The polyelectrolyte complex film was found to have a density- shear modulus product on the order of 10^7 Pa-g/cm^3 at 15 MHz (n=3) and

a viscoelastic phase angle at 15 MHz of about 50^{o}($\phi = 0$ for purely elastic materials and 90 for newtonian liquids). It is interesting that the film becomes more elastic as it increases in thickness, a phenomenon we attribute to the increasing polymer volume fraction in the film as it evolves.

These values compliment the low-frequency mechanical test results previously reported for polyelectrolyte multilayers. Han *et al.* performed AFM nanoindentation of the PAA/PAH system, reporting modulus values as a function pH and ionic strength on the order of megapascals.[94] Jaber *et al.* performed dynamic mechanical tests on the PDADMA/PSS system, with moduli on the order of few megapascals and phase angles between 10-40^{o}.[95, 96] The larger moduli and lower viscosities obtained in our experiments are consistent with the much higher frequency of the QCM measurement in comparison to traditional dynamic mechanical tests.[6, 95, 96, 97] Our modulus values also agree reasonably well with previously reported values for PAA/PAH multilayers using QCM-D.[92, 98] The magnitude of the complex viscosity at 15 MHz, which we refer to as η_3^*, provides a more straightforward comparison to the properties of the polyelectrolyte complex film in comparison to water. Water has a frequency-independent viscosity of $\approx$1 mPa-s $\left(10^{-3}\,\mathrm{Pa-s}\right)$ at room temperature. The magnitude of the complex viscosity of the films corresponding to Figure 2.2b are $\approx$ 200 times this value, assuming a film density of 1 g/cm^3.

Our ability to quantify mechanical properties of an adsorbed film with the QCM requires that measurable deviations from the Sauerbrey equation are observed. If a film is too thin it will fall under the Sauerbrey regime (Figure 2.5), where no information about viscoelastic properties can be obtained. The QCM is only sensitive to the mass loading here. For films of intermediate thicknesses, the mass loading, modulus and phase angle can be calculated by quantifying the deviation from the Sauerbrey regime.[39] This is the regime we operate in for the experiments in this chapter, and it is $\approx$ 600 - 2000 nm. While viscoelastic information can be obtained from thinner films[22, 92, 99], the inherent error in the properties extracted in this regime are much larger than in the thickness regime that we choose to analyze. Indeed, it is possible to deposit films much greater

than 1 μm using our electrochemical approach. However, for very thick films the crystal resonance is damped so strongly that it is no longer possible to obtain useful information with the QCM. It is still important to recognize that in almost all cases the Sauerbrey equation is still accurate to within 10 or 20 percent, provided that one is only interested in the film mass. This is illustrated in Figure 2.3a, where we plot the ratio of ρd obtained from the complete viscoelastic analysis to the value of ρd obtained from the Sauerbrey equation (eq 1.3). For sufficiently thick films the Sauerbrey equation will become quite inaccurate, since the frequency shift becomes independent of d when d is much larger than the decay length, δ. For our experiments the film thickness is always less than δ, as shown in Figure 2.3b. These values of δ were obtained from the values of ϕ_n and $\rho|G_n^*|$ obtained from our full viscoelastic solution. Our experiments are therefore being conducted in a thickness range where d is large enough so that values of the viscoelastic properties of the film can be obtained from the deviations to the Sauerbrey equation, but small enough so that measured frequency and dissipation shifts are sensitive to the total film mass.

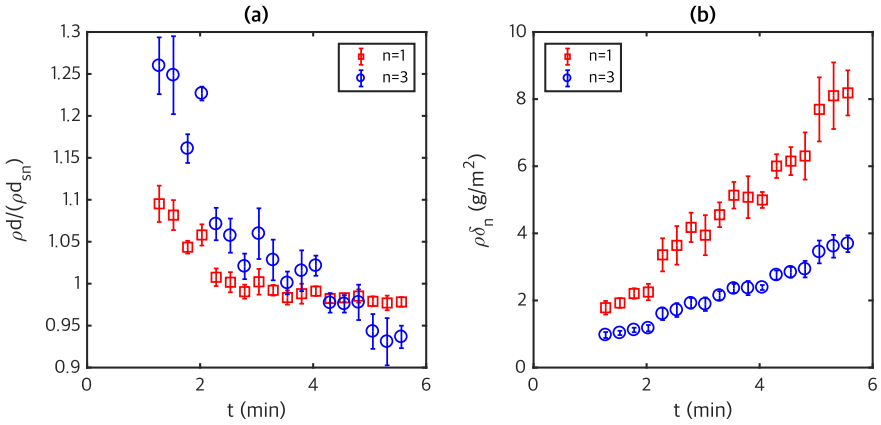

Figure 2.3: (a) Deviation from the Sauerbrey limit of the viscoelastic film and (b) the decay length (eq 2.7) of the shear wave as a function of time for the deposition outlined in Figure 2.2. The quantity $\rho d/(\rho d)_{sn}$ is the ratio of the areal mass obtained from solving eq 2.2 to that calculated from the experimentally measured frequency shift using eq 1.3. Error bars presented are the standard errors of three experiments. Note that 1 g/m^2 = 1 μm for ρ = 1 g/cm^3.

The voltammetry performed in Figure 2.1 provided an initial guess for setting the working elec-

trode potential, but we speculated that changing the potential would greatly affect the rate of mass deposition. To investigate this further, potential step tests were performed in which the potential at the working electrode was cycled between the open circuit potential (≈ 0.6 V) and the deposition potential (≈ -0.5 V). Figure 2.4a shows that there is a small delay (≈ 30 s) between the time when the potential is switched on and the time of mass increase. The mass continues to increase linearly while the potential is maintained, and spikes immediately as the potential is switched back to the open circuit potential. The spike in mass corresponded with a spike in the dissipation shift, suggesting that the film swelled before dissolving away at this low solution pH. This pH dependent swelling behavior of PAA/PAH has been documented previously for multilayers, and the electrodeposited films in this work appear to behave similarly.[100] Next, the potential was stepped from -0.35 V to -0.55 V in increments of -0.05 V, as shown in Figure 2.4b. We recorded negligible mass increase at -0.35 V, but the deposited mass scaled with the potential decrease thereafter. At the final potential of -0.55 V, we observed a mass increase followed by a quick decrease before swelling and dissolution (Figure 2.4d). A film could not be maintained at this potential without lowering the salt concentration, suggesting that there is a complex interplay between salt, potential and pH that determines film mechanical properties and stability. This coupling of process variables has been previously observed, although has not been fully explained. [80, 81] Determining the exact nature of this potential/salt based dissolution is beyond the scope of the current work, but we suspect that at lower potentials the pH in the vicinity of the electrode could become too basic such that PAH is significantly deprotonated and therefore a stable film cannot be formed.

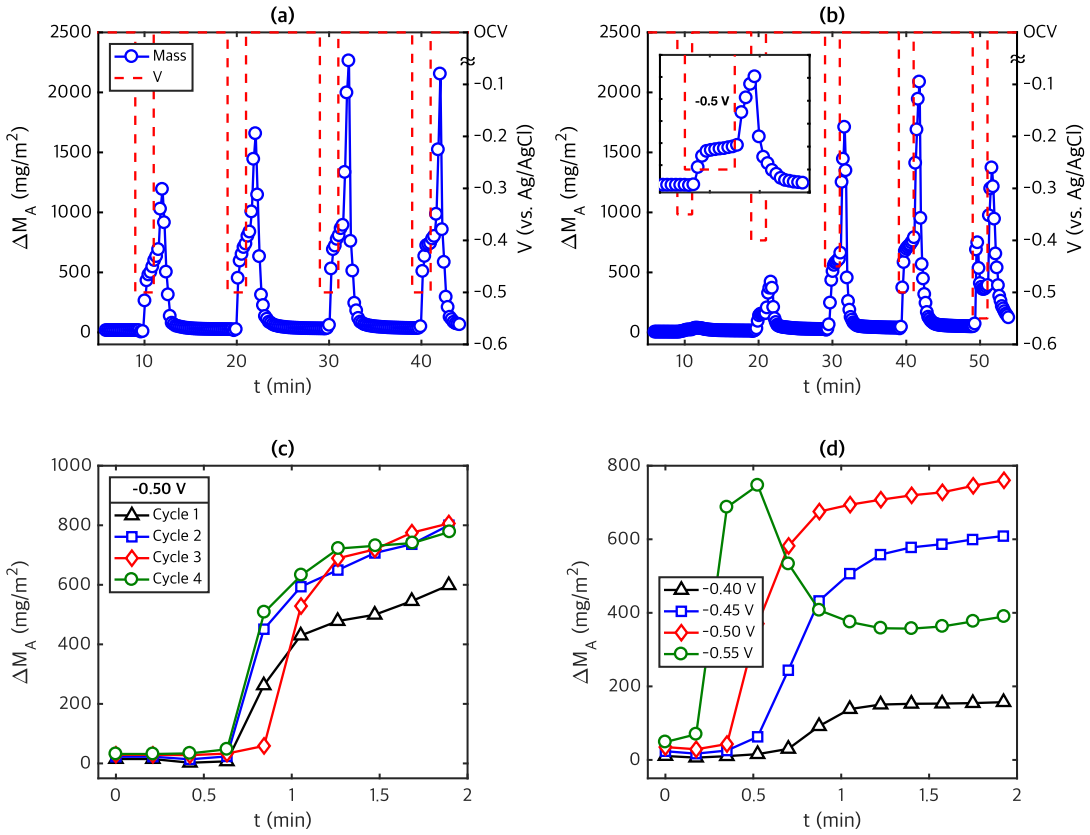

Figure 2.4: Potential step tests conducted in a solution of pH 1.95, 120 mM H_2O_2, 30 mM NaCl, 26.7 mM PAH and PAA each. Two minute potential steps were applied from the open circuit potential (OCV $\approx$ 0.6 V) to (a) -0.5 V, and (b) sequentially decreased from -0.35 V to -0.55 V at -0.05 V increments. (a) and (b) depict film deposition when the potential is switched on, followed by swelling and dissolution (see inset) when it is switched off. (c) Showing only the deposition while the potential is on from (a), and (d) showing the effect of the electrode potential on the deposition from (b). The mass reported here is the Sauerbrey mass (eq 1.3) calculated at the first harmonic, which is accurate to within 10% (Figure 2.3a).

2.3.3 Error Analysis

To solve eq 2.2 numerically, we first note that it is a function of ρd, d/λ_n and ϕ. Next, we define a harmonic ratio (r_h) and a dissipation ratio (r_d), which for the 1:3,3 calculation assumes

the following form:

$$r_h = \frac{\Delta f_3}{3\Delta f_1} = \frac{\text{real}(\Delta f_3^*/\Delta f_{s3})}{\text{real}(\Delta f_1^*/\Delta f_{s1})} \tag{2.13}$$

$$r_d = -\frac{\Delta \Gamma_3}{\Delta f_3} = -\frac{\text{imag}(\Delta f_3^*/\Delta f_{s3})}{\text{real}(\Delta f_3^*/\Delta f_{s3})} \tag{2.14}$$

Next, we redefine ρd with a modified form of the Sauerbrey eq:

$$\rho d = \frac{\Delta f_3 Z_q}{6 f_3^2} \text{real}\left[\frac{\Delta f_3^*(\phi_n, d/\lambda_3)}{\Delta f_{s3}}\right] \tag{2.15}$$

where Δf_3^* is given by eq 2.2. Finally, we assume $|G_n^*|$ has a power law dependence on the frequency, with same the phase angle at both n_1 and n_3. We previously demonstrated that the error due to this "constant phase angle approximation" is quite small.[24, 39] The power law frequency dependence and the constant phase angle approximation yield the following relationships:

$$|G_3^*|/|G_1^*| = 3^{\phi/90} \tag{2.16}$$

$$|D_3^*|/|D_1^*| = 3^{(1-\phi/180)} \tag{2.17}$$

Here, D_n^* is given by eq 2.4. When eq 2.17 is combined with eq 2.2, eqs 2.13-2.15 provide a system of equations that can be solved numerically to find self-consistent solutions for ϕ, d/λ_n and ρd. Eq 2.6 is then used to obtain $\rho|G_n^*|$ from d/λ_n.

Figure 2.5a,b plots the contour maps of eq 2.2 showing how Δf_3^* deviates from the Sauerbrey limit as a function of ϕ and d/λ_n at 15 MHz and time t = 3.5 min. The time point is highlighted in red in Figure 2.2, and the corresponding calculated solution is marked with a "+" in Figure 2.5. Figure 2.5b,c plots the change in r_h and r_d also as function of ϕ and d/λ_n. In the data presented in Figure 2.2, we typically observed a variation of about 3% between repetitions. The black solid lines overlayed on these plots show all potential solutions of r_h that are within 3% of

the calculated solution and the dashed lines outline all potential solutions within 3% of r_d. The region of intersection marks the unique solution to the system of equations. Furthermore, in the deposition experiment reported in Figure 2.2, the QCM is insensitive to the viscoelastic properties of the film until about 30 s. This is due to the fact that for very thin films, the Sauerbrey limit holds even for viscoelastic layers.[46] Figure 2.5a, graphically represents this phenomenon; very thin films ($d<<\lambda_n$) are in the Sauerbrey regime, where ($\Delta f_3/\Delta f_{s3} \approx 1$). Practically, we find that d/λ_3 must be larger than ≈ 0.05 for accurate property values to be obtained.

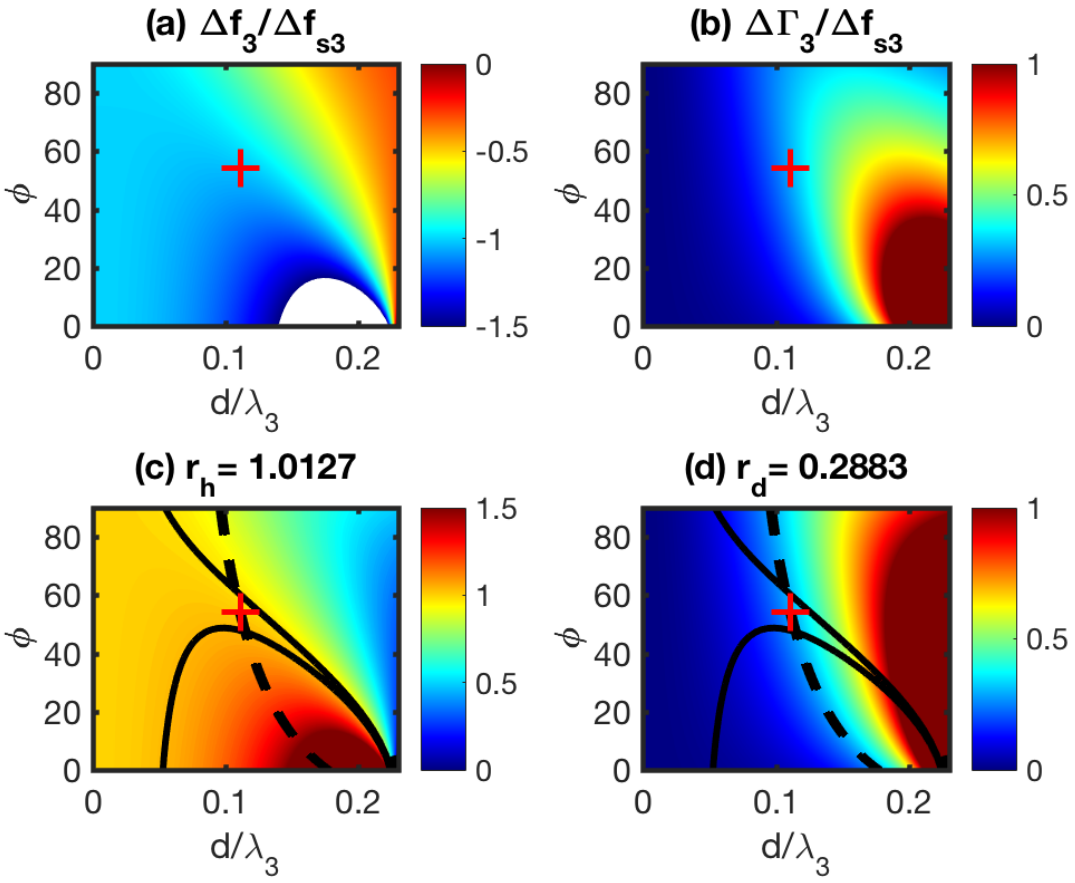

Figure 2.5: (a) $\Delta f_3/\Delta f_{s3}$ and (b) $\Delta\Gamma_3/\Delta f_{s3}$ as a function of ϕ and d/λ_3 as calculated from eq 2.2 for the indicated point at $t = 3.5$ min in Figure 2.2. (c) Variations in r_h and (d) r_d, also as a function of ϕ and d/λ_3. The solid black lines in (c) and (d) outline all possible combinations of ϕ and d/λ_3 that give a harmonic ratio within 3% of 1.01; the dashed lines outline all possible combinations that give a dissipation ratio within 3% of 0.29. The center of the intersection between these two regions is marked a "+" on all four plots and represents the solution to eqs 2.13-2.15 at t = 3.5 min of the film deposition.

2.3.4 Numerical Modeling and Acid-Base Titrations

Numerical modeling was performed to quantify the pH and hydrogen peroxide concentration at the electrode surface during the initial stages of film growth. Modeling was not performed beyond the initial period due to difficulties in quantifying diffusion through a polymer film that is growing as

a function of time. The aim of this portion of the study was to gain an intuition behind the rate of proton and hydrogen peroxide depletion at the electrode-electrolyte interface. The current density at the working electrode boundary was specified to be the current measured from the experiment presented in Figure 2.2. Figure 2.6 plots the surface pH and peroxide concentration as a function of time after a step change in the electrode potential from open circuit to -0.5 V. During film deposition, a significant shift in the quartz resonant frequency was not observed until $\approx$ 30 s after the potential was switched on. This delay in response is arguably due to the time required to raise the pH sufficiently to precipitate out a polyelectrolyte complex. Our model suggests that the pH increases about one unit within the first few seconds, corresponding with a drop in the local peroxide concentration, as shown in Figure 2.6.

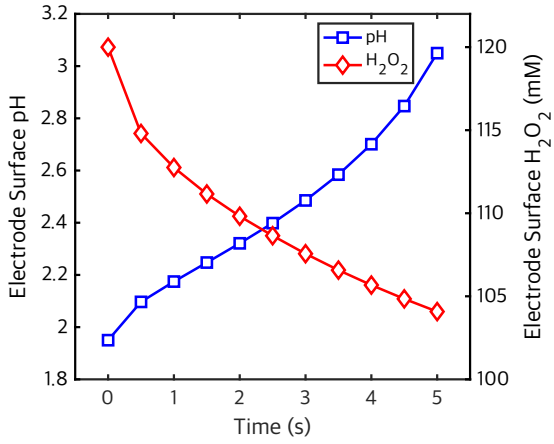

Figure 2.6: Numerical modeling results displaying the pH evolution and hydrogen peroxide depletion at the electrode-electrolyte interface, i.e., at a distance x=0 from the electrode. Solution conditions used as model inputs are reported in Table 2.1.

A change in pH would result in a change in the degree of ionization (α) of PAA and PAH, thus causing a time dependent complexation at the electrode-electrolyte interface. The extent of complexation depends on the relative degrees of ionization of each polymer chain. To calculate α as a function of pH, acid-base titrations were conducted to determine the fraction of protonated monomer units (f_p) for each polymer. 'Solvent' solutions were prepared with 30 mM NaCl, while

the 'PAH' and 'PAA' solutions contained 0.250% and 0.192% (w/v) (26.7 mM), respectively. No solutions contained hydrogen peroxide. After raising the pH of the solutions to 12 using NaOH, HCl was added in increments while a pH meter simultaneously measured the solution pH. The fraction of protonated amine/acid groups, f_p, at each incremental addition of HCl was determined by:

$$f_p = \frac{10^{-pH_s} - 10^{-pH_p}}{[Monomer]_{tot}} \tag{2.18}$$

where pH_p and pH_s are the pH values of the solutions with and without any polymer, respectively. $[Monomer]_{tot}$ is the total molar concentration of protonizable amine/acid functional groups, determined from the dissolved polymer concentration. For PAH, α is simply equal to f_p, while for PAA it is equal to (1-f_p). Figure 2.7a and b plots the titration curves for the solution, PAH and PAA, and Figure 2.7c displays α as a function of pH. We observed a pK_a of about 5.5 for PAA and 8.8 for PAH under the low salt conditions used in this work, similar to previously reported literature values.[101, 102]

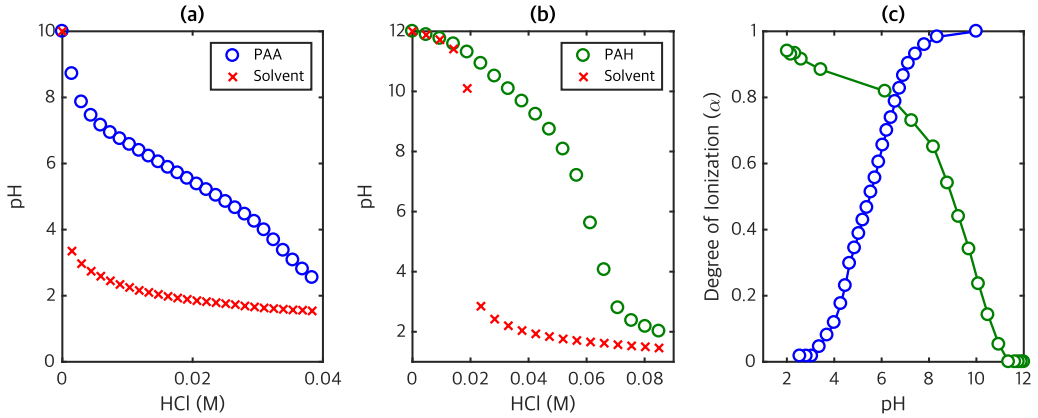

Figure 2.7: Titration curves for 26.7 mM (a) PAA and (b) PAH dissolved in 30 mM NaCl. The blank "solvent" consisted of just 30 mM NaCl in deionized water. (c) The degree of ionization as a function of pH for PAA and PAH as calculated from eq 2.18.

At pH 2, PAH was found to be about 96% charged at this concentration while PAA was completely uncharged. According to the modeling results, the electrode surface pH is about 3 after 5 s,

which corresponds to PAA and PAH being roughly charged at 2% and 92%, respectively, according to the titration of the individual polymers. The situation is markedly different when both PAA and PAH are present together at this pH. The presence of fully charged PAH effectively increases the solubility of PAA by shifting the equilibrium towards ion pairing. PAA is thereby deprotonated at a lower pH than what one would expect from the degree of ionization behavior of PAA individually. We used dynamic light scattering to monitor the hydrodynamic radii of PAA, PAH and their complexes as a function of pH as listed in Table 2.2, and observed that significant aggregates formed at pHs as low as 2.1. We report the Z-average radius and the peak of the volume percent vs. size distribution (R_v). As expected, both of these metrics of the complex size appeared to increase with pH.

Table 2.2: Hydrodynamic radii of PAH, PAA, and the PAA/PAH complex at different pH. The concentration of each polymer was 26.7 mM, and the NaCl concentration was 30 mM. The error reported is one standard deviation of four measurements.

System	**pH**	**R_v(nm)**	**Z-avg. Radius (nm)**
PAH	2.0	5.4±0.4	40±5
PAA	2.0	28±5.6	110±30
PAA/PAH	1.9	15±3.0	112±15
PAA/PAH	2.0	28±4.0	152±12
PAA/PAH	2.1	59±9.0	192±18
PAA/PAH	2.2	85±24	151±21

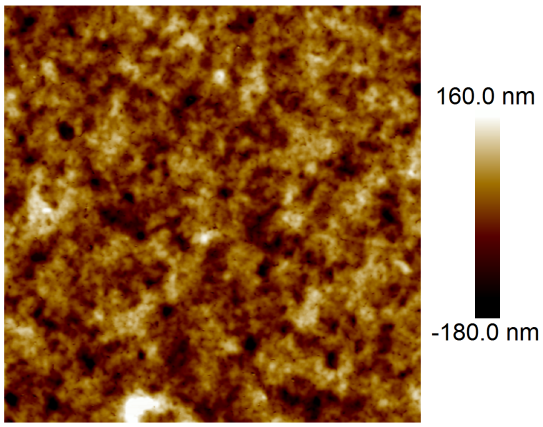

Figure 2.8: AFM image of a dried electrodeposited PEC film prepared with the same conditions outlined in Figure 2.2. The scan area was 25 by 25 μm with a root-mean-square roughness of 50 nm. The dry average thickness of the film from five measurements was determined to be 750 $\pm$ 50 nm using profilometry.

2.3.5 Film Morphology

The pH is known to strongly affect the morphology of PAA/PAH multilayers even when exposed to acidic conditions for short period of times [100]. What could be the structure of rapidly electrodeposited PAA/PAH films using a time-dependent pH gradient? Under the low salt conditions utilized in this work it is possible that the complex size indicated by R_v in Table 2.2 are nano-precipitates rather than coacervate-like phases, which would suggest a mechanism of precipitation in solution followed by nucleation at the electrode. Cho *et al.* reported that LbL films exhibited morphological changes under potential biases (4.0 V vs. Ag/AgCl) resulting from the local pH change and water oxidation.[73] These films showed changing porosity and roughness based on the duration of the applied potential, with the root-mean-square (RMS) roughness becoming as high as 90 nm. Since we electrodeposit PEC films under mild reducing potentials, we do not expect gas bubble induced porosity or roughness in our films. However, if the mechanism of deposition is precipitation in solution followed by adsorption to the surface, it could be a source of porosity and roughness. Figure 2.8 shows an AFM image of a dried electrodeposited PEC film

taken out of solution immediately after deposition. This film possessed a RMS roughness of 49 nm and an assortment of pore-like structures. While a more detailed investigation of film morphology based on the processing parameters is currently underway in our lab, we can offer a qualitative explanation: since the deposition rate of our films are quite fast, highly non-equilibrium structures are formed that are essentially frozen. Carefully controlling the rate of deposition may result in smoother films. Annealing in subsequent salt solutions could also swell and smooth these films.

2.4 Conclusion

In this work, a facile electrochemical deposition technique was developed for rapidly depositing a polyelectrolyte complex (PEC) film at the electrode of an electrochemical quartz crystal microbalance (EQCM) by exploiting the reduction of hydrogen peroxide to trigger the pH responsive self-assembly of PAH and PAA. This approach yielded thick PEC films ($1\mu m$) within short experimental time scales (5 min). It was demonstrated that hydrogen peroxide is an ideal molecule for inducing the pH gradient due to its simple chemistry, moderate reduction potential, and absence of a gaseous product. The EQCM was used to quantify the *in-situ* viscoelastic properties of a PEC film by observing the deviation in the complex frequency shift from the Sauerbrey prediction. Using this approach, the areal mass (ρd), the density-modulus product ($\rho|G_n^*|$) and the viscoelastic phase angle (ϕ) was determined as a function of time during electrodeposition. Our calculation indicates that the film that forms at the working electrode has a phase angle of about 50^o and a density-modulus product of around 10^7 Pa-g/cm^3 at 15 MHz and after five minutes of deposition. Finally, we presented finite element modeling results to guide the intuition behind the time evolution of the pH gradient at the electrode surface, showing that the pH rises by one unit within the first 5 s of deposition, with a complimentary drop in the hydrogen peroxide concentration.

Chapter 3

Influence of Hydrophobicity on Polyelectrolyte Complexation

Abstract: Polyelectrolyte complexes are a fascinating class of soft materials that can span the full spectrum of mechanical properties from low viscosity fluids to glassy solids. This spectrum can be accessed by modulating the extent of electrostatic association in these complexes. However, to realize the full potential of polyelectrolyte complexes as functional materials their molecular level details need to be clearly correlated with their mechanical response. The present work demonstrates that by making simple amendments to the chain architecture it is possible to affect the salt responsiveness of polyelectrolyte complexes in a systematic manner. This is achieved by quaternizing poly(4-vinylpyridine) (QVP) with methyl, ethyl and propyl substituents– thereby increasing the hydrophobicity with increasing side chain length– and complexing them with a common anionic polyelectrolyte, poly(styrene sulfonate). The mechanical behavior of these complexes is compared to the more hydrophilic system of poly(styrene sulfonate) and poly(diallyldimethylammonium) by quantifying the swelling behavior in response to salt stimuli. More hydrophobic complexes are found to be more salt resistant, yet the mechanical properties of the complex remain contingent on the water content and overall swelling ratio of the complex itself, following near universal

swelling-modulus master curves that are quantified in this work. The rheological behavior of QVP complex coacervates are found to be approximately the same, only requiring higher salt concentrations to overcome strong hydrophobic interactions, demonstrating that hydrophobicity can be used as an important parameter for tuning the stability of polyelectrolyte complexes in general, while still preserving the ability to be processed "saloplastically". This work partially appears in *Macromolecules* 2017, 50, 23, 9417-9426.

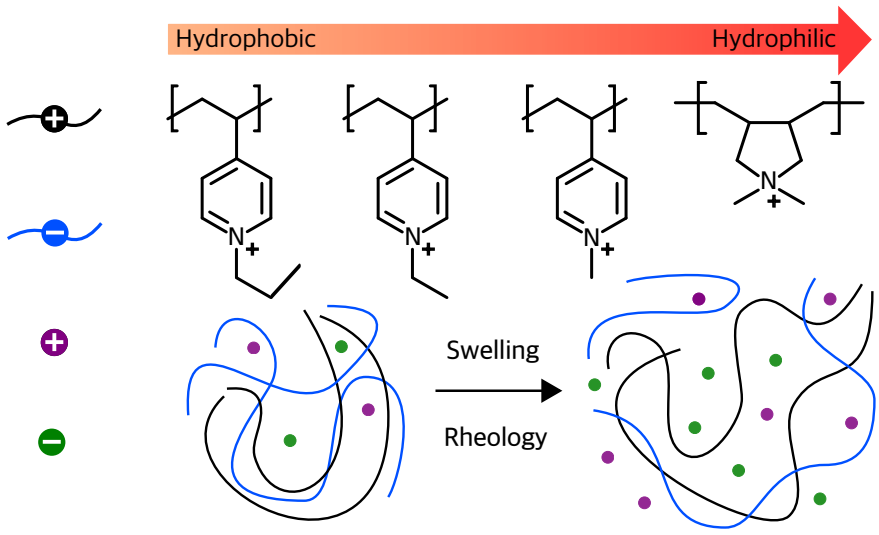

3.1 Introduction

The associative behavior of oppositely charged polyelectrolytes is a phenomenon relevant to many biological processes as well as many synthetic applications. In complex biomacromolecules, the details of the charge distribution, hydrophobic moieties and steric effects dictate the shape, conformation and ultimately the function of those molecules.[103, 104] In synthetic applications, the polyelectrolyte complexes can be engineered to form micelles[105], gels[106, 107],

and coatings.[58] In all of these contexts, the dynamic ionic bonds formed between oppositely charged ions help dictate the responsiveness and properties of the final material. These dynamic bonds impart a continuum of properties to polyelectrolyte complexes (PECs), which can be accessed by controlling the extent of electrostatic association in the system.[6] While the effects of pH and salt on the responsiveness of PECs are becoming better understood, the effects of hydrophobicity and chain architecture remain more open questions.[108]

In the present work, we utilize a series of quaternized poly(4-vinylpyridines) (QVPs) to build a spectrum of hydrophobic polyelectrolytes and study their mechanical properties in terms of their salt responsiveness. The addition of methylene groups to the side chain of QVP tunes its hydrophobicity, and is therefore expected to affect the salt responsiveness of the materials.[109, 110] However, it is unclear how *differential* changes in hydrophobicity, which is often nebulously defined, would affect the *differential* mechanical response of PECs, both in the low salt regime where doped solid-like complexes form, and in the high salt regime where coacervate phases form. Further complications arise from the fact that the method of determining mechanical responses for the solid complexes and coacervates are often quite different. For example, when complexes are formed in the thin film format such as in layer-by-layer assemblies, nano/micro-indentation and dynamic mechanical analysis may be the choice of mechanical analysis.[94, 95] When complex coacervates are concerned, the mechanical analysis of choice is almost always traditional cone-plate rheology.[3, 97, 111] Each of these techniques has its own advantages and disadvantages, and the data obtained from these separate techniques must be compared with caution, even when the same material system is being investigated.

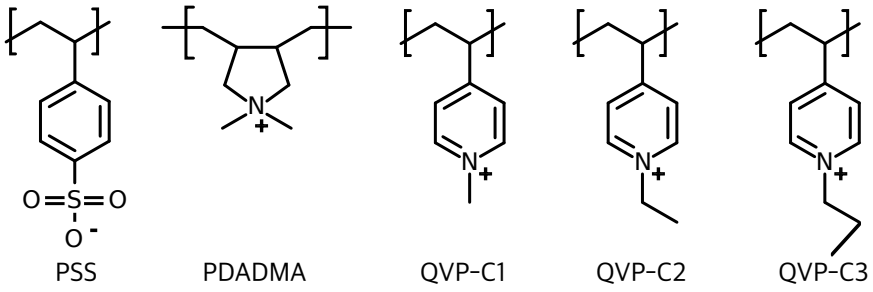

Figure 3.1: Structures and designations of the polyelectrolytes in this work.

In a series in insightful works, Schlenoff and coworkers have demonstrated that salt induced breakage of ion-pairs in PECs can be used for "saloplastic" processing, and that coacervation spans a continuous bridge between doped solids and single phase solutions.[6] It is desirable to quantify this spectrum of mechanical properties of PECs on a single characterization platform so that changes in viscoelasticity between the coacervate and solid complex of the same material may be directly comparable. We have recently developed the analysis required to obtain accurate viscoelastic information using the quartz crystal microbalance (QCM), and have demonstrated its versatility as a high frequency rheometer in several contexts such as electrodeposition[13], corrosion[24] and curing of thermosets.[36, 41] The great utility of the QCM lies in its ability to quantify the fixed frequency (15 MHz in the present work) mechanical response of both thin films deposited on the quartz crystal surface, as well as of any viscous medium in which the crystal is immersed. This versatility makes the QCM a unique platform capable of quantifying the *mechanical spectrum* associated with the continuous transitions of PECs. Additionally, QCM experiments with a complete viscoelastic analysis of the frequency and dissipation shifts allow the most accurate measure of swelling behavior of homogeneous thin films. However, the QCM provides only the single high frequency response of the material, and so the low frequency (0.1-300 rads s^{-1}) tests of more traditional cone-plate rheology are needed to build a picture of the dynamic mechanical behavior.[97, 111]

In this work we aim to develop a unifying mechanical picture of PECs spanning the entire

spectrum of their mechanical response, from solid-like complexes to low viscosity coacervates, and encompassing polyelectrolyte hydrophobicity and salt hydration effects. We first quantify the swelling and mechanical behavior of PSS:PDADMA, which is the most hydrophilic pair in Figure 3.1. The mechanical response is characterized in terms of the effectiveness of salt identity in swelling thin films of PSS:PDADMA, resulting in well-defined swelling-modulus master curves that appear to be universal for the specific set of cationic and anionic polyelectrolyte of interest. Next we complex QVP with varying alkyl side chain lengths with PSS and measure their swelling, modulus and viscoelastic phase angle in response to added KBr, and draw a comparison to PSS:PDADMA. We explore the dynamic response of PSS:QVP coacervates using cone-plate rheology, and quantify their power-law frequency response and relaxation spectra.

3.2 Results & Discussion

When two oppositely charged polyelectrolytes are mixed, the driving force for complexation is almost purely entropy driven due to counter ion release.[112] These complexes remain stable until addition of externally added salt breaks ion pairs, increasing the screening between polyelectrolyte chains. Spruijt *et al.* drew the analogy between salt and temperature, arguing that addition of salt increases the mobility of chains inside a complex.[113] This concept was further used to introduce "saloplastic" processing of PECs[6, 66, 114], analogous to thermoplastic processing of glassy homopolymers. While thermal transformations in PECs can be distinct[115], the saloplastic transition from solid complex to coacervate to single phase solution is a spectrum where a continuous change in physical properties is observed as the salt concentration is increased.[6] The question then naturally arises about what the associated change in physical properties is of the polyelectrolyte complex continuum. As indicated earlier, the QCM is uniquely suited for quantifying mechanical properties of viscous solutions and viscoelastic solids, as schematically shown in Figure 3.2.

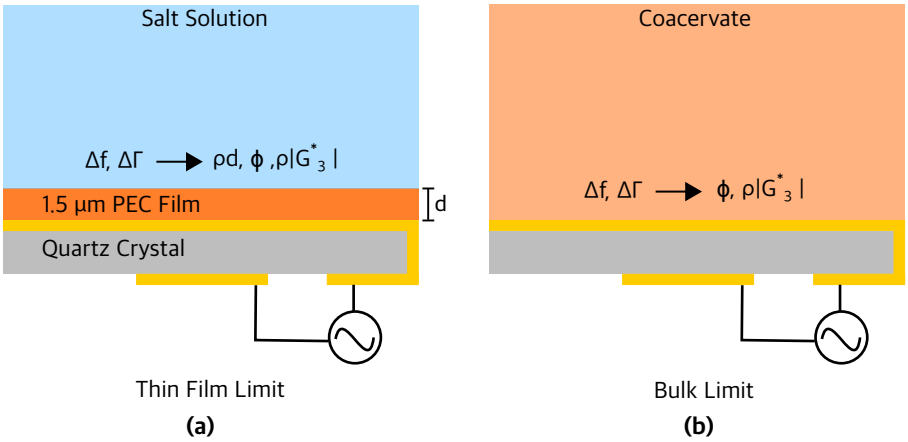

Figure 3.2: (a) The Thin Film Limit of the QCM allows measurement of the areal mass (ρd), density-shear modulus product ($\rho|G_3^*|$) and the phase angle (ϕ) of a deposited film from the experimentally measured frequency (Δf) and dissipation shifts ($\Delta\Gamma$). (b) The Bulk Limit provides the $\rho|G_3^*|$ and ϕ of the viscous medium in which the crystal is immersed (Eqs. 1.5 and 1.6). The subscript 3 refers to the third crystal harmonic corresponding to a frequency of 15 MHz.

For thin *rigid* films, the well known Sauerbrey equation provides a very accurate measurement of the areal mass, $d\rho$, where d is the film thickness and ρ is its density.[24] For thin *viscoelastic* films applied at the crystal surface, a measurable deviation from the Sauerbrey equation occurs which can be used to quantify the film's $\rho|G^*|$ and ϕ in addition to its $d\rho$. While the full mathematical description of the Thin Film Limit is not as simple as that of the Bulk Limit, we have detailed this approach in Chapter 1. If the film is immersed in water, the physical properties of the layer can be observed as a function of external stimuli such as ionic strength, pH, temperature and etc. Therefore, the Thin Film Limit proves to be exceptionally valuable for studying the salt responsive mechanics of PEC films as their swelling behavior can be directly quantified along with the modulus and phase angle. We define the percent swelling in terms of $d\rho$ using eq 3.1:

$$Swelling\,\% = \frac{Weight_{water}}{Weight_{polymer}} \times 100 = \frac{d\rho - (d\rho)_{dry}}{(d\rho)_{dry}} \times 100 \tag{3.1}$$

Here, $(d\rho)_{dry}$ is the areal mass of the PEC film after equilibration over drierite in an enclosed

environment, which extracts almost all water molecules from the film.

3.2.1 Mechanical Behavior of PSS:PDADMA Complexes

Figure 3.3 presents the mechanical spectrum associated with exposing stoichiometric PECs of PSS:PDADMA to KBr. Under low salt (<1.0 M) conditions, the properties of the complex are dominated by salt doping, which also increases the water content within the complex. Here, both salt and water can be thought of as plasticizers to an initially glassy material. As salt concentration increases, the PEC becomes more viscoelastic, until a clear coacervate phase forms with ϕ between 50° and 85°. This complex to coacervate transition was recently reported as a gelation phenomenon.[3] Addition of more salt results in dissolution of the coacervate into a single phase solution with properties very close to that of water itself.

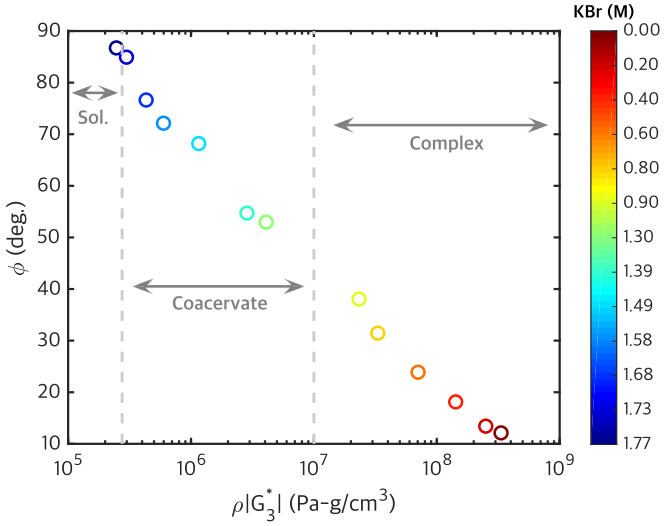

Figure 3.3: The mechanical spectrum of PSS:PDADMA complex as a function of salt concentration. The QCM was used to elucidate the continuous transition from complex to coacervate to a single phase solution at 15 MHz. Note that in this MHz regime, water has a $\rho|G^*|$ of 10^5 Pa-g/cm^3 and ϕ of 90°. Purely glassy films have $\rho|G^*| \approx 10^9$ and $\phi < 10°$.

KBr is known to be one of the most effective salts in breaking up ion pairs in PECs. Salt identity has a significant effect on its PEC doping capacity, with strongly hydrated salts interacting

more weakly with PECs. For applications of PECs as membranes, it is of interest to know how the physical properties of the complex changes with respect to salt identity. In other words, what is the stability of PECs against different salt solutions? To investigate this question we exposed PSS:PDADMA films to salt solutions with varying ionic strengths and salt identity as shown in Figure 3.4. The limit of 1 M ionic strength is appropriate here since all data points can be considered to fall in the solid-like regime. Significant loss of mechanical function occurs for PEC films exposed to KBr concentrations above 0.5 M, while LiCl and $CaCl_2$ only have a marginal effect on the mechanical stability of PSS:PDADMA in this salt range. These trends follow the electronegativity of the salts, which is closely related to their hydration.[116] At higher concentrations, all salts weaken PECs.

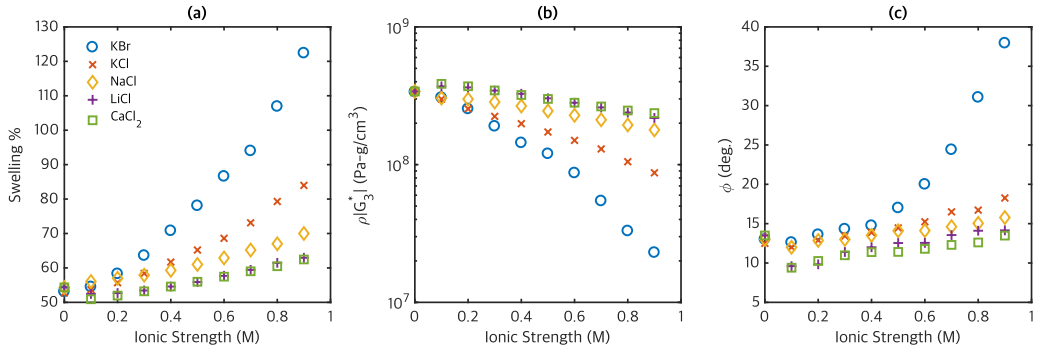

Figure 3.4: (a) Swelling behavior (b) density-shear modulus and (c) viscoelastic phase angle as a function of ionic strength and salt identity for spin-coated PSS:PDADMA films. Swelling % is calculated in reference to the dry PEC film. $\approx 1\mu m$ PEC films were spun-cast from an equilibrated coacervate of PSS:QVP-C2 directly on to the quartz crystal for measurements.[2] For reference, polymer glasses have a shear modulus of $\approx 2 \times 10^9$ Pa and a $\phi \approx 1^o$ at this frequency (15 MHz), and $G^* = G' + iG''$ and $\phi = \arctan(G''/G')$ as usual.

Figure 3.4 initially suggests that salt identity plays a critical role in determining the mechanics of PECs. However, plotting $\rho|G_3^*|$ and ϕ against the swelling % of the complex (Figure 3.5) leads to an insightful conclusion: it is the overall swelling of the the complex that determines its mechanical behavior and not the identity of the salt used to swell it. Changing the salt identity only allows movement along the same master curve, both for the modulus and the phase angle. Higher

concentrations of strongly hydrated salts are needed to swell the complex to the same degree that can be achieved via a weakly hydrated salt at lower concentrations. The fact that PECs follow well defined master curves suggests that ultimately it is the amount of water inside the complex that determines the overall mechanical behavior, and that the properties of the complex can be further tuned by controlling the hydrophobicity of the polyelectrolytes used to make the complex.

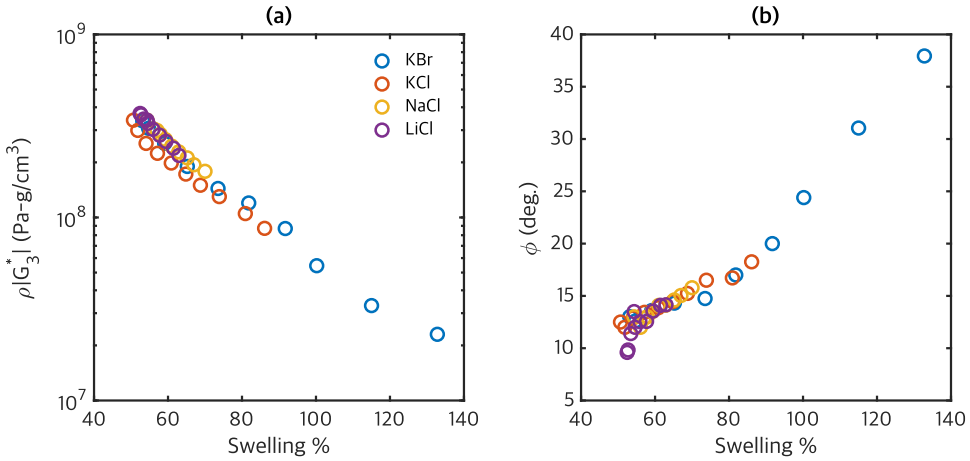

Figure 3.5: (a) Swelling-modulus and (b) swelling-phase angle master curves for PSS:PDADMA films in salt solutions of up to 1.0 M.

3.2.2 Mechanical Behavior of PSS:QVP-C1, C2 & C3 Complexes

QVPs are interesting strong cationic polyelectrolytes due to their versatility, chief among which is the ability to easily vary the quaternizing substituent. Poly(4-vinylpyridine) is known to exhibit a strong hydrophobic to hydrophilic transition based on pH, which can be exploited to achieve novel swelling behavior.[117] Partial quaternization can be used to precisely control the pH independent charge density, while preserving some of the hydrophobic and pH responsive pyridine units as additional tuning parameters.[118] Yet given such immense versatility and control over structure and function, QVPs have been understudied as components in polyelectrolyte complexes, and even in layer-by-layer assemblies. In some ways, QVPs may be considered a more natural cationic polyelectrolyte for complexing with PSS than PDADMA, given the similarity of their structure. Addi-

tionally, the mismatch of the repeat unit size that exists for PSS:PDADMA is avoided for PSS:QVP complexes. However, PSS:PDADMA remains one of the most easily processable combination of polyelectrolytes, and serves as a good model system for many fundamental investigations.[6, 112] In our work, PSS:PDADMA serves as the hydrophilic pair to which more hydrophobic combinations can be compared. Figure 3.6 compares the swelling behavior of increasingly hydrophobic complexes with response to the common salt of KBr.

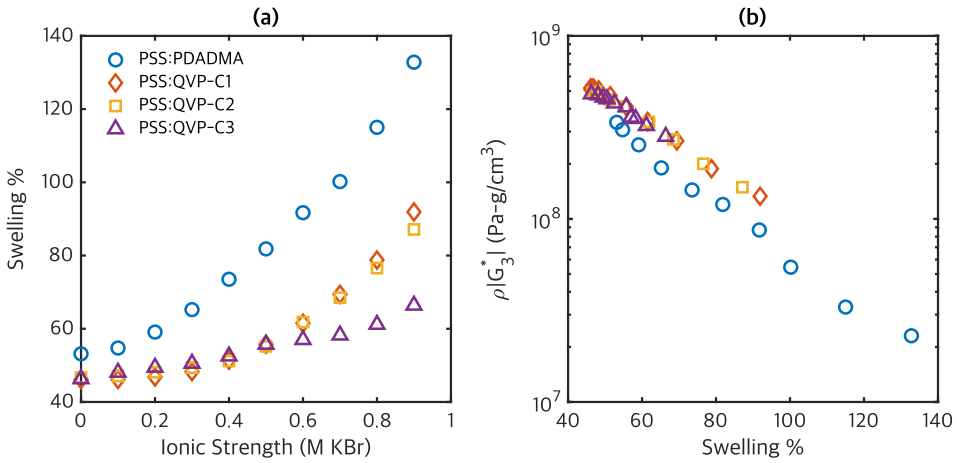

Figure 3.6: (a) The swelling behavior of QVP complexes in comparison to PSS:PDADMA as a function of KBr ionic strength. (b) Swelling-modulus master curves for both PSS:PDADMA and PSS:QVP complexes. Error in the measurements are on the order of the size of the symbols used.

Upon immersion in water, all complexes swell about 50% compared to their dry state, corresponding to approximately 8 water molecules per ion pair in the complex. While it is well known that 8 water molecules associate to PSS:PDADMA upon immersion in water[6, 109], the fact that PSS:QVPs also exhibit the same behavior hints that in the absence of salt the swelling behavior is determined by the hydration of the ions within the complex. Since the identity of the charged groups do not change in these complexes, it is reasonable to expect this behavior. The effect of hydrophobicity within the salt range explored becomes more pronounced at higher ionic strengths, where there is a significant difference between PSS:PDADMA and PSS:QVP-C3. C1 and C2 remain closely matched, only appearing to deviate at the highest salt concentration. This behavior

suggests that the effect of adding methylene groups on the QVP side chain on the mechanical behavior is not linear; the differential change in mechanical properties increase with increasing hydrophobicity. Further insights can be gleaned from constructing swelling modulus master curves. It is clear from Figure 3.6b that changing the side chain length does not change the modulus-swelling behavior, and only affects how much of the master curve is accessible for a given concentration of salt. Furthermore, the effect of hydrophobicity may be directly compared to the response of PECs to salt identity. Just like changing salt identity only affects the extent of movement along the same master curve, changing the hydrophobicity of the complex has the same effect. It is the overall swelling ratio that ultimately determines properties, which posits the idea that by tuning the swelling behavior (using hydrophobicity or otherwise) it is possible to engineer the stability of these complexes over a wide range.

Figure 3.6b also shows that the master curves for PSS:PDADMA and PSS:QVP, while similar, are not the same. PSS:PDADMA appears to have a more negative slope than PSS:QVP, a difference that is significant but not large. We suspect that this subtle difference arises from the mismatch in repeat unit sizes between PSS and PDADMA, but could also be from other detailed effects such as the complex's exact glass transition temperature, chain flexibility, or complex non-stoichiometry.

Thus far in our discussion the QCM has proved to be a uniquely suitable instrument for studying the detailed mechanics of PECs. However, due to its fixed frequency it cannot probe the dynamic behavior of PECs, for which traditional cone-plate rheology is appropriate. Since more hydrophobic complexes are more difficult to dope, the salt concentrations over which coacervates form move toward higher salt conditions. Figure 3.7 illustrates this phenomenon using frequency sweeps on coacervates of PSS:QVP-C1, C2 and C3, each with three salt concentrations such that time-salt superposition[113] may be used to elucidate the mechanical response over a larger frequency domain. It is qualitatively evident that the same rheological behavior is observed, only at higher salt concentrations following the trend in hydrophobicity of the PECs. The non-linear ef-

fect of hydrophobicity is evident once again in the salt concentration dependent shift factors which move to higher ionic strengths.

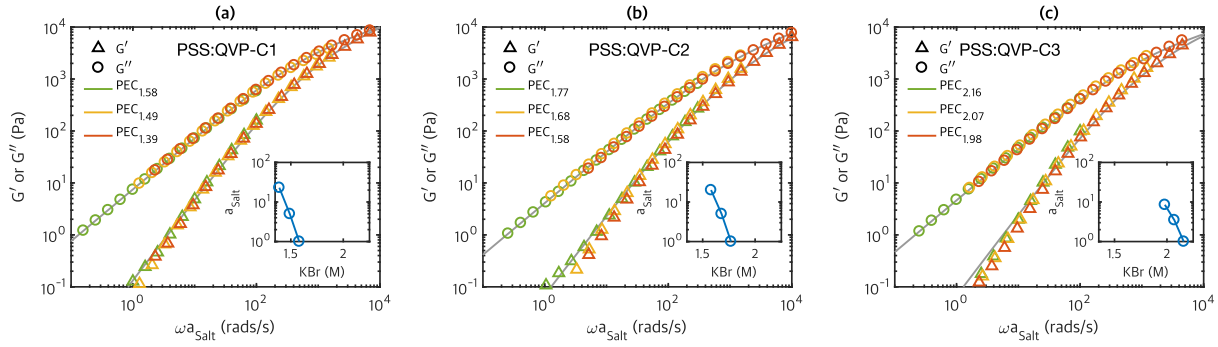

Figure 3.7: Time-Salt Superposition of frequency sweeps at 20 °C of (a) PSS:QVP-C1, (b) PSS:QVP-C2 and (c) PSS:QVP-C3. The designation of PEC_x corresponds to formulations provided in Table 3.2, where x is the molar KBr concentration. Curves are shifted with respect to the highest salt concentration in each case. Solid gray lines correspond to fits of Eq. 3.7 for calculating β and τ_{ref}. Note that no vertical shifting was done since the polymer concentration in these complexes do not vary significantly.[3]

Figure 3.7 demonstrates that PSS:QVP complexes behave like liquids at high salt concentrations and low frequencies, and appear to approach a power-law behavior at low salts and high frequencies. Similar behavior has been previously reported for a variety of polyelectrolyte systems.[3, 97, 111] Since coacervates of strong polyelectrolytes formed at low salt concentrations take several months to equilibrate, it is very difficult to obtain higher frequency response using time-salt superposition as done in Figure 3.7. However, by taking a low salt concentration coacervate and performing a time-temperature superposition it is possible to probe the higher frequency response. Figure 3.8 verifies that the coacervates do assume a power-law behavior at higher frequencies. We fit the temperature shift factors to the Vogel-Fulcher-Tammann form (Eq. 3.2), and find the values of B = 290 °C and $T_\infty = -65$ °C. We now quantify the power-law behavior of complex coacervates in the following section.

$$log(a_T) = \frac{-B}{T_{ref} - T_\infty} + \frac{B}{T - T_\infty} \tag{3.2}$$

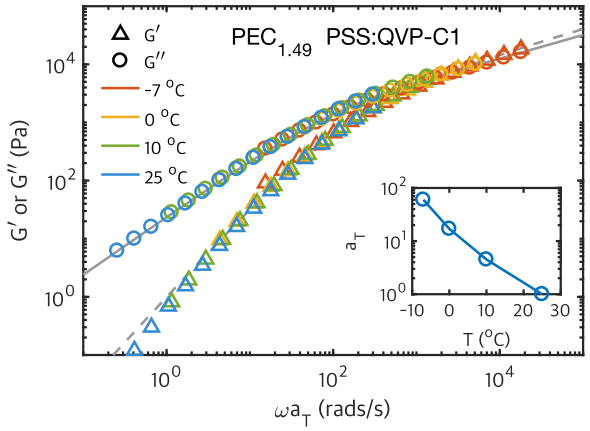

Figure 3.8: Time-Temperature Superposition of PSS:QVP-C1 formed at a KBr concentration of 1.49 M. The lowest temperature of -7 °C could be measured before the onset of freezing effects. Gray lines correspond to fits of Eq. 3.7 for calculating β and τ_{ref}. Shift factors were fitted to the Vogel-Fulcher-Tammann form (Eq. 3.2) of the WLF relation, giving B = 290 °C and $T_\infty = -65$ °C.

3.2.3 Power-law Rheology & Relaxation Spectrum

A single Maxwell element has a spring of modulus, E, in series with a viscous element (viscosity, η) as shown in Figure 3.9a. The complex dynamic modulus for a Maxwell element is given by the following expression:

$$E^*(\omega) = \frac{Ei\omega\tau}{1+i\omega\tau} \tag{3.3}$$

where $\tau \equiv \eta/E$ is the relaxation timescale of the model. As demonstrated in Figure 3.8, the PECs of PSS:QVP approach a distinct power-law behavior. Such behavior is poorly described by Maxwell elements, or generalized Maxwell models, which often require a large number of mechanical elements to capture the material behavior. Spring-pots (Figure 3.9b), which are power-law elements with a constant phase angle, offer a more natural description of power-law like rheological behavior.[119, 120] Additionally, the Rouse theory for dilute polymer solutions can be reduced

to a form where the total stress is contingent on the fractional half-derivative of the polymer contribution in terms of strain history.[121] Thus, the Rouse theory itself provides a basis for considering spring-pot elements to describe viscoelasticity. The spring-pot corresponds to an element with the following frequency- dependent complex modulus:

$$E^* = E^s(i\omega/\omega_o)^\alpha \tag{3.4}$$

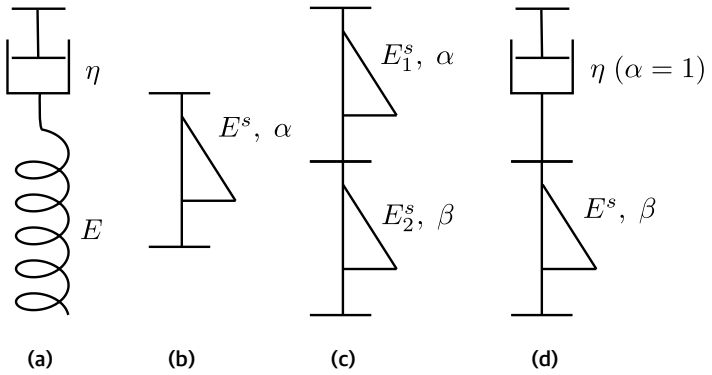

Figure 3.9: (a) A Maxwell element, (b) a spring-pot element, (c) two spring-pot elements in series (fractional Maxwell model[**?**]) with power-law exponents of α and β, and (d) a purely viscous dashpot in series with a spring-pot (fractional Maxwell liquid).

The properties of a spring-pot are quantified by two independent parameters. One of these is the power law exponent, α. This quantity is the order of the fractional derivative in the corresponding constitutive equation and can be thought of as a bridge between a completely viscous dashpot ($\alpha = 1$) and an elastic spring ($\alpha = 0$).[119] The second property of the spring-pot is a parameter (a *quasi-property*[119]) giving the magnitude of the modulus. There are a couple of ways to specify this quantity. Perhaps the most straightforward way is to consider the product $E^s\omega_o^{-\alpha}$, but this quantity has units of a stress multiplied by a fractional power of time. Instead, we specify E^s, which corresponds to $|E^*|$ at a reference frequency, ω_o. If two spring-pots are in series with one another, as shown in Figure 3.9c, a *fractional Maxwell model* is formed, as referred to by Jaishankar and McKinley.[119] The Maxwell model of Figure 3.9a is a specific version of the more general

fractional Maxwell model, with $\alpha = 1$ and $\beta = 0$.

We use a simplified form of the fractional Maxwell model to describe our polyelectrolyte complexes. In this model, which we refer to as a *fractional Maxwell liquid* (Figure 3.9d) one of the spring-pots gives a purely viscous response, *i.e.,* $\alpha = 1$. Summing the compliances of each unit we have:

$$\frac{1}{E^*} = \frac{1}{E^s(i\omega/\omega_o)^\beta} + \frac{1}{i\omega\eta} \tag{3.5}$$

ω_o may be defined as any frequency of interest, but we define it analogously to that of the Maxwell model, *i.e.* the frequency where the magnitudes of the two terms on the right hand side of Eq. 3.5 are equal to one another:

$$\omega_o = \frac{E^s}{\eta} = \frac{1}{\tau} \tag{3.6}$$

The last two equations can be used to derive an expression for the normalized modulus:

$$\frac{E^*}{E^s} = \frac{(i\omega\tau)^\beta}{1+(i\omega\tau)^{\beta-1}} \tag{3.7}$$

This same math holds for shear moduli as well: :

$$\frac{G^*}{G^s} = \frac{(i\omega\tau)^\beta}{1+(i\omega\tau)^{\beta-1}} \tag{3.8}$$

We take the real and imaginary parts to obtain G' and G'', respectively. Note that a well-defined zero shear viscosity, η_o is obtained, provided that $\beta < 1$**:**

$$\eta_o = \lim_{\omega\to\infty} \frac{G''}{\omega} = G^s\tau \tag{3.9}$$

For a given value of β, the material behavior is determined by G^s and a single additional

parameter, τ. Eq. 3.7 can now be used to fit the frequency master curves obtained by time-salt or time-temperature superposition to calculate β and τ. Results are shown in Table 3.1. We refer to the reference time scale associated with ω_o of the master curves as τ_{ref} such that $\tau = a_{Salt}\tau_{ref}$ and $\tau = a_T\tau_{ref}$. While our results imply that $\tau = a_{Salt}a_T\tau_{ref}$, further work is necessary to determine if the salt and temperature effects are truly separable in this way. In general, vertical shifting may need to be applied as well, since the overall polymer concentration depends on the added salt. In our case this can be accounted for by adjusting G^s. This shifting is not necessary in our case, however, because the salt is being adjusted over relatively narrow concentration range, where changes in the overall concentration are relatively small.[6] This behavior is consistent with the recent results of Liu *et al.*, who found that the vertical shift factors were independent of salt concentration in a similar composition range for a related coacervate system.[3]

Sample	β	G^s (Pa)	τ_{ref} (s)	[KBr] (M)	T (^{o}C)	a_{Salt}	a_T
PSS:QVP-C1 (Fig. 3.7a)	0.42	5070	0.0015	1.39	20	23	
				1.49	20	5	
				1.58	20	1	
PSS:QVP-C2 (Fig. 3.7b)	0.44	4150	0.0010	1.58	20	20	
				1.68	20	5	
				1.77	20	1	
PSS:QVP-C3 (Fig. 3.7c)	0.42	4250	0.0011	1.98	20	9	
				2.07	20	4	
				2.16	20	1	
PSS:QVP-C1 (Fig. 3.8)	0.42	3410	0.0071	1.49	-7		60
					0		17
					10		4.5
					25		1

Table 3.1: Values of β and τ_{ref} for the rheological response of PSS:QVP complex coacervates.

The shift factors listed in Table 3.1 depend on the details of the coacervate, with higher salt concentrations required to give a given value of τ for a more hydrophobic cationic polymer in the polyelectrolyte complex. The concentration dependence of these relaxation times appears to have some universal features, which can be seen from the plots of a_{Salt} (which is proportional to τ) in

the insets of Figure 3.7. From these plots we see that the logarithm of a_{Salt} is linear in the salt concentration, suggesting that the shift factors can be written in the following form:

$$\log_{10} a_{Salt} = B_{Salt}\left(1 - [\mathrm{KBr}]/C_{ref}\right) \tag{3.10}$$

Here C_{ref} is a reference KBr concentration where a_{Salt} is defined to be equal to one. The salt dependence of the relaxation times is determined by the constant B_{Salt}. The salt shift factors from Table 3.1 are plotted in Figure 3.10, along with the prediction of Eq. 3.10 with $B_{Salt} = 12$. The values of a_{Salt} and C_{ref} have been adjusted slightly from the shift factors and concentrations listed in Table 3.1 in order to give $\tau = 0.001$s when $a_{Salt} = 1$, using Eq. 3.10 with $B_{Salt} = 12$ to apply the necessary shifts.

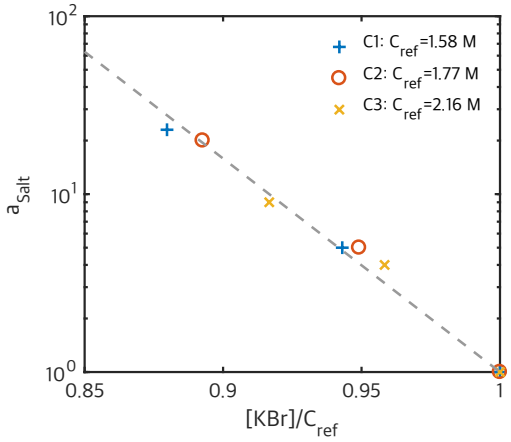

Figure 3.10: Normalized plots of the salt shift factors obtained from the data in Table 3.1, shifted to a reference salt concentration where τ =0.001 s. The dashed line is Eq. 3.10 with B_{Salt}=12.

Use of the the fractional Maxwell liquid model has several advantages. Perhaps most importantly, the entire rheological response of the polyelectrolyte complexes is described by three parameters; G^s, β and τ. Since the value of β is very similar (≈ 0.42) for each of the systems that we have studied, rheological differences are characterized by G^s and τ. Finally, an elegant analytical expression exists for the relaxation spectrum ($H(\lambda)$) for the fractional Maxwell model.

Obtaining $H(\lambda)$ usually requires iterative fitting, as exemplified in the seminal work by Spruijt *et al.* where the storage, loss and relaxation modulus were fitted.[97] However, Palade *et al.* derived the explicit expression for $H(\lambda)$ for the fractional Maxwell liquid[122], which in the present case may be written as follows:

$$\frac{H(\lambda)}{G^s} = \frac{1}{\pi} \frac{(\lambda/\tau)^{-1} \sin(\pi\beta)}{(\lambda/\tau)^{(\beta-1)} + (\lambda/\tau)^{(1-\beta)} + 2\cos(\pi(1-\beta))} \tag{3.11}$$

Eq. 3.11 implies the following two scaling relationships for $\alpha = 1$:

$$\lim_{\lambda \to 0} H(\lambda) \propto \lambda^{-\beta}$$

$$\lim_{\lambda \to \infty} H(\lambda) \propto \lambda^{-(2-\beta)}$$

Figure 3.11 plots the relaxation spectra for PECs showing that the relaxation behaviors of PSS:QVP- C1, C2 and C3 remain identical by following well defined scaling relationships, albeit occurring at higher salt concentrations with increasing hydrophobicity. The shape of the relaxation spectrum resulting from the power-law rheological response offers a pathway to engineer materials with damping properties over a broad range of timescales, with salt and/or hydrophobic effects being key tuning parameters.

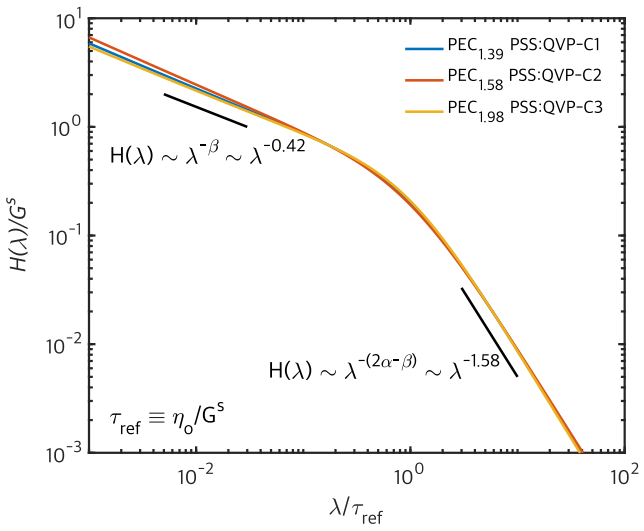

Figure 3.11: The relaxation spectrum of PSS:QVP-C1, C2 and C3 obtained by plotting eq 3.11 using the power-law exponent (β) calculated from frequency sweep data presented in Figure 3.7.

3.2.4 PEC Phase Behavior

In Figure 3.4 the salt responsiveness of PSS:PDADMA was quantified, and in Figure 3.6 we compared the swelling behavior of PSS:PDADMA to complexes involving QVP-C1 to C3. Complexes using the QVP polyelectrolytes were found to be mildly more hydrophobic, which resulted in a diminishing responsiveness to KBr concentrations. This suggested that hydrophobicity is a simple tuning parameter to control stability. We now quantify the swelling behavior of PSS:QVP-C2, which is mildly more hydrophobic than PSS:PDADMA, to different salts and the results are plotted in Figure 3.12. PSS:QVP-C2 complex remains stable in all common salt solutions, with little swelling at up to 1.0 M ionic strength. Correspondingly, the $\rho|G_3^*|$ remains nearly constant in this salt concentration regime, and ϕ remains low, indicating the materials are primarily elastic. KBr was the only ion combination to effectively swell the complex and diminish $\rho|G_3^*|$ due to both potassium and bromine being poorly solvated ions.[1, 2, 66] This selective salt responsiveness is extremely beneficial as it allows the PEC to be processed like a traditional polymer with concen-

trated KBr solutions, while preserving resistance to common ions. In other words, making the complex very mildly hydrophobic modulated out the interaction of most ions, while preserving the ability to process the complex "saloplastically."

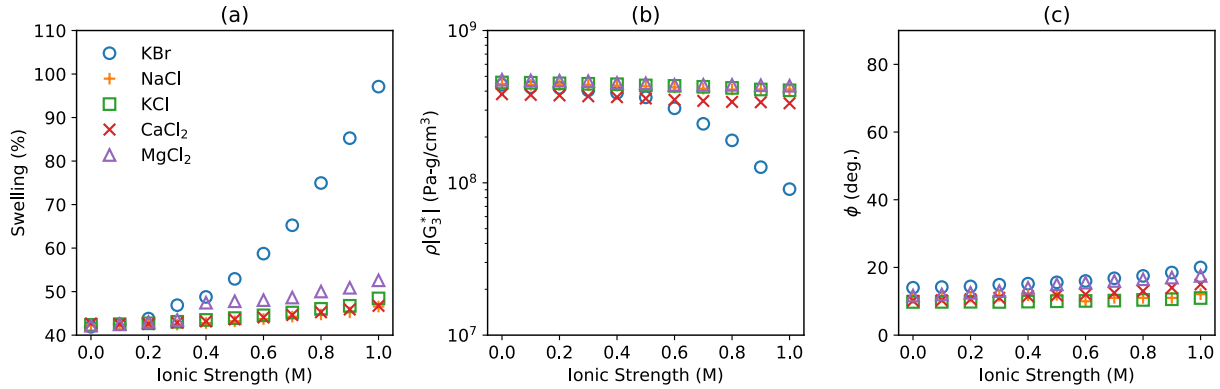

Figure 3.12: (a) Swelling %, (b) density-shear modulus product, and (c) viscoelastic phase angle at 15 MHz of PSS:QVP-C2 in response to increasing ionic strengths of different salt identities. KBr is the only salt that can effectively swell and dissolve this complex by breaking ion-pairs between PSS and QVP-C2, while other salt ions do not significantly affect the mechanical integrity of the complex, and therefore also do not effectively dissolve the complex. This essentially allows PSS:QVP-C2 membranes to be processed from KBr solutions, while maintaining stability in a variety of commonly encountered salts at ambient to high concentrations.[4] A $\approx$ 43% increase in thickness relative to the dry film is observed for the complex immersed pure water which is attributed to charge hydration.[1, 5]

The swelling behavior that was quantified thus far builds a quantitative picture of ion-specific and hydrophobic effects in PECs. However, these effects are ultimately a reflection of the underlying phase behavior of these materials. Figure 3.13 plots the ternary phase map of PSS:QVP-C2 with added KBr. A solid complex of composition *S* (30 % water, 70 % polymer) is the stable composition in the absence of salt. Here, the intrinsic 30 wt% water content ($\approx$ 43% swelling) is a result of solvating the charges present within the complex. Clear, one phase solutions are obtained for overall salt concentrations above $\approx$ 20 wt. %. At salt concentrations below 20 wt. % the system separates into a phase with almost no polymer and polymer-rich coacervate phase with a polymer concentration that decreases with increasing salt concentration. The addition of 15.1 wt % KBr

results in a clear liquid-like coacervate with a polymer concentration of 32 wt %, hence we refer to this coacervate solution as C_{32}. The addition of more salt further increases the water content of the coacervate, with a 17 wt % KBr giving a coacervate phase with a polymer concentration of 20 wt % (C_{20}) and a 18.3 wt % KBr giving a coacervate phase with a polymer concentration of 12 wt % (C_{12}). Solutions drawn from these coacervate phases can be cast into thin-films using established blade or bar casting methods onto any desirable substrates.

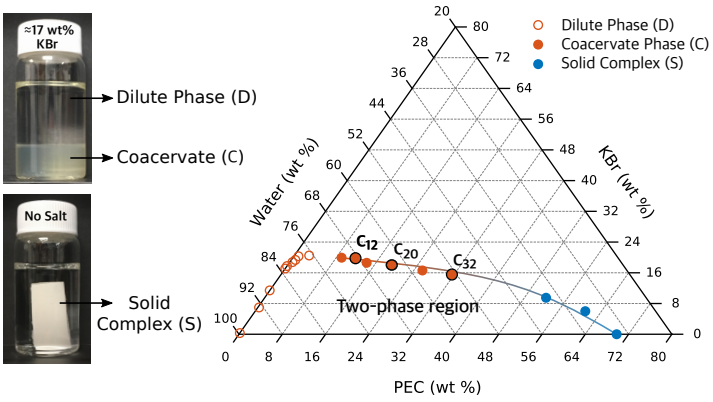

Figure 3.13: Phase behavior of PSS:QVP-C2 complex. In the absence of salt, the two polyelectrolytes neutralize each other into a solid complex, *S*. Increasing the salt concentration results in a liquid-liquid phase separation between a polymer rich coacervate phase and a polymer dilute phase.[1, 3, 6] The coacervate is a viscous polymer solution that can be cast into films of controllable thicknesses.

We now summarize the observation that hydrophobic effects increase the stability of complexes by comparing the phase behavior of PSS:QVP-C2 and C3, plotted in Figure 3.14a as a binary map which is a bit easier to visualize than the ternary one. We find that the reason for the increase in stability with increasing hydrophobicity is because the critical salt concentration needed to dissolve the complex increases with enhanced hydrophobic interactions, which also expands the two-phase region. Interestingly, we find that the tie lines for the phase map are slightly negative, a phenomenon that was discussed in more detail by Lu et al.[67]

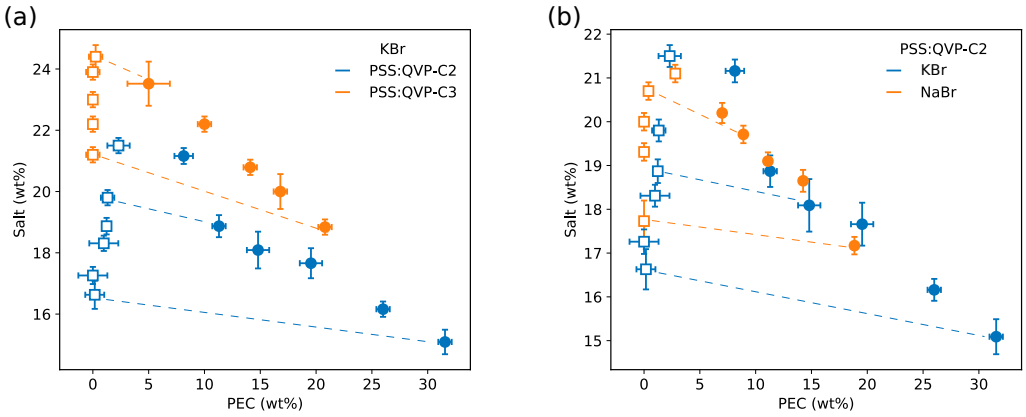

Figure 3.14: (a) Phase behavior of PSS:QVP-C2 in comparison with PSS:QVP-C3. Increased hydrophobicity expands the two phase region. (b) Phase behavior of PSS:QVP-C2 in response to NaBr and KBr. Both salts exhibit similar phase behavior, but it should be noted that NaBr has a smaller molar mass, therefore, overall a higher molar ratio of salt to PEC is needed. Note that in all cases the tie lines are slightly negative.

3.3 Conclusion

In the present work we described the most detailed study to date of hydrophobicity on polyelectrolyte complexation by adding single methylene groups to the side chain of quaternized poly(4-vinylpyridine), and complexing it with a common anionic polymer. This simple modification to the chain architecture led to measurable changes in the mechanical behavior, which were accurately quantified in terms of swelling, density-shear modulus product at 15 MHz and the viscoelastic phase angle at this same frequency. We used these hydrophobic effects to quantify properties of these complexes across the whole spectrum of their mechanical behavior, from solid-like complex to coacervate to single phase solutions. Our results show that hydrophobicity plays a crucial role in determining the stability of polyelectrolyte complexes against concentrated salt solutions, allowing a simple yet powerful tuning parameter over their mechanical response. Additionally, the effect of differential changes in hydrophobicity of the parent chain was shown to have a non-linear influence on mechanical properties; increasing hydrophobicity of the complexes resulted in increasing resis-

tance to swelling in salt solutions. We also demonstrated that hydrophobic effects only tune the salt responsiveness of the PSS:QVP system without altering its rheological behavior, that is, the power-law exponent (β) and the shape of the relaxation spectrum (Figure 3.11) remain the same. The effect of salt and temperature can therefore be quantified by the effect these variables have on a single characteristic time, τ. This time was defined in terms of a fractional Maxwell liquid model, which replaces the large number of relaxation modes required using Maxwell elements with minimal fit parameters, and provides an elegant analytical expression for the relaxation spectrum. The rheological behavior coupled with swelling master curves (Figure 3.5 and 3.6) and the mechanical spectrum (Figure 3.3) painted a unifying mechanical picture of polyelectrolyte complexes.

3.4 Experimental Methods

Materials: Poly(styrene sulfonate) sodium salt (PSS, MW 200K g mol^{-1}), poly(diallyldimethyl) chloride (PDADMA, MW 200-350K g mol^{-1}) and poly(4-vinylpyridine) (P4VP, MW 60K g mol^{-1}) were purchased from Sigma Aldrich. Iodomethane, 1-bromoethane, 1-bromopropane, NaCl, KCl, LiCl, $CaCl_2$and KBr were also purchased from Sigma-Aldrich. Deionized water (conductivity $\approx 5\,\mu S/cm$) was used for making all solutions except when forming coacervates where 18.2 MΩ*cm MilliQ water was used.

Quaternization of poly(4-vinylpyridine): In our nomenclature we refer to methyl, ethyl and propyl substituted P4VP as QVP-C1, QVP-C2 and QVP-C3 respectively. QVPs were synthesized by dissolving 8 wt% P4VP in dimethyl sulfoxide before adding a molar excess of the methyl iodide, ethyl bromide or propyl bromide. QVP-C1 was synthesized by adding 20% molar excess of methyl iodide while keeping the solution well stirred for 4 hours at room temperature. QVP-C2 (QVP-C3) was synthesized by adding 70% (100%) molar excess of ethyl (propyl) bromide while keeping the solution well stirred for 24 hours at 40 ^{o}C. Once the reaction was complete, QVP-C1 was precipitated in ethanol and QVP-C2 and C3 in tetrahydrofuran followed by vacuum filtration.

The precipitate was then dissolved in 1.0 M NaCl and dialyzed against 0.2 M NaCl for 3 days, and another 3 days against deionized water, with the external solution replaced every 24 hours. Subsequent lyophilization yielded dry polymer chloride salts. The success of the ion exchange was verified by precipitating the counter ions using $AgNO_3$, and by noting that AgCl is white and AgI is yellow. The degree of quaternization was verified to be 100% by H^1-NMR using a Bruker Avance III 500 MHz system, Ag500.

Stoichiometric PECs: PECs were made from PSS:PDADMA in a similar "backwards" manner previously reported by Wang and Schlenoff.[6] Briefly, individual PSS or PDADMA solutions were prepared at a concentration of 0.25 M and then added simultaneously to a well stirred beaker of deionized water. The PEC precipitated out as a white solid which was isolated by vacuum filtration. These PECs were then re-immersed and stirred in a large beaker of deionized water. The precipitates were allowed to settle periodically, and the supernatant decanted, and subsequently then re-immersed in fresh deionized water. This process was repeated until the conductivity of the supernatant fell to $\approx 50\,\mu S/cm$. The precipitates were then vacuum filtered once more and the dried at 120 ^{o}C for 12 hours.

PSS-QVP PECs were made analogously. Once the quaternization reaction was completed (in DMSO), the moles of QVP repeat units were calculated, and the equivalent amount of PSS was dissolved in equivalent volume of water separately. The two solutions were then simultaneously added to a third beaker of water under stirring. The PECs again precipitated out as a white solid that was subjected to the same washing procedure as PSS:PDADMA. Since pyridines have poor thermal stability, these precipitates were dried at 70^{o}C and in the presence of drierite for 12 hours.

Coacervates: Coacervates were formed from the dry PECs by dissolving them in solutions of KBr. In all cases, 1.50 g of dry PEC was dissolved in 10 g of MilliQ water (18.2 MΩ cm) and X grams of KBr (Table 1). Once the PECs dissolved, an additional 5 g of water was added while keeping the solution well stirred. Once the coacervate phase began to form, the solution was

annealed at 60^{o}C for 30 min. The solutions were then allowed to equilibrate between 1 week to 3 months, depending on the sample. Coacervates formed at lower salts required longer equilibration times.

Sample	PEC (g)	H_2O (g)	KBr (g)	KBr (wt%)	KBr (M)
$PEC_{1.30}$	1.5	15	2.5	13.15	1.30
$PEC_{1.39}$	1.5	15	2.67	13.92	1.39
$PEC_{1.49}$	1.5	15	2.85	14.72	1.49
$PEC_{1.58}$	1.5	15	3.03	15.51	1.58
$PEC_{1.68}$	1.5	15	3.21	16.28	1.68
$PEC_{1.77}$	1.5	15	3.39	17.04	1.77
$PEC_{1.86}$	1.5	15	3.57	17.78	1.85
$PEC_{1.98}$	1.5	15	3.95	19.31	1.98
$PEC_{2.07}$	1.5	15	4.13	19.94	2.07
$PEC_{2.16}$	1.5	15	4.31	20.63	2.16
$PEC_{2.25}$	1.5	15	4.47	21.32	2.25

Table 3.2: Sample designations and coacervate compositions.

Rheology: Rheology was performed using an Anton-Paar MCR 302 rheometer with the cone-plate geometry. 50 mm diameter plates with a cone angle of 2^{o}were used to perform frequency sweeps between 0.1-300 rads s^{-1}. A 1% strain amplitude was used which was verified to be well within the linear viscoelastic regime using amplitude sweeps. Once the coacervates were loaded, they were allowed to relax for at least 10 min at room temperature. Solvent evaporation was mitigated by placing a small trough of water around the bottom plate of the rheometer and isolating the sample inside a custom chamber. Frequency sweep master curves were fitted to the fractional Maxwell liquid model using MATLAB's *lsqnonlin* function, with the solver tolerance set to 10^{-10}.

Quartz Crystal Microbalance: A custom quartz crystal microbalance (QCM, AWSensors, Valencia, Spain) was used in conjunction with a N2PK impedance analyzer (Thornhill, Canada) for swelling and viscoelastic measurements of spin coated polyelectrolyte complex films. 1.5 μm polyelectrolyte complex films were directly spin-coated onto 1" quartz crystals with Au electrodes

(Inficon, East Syracuse, NY) from the polymer rich coacervate phase. Accurate QCM experiments require highly homogeneous and smooth films. Such high quality films could be obtained by spin-coating coacervates between 3000-9000 RPM for 20 s, and then immediately immersing them into low ionic strength KBr solutions to extract residual salt in the film. PSS:PDADMA films were spin coated from $PEC_{1.58}$, and annealed in 0.5 M KBr for 12 hours. PSS:QVP-C1 (C2, C3) films were obtained from $PEC_{1.68}$ ($PEC_{1.96}$, $PEC_{2.25}$) and annealed in 0.75 M KBr (1.0, 1.25 M KBr) for 12 hours. After salt solution annealing the films were rinsed with excess deionized water and dried in air. The QCM experiments were performed as described in our previous work[13, 24], but a brief description is provided. The QCM provides changes in the resonance frequency (Δf_n) and dissipation ($\Delta\Gamma_n$) of the piezoelectric quartz crystal at the odd n^{th} harmonic of the fundamental frequency (5 MHz for the crystals used in this work). We monitor Δf_n and $\Delta\Gamma_n$ at n = 1, 3, 5 by fitting a lorentzian peak to the conductance and suseptance in the frequency domain (note that this is in contrast to the widely used Q-sense instrument that operates in the time domain, with $\Delta D_n = 2\Delta\Gamma_n/f_n$ where D is the dissipation factor). The time domain experiment is poorly suited for studying thicker ($\approx 1.5\ \mu$m) films that are necessary for calculating accurate viscoelastic properties.

Chapter 4

Guanidinium Can Both Break and Form Strongly Associating Ion-Complexes

Abstract: Guanidinium is one of nature's strongest denaturants and is also a motif that appears in several interfacial contexts such as the RGD sequence involved in cell adhesion, cell penetrating peptides, and anti-microbial molecules. It is important to quantify the origin of guanidinium's ion-specific interactions, so that its unique behavior may be exploited in synthetic applications. The present work demonstrates that guanidinium ions can both break and form strongly associating ion-complexes in a context-dependent way. These insights into guanidinium's behavior are elucidated using polyelectrolyte complexes (PECs), where inter-polymer ion-pairs between oppositely charged polymers play an important role in determining material stability. Different polycation-polyanion combinations can span a large range of association affinities, where more strongly associating complexes can remain insoluble in concentrated salt solutions and/or in extreme pH conditions. This high stability is desirable in several application contexts for PECs, but also renders them challenging to process– and therefore, to study– since they cannot be dissolved into polymer solutions. Here we demonstrate that guanidinium salts are very effective in dissolving the poly(styrenesulfonate)/poly(allylamine) (PSS:PAH) complex, which has one of the high-

est measured polycation-polyanion association affinities. We also demonstrate the importance of charge identity by functionalizing guanidinium directly into poly(allylamine) resulting in a complex that remains stable under highly denaturing conditions. The model system of PSS:PAH is used to glean insights into guanidinium's denaturing activity, as well as to broadly comment on the nature of ion-specific interactions in charged macromolecules. This work appears in *ACS Macro Lett.* 2019, 8, 2, 117-122.

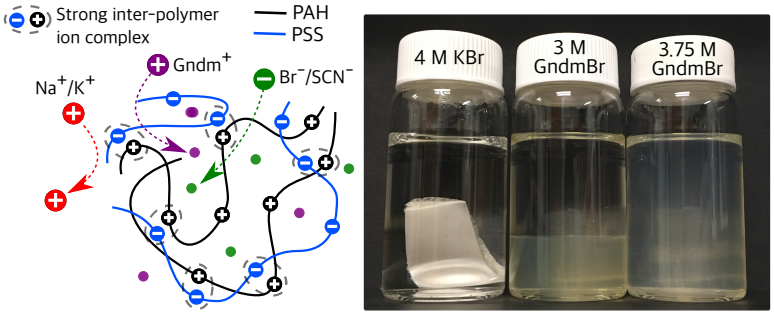

4.1 Introduction

Polyelectrolyte complexes (PECs) were difficult to process into functional materials before development of the layer-by-layer (LbL) assembly technique. This approach led to an explosion of work using these materials to obtain coatings for a variety of applications.[69, 123] A similarly important advancement in the field was made when salt-mediated processing ("saloplastics") was introduced to process bulk PECs.[6, 114] Here, salt is an analog for temperature where a solid-like complex can be "melted" in appropriate salt concentrations into an associating polymer solution, commonly known as the coacervate phase. The liquid-like coacervate phase is more tractable from a processing standpoint, where the salt concentration can be tailored to modulate the viscosity, and ultimately be cast into more useful formats such as films[1], rods[114] or fibers.[124] Since the number of potential polyelectrolyte combinations is large, a collective understanding of how the

constituting polymer identities– and the associated details such as charge identity, topology, and hydrophobicity– dictate the observed macroscopic material response is only incipient. Given the vast number of applications to which polyelectrolyte complexes, or polyelectrolytes in general, are relevant it is important to clearly correlate these molecular level details to measurable material parameters.

While different salts used to swell PECs result in a material response in a fairly predictable manner according to ionic solvation[1], different polycation/polyanion combinations exhibit more complex trends. Specifically, different constituting polyelectrolyte pairs have very different association affinities.[125] Weakly associating complexes have a low salt resistance, defined as the critical salt concentration needed to completely dissolve the material by charge screening.[67] On the other end of the spectrum, strongly associating complexes have a very high salt resistance and are frequently insoluble. Such strongly associating complexes are often found in nature, in protein-protein interactions for example.[126] The measured salt resistance of a specific complex is a non-trivial function of the ion-pairing strength[125], chain topology[108], hydrophobicity[1] and molecular weight.[67] Importantly, the salt resistance of a complex is also dependent on the specific salt being considered– a complex will have a low salt resistance against a salt which is effective for breaking that particular complex.[127] The most well-studied complex with high salt resistance is the pairing of poly(allylamine) with poly(styrenesulfonate) (PSS:PAH), which has been popular for LbL assemblies precisely due to its high association affinity that makes processibility simpler, but also precludes salt mediated dissolution into a coacervate phase.[125, 128] Indeed, PSS:PAH cannot be dissolved in potassium bromide solutions, which is one of the most effective salts in breaking ion-pairs.[1, 6, 127] Yet it remains desirable to be able to process PSS:PAH saloplastically since once it is formed into functional materials, the final product would be highly stable under many conceivable application environments.

4.2 Results and Discussion

As mentioned earlier, hydrophobic effects, ion-pairing associations, molecular weights, and chain topology can all ascribe stability to PECs against salt solutions and/or pH changes. Since molecular weight effects are more pronounced at low degrees of polymerization, and because the most common chain topology is linear, we focus here in the limit of linear high molecular weight chains but note that these factors are important and have been considered elsewhere.[67, 108] This leaves us to consider the roles of hydrophobicity and ion-pairing association in charged complexes, which are also two important factors determining protein stability. In our recent work, we demonstrated that more hydrophobic complexes are more salt resistant, showing greater and greater stability in salt solutions as the complex is made progressively more hydrophobic.[1] Let us now consider the polycations PAH and poly(N-ethyl-4-vinylpyridinium) (QVP-C2), where the latter is expected to be relatively more hydrophobic. The relative hydrophobicity/hydrophilicity of these two polyelectrolytes can be quantified by their propensity to segregate at water/chloroform interfaces as measured from a drop in the interfacial tension. Figure 4.1 shows that QVP-C2 readily partitions to a water/chloroform interface due to its hydrophobic character, while poly(allylamine) has no observed interfacial affinity due to its relatively hydrophilic nature. If hydrophobicity is a dominating non-covalent interaction in complexes of these two polycations with the same polyanion, then one would expect the more hydrophilic complex involving poly(allylamine) to be more weakly associating with a lower salt resistance.[1] Yet, we find this not to be the case.

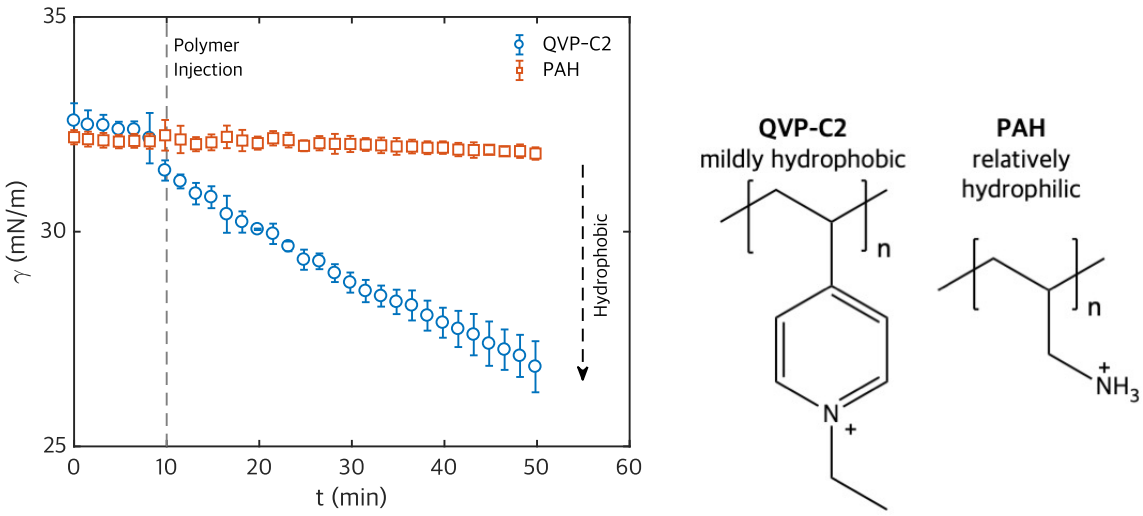

Figure 4.1: Effect of poly(allylamine) HCl (PAH) and poly(N-ethyl-4-vinylpyridinium) (QVP-C2) adsorption on the interfacial tension (γ) at a water/chloroform interface. More hydrophobic molecules adsorb to a greater extent, thus lowering the tension from the pristine water/chloroform value of $\approx$ 32.8 mN/m. The polymers were added to the aqueous phase at a repeat unit concentration of 5 mM. 5 mM $NaClO_4$ was also present in the aqueous phase. A more detailed use of these tension experiments to elucidate ion-specific behavior is provided in Chapter 6.

Figure 4.2 plots the salt responsiveness of PSS complexed with PAH and QVP-C2, showing that the more hydrophobic complex of PSS:QVP-C2 swells $\approx$40 % in water while PSS:PAH only swells $\approx$30 %. These data were obtained with the quartz crystal microbalance, which is able to measure the linear viscoelastic behavior of PEC films ($\approx$ 1.5 μm) at a frequency of 15 MHz.[1, 5] This technique is advantageous because it allows mechanical characterization while simultaneously recording the swelling ratio of pore-free thin-films with a high degree of precision. The swelling ratio is directly related to the water content of the PEC films. Here, the modulus of PSS:PAH initially is nearly glass-like at $\approx 9 \times 10^8$ Pa (for reference, polystyrene at room temperature is $\approx 2 \times 10^9$ Pa). Even more surprisingly, PSS:PAH appears insensitive to swelling with increasing ionic strength of KBr after an initial response at low salt concentrations. During this response, the complex was observed to swell to 40-50% from the initial swollen state of about 30% in pure water. While this initial swelling response at low ionic strengths is somewhat peculiar, con-

flicting reports exist in literature where similar behavior has been observed in some polyelectrolyte multilayers involving poly(allylamine)[129, 130], but not in others.[131, 132] In our experiments, we observe that this initial swelling at 0.1 M occurs over several hours, consistent with at least one study explicitly reporting it.[129] Therefore, the slow timescales associated with this phenomenon could be a reason for the experimental discrepancies, as the measurement timescale becomes critical, and more detailed investigations are required to elucidate the underlying mechanisms.[133] However, the majority of studies acknowledge PSS:PAH's relatively high modulus/lower water content[132, 134] and insensitivity to salt[131, 132, 135, 136], consistent with our own observations in the present work. The relatively high modulus and low water content of the PSS:PAH complex– even though it is quantifiably more hydrophilic– may be attributed to the tighter/stronger ion-pairs that form between the two monomers. This observation is complimentary to other reports which have found PSS:PAH to be highly stable in a variety of salt solutions.[125] Understanding this stability is desirable since materials and soft assemblies formed using this unique ion-pair would also be highly stable. Figure 4.2 also shows that at increasing ionic strengths, PSS:QVP-C2 keeps swelling, and the modulus keeps decreasing, as expected.

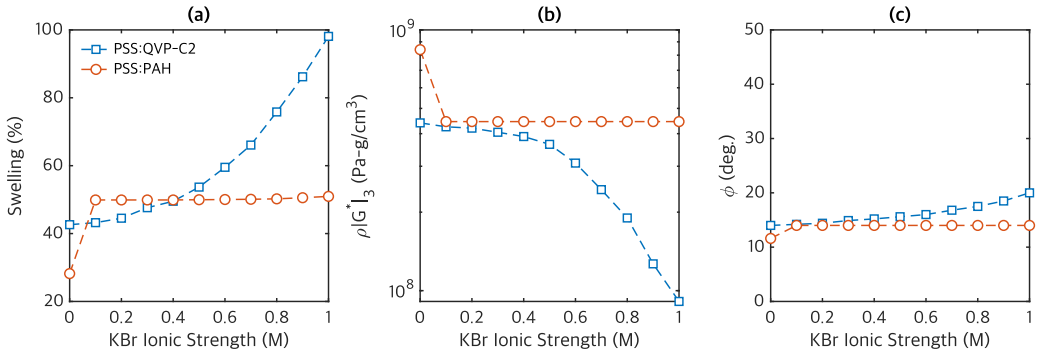

Figure 4.2: (a) Swelling behavior, (b) density-shear modulus product, and (c) viscoelastic phase angle (ϕ) as a function of ionic strength for spin-coated PSS:PAH films. Swelling % is calculated in reference to the dry film. PSS:PAH shows little sensitivity to increasing concentration of KBr, which is one of the most effective salts for dissolving polyelectrolyte complexes. PSS:QVP-C2 exhibits increased swelling and diminished mechanical properties with increasing salt concentration. Viscoelastic properties were measured at 15 MHz using the quartz crystal microbalance as described previously.[1, 5] For reference, polymer glasses have a shear modulus of $\approx 2 \times 10^9$ Pa and a $\phi \approx 1^o$ at this frequency, and $|G^*| = |G' + iG''|$ and $\phi = \arctan(G''/G')$ as usual. pH of all solutions were ambient at $\approx 5.5 - 7$.

Thus far intuition has misled expectations in terms of PEC stability, and it appears that processing PSS:PAH remains difficult. Numerous publications have focused on the interaction of Hofmeister series of salts to study interaction with PECs, usually focused on the anions.[137] Poorly solvated salt species are generally found to interact more strongly with complexes, and well-solvated species such as lithium typically interact weakly.[1] KBr is one of the best salts for dissolving PECs since the bromide ion can efficiently break ion-pairs but does not precipitate polycations at high concentrations. More poorly solvated anions such as perchlorate and thiocyanate tend to precipitate out some polycations.[138] However, we speculate that it may be possible to use a more poorly solvated cation than potassium to process PECs. This speculation was inspired by observing the well-known role of guanidinium ions in protein denaturation.[139, 140] Guanidinium thiocyanate is one of the strongest known denaturants, and also happens to be a very weakly solvated salt.[139] Many essential molecular details that contribute to protein stability are also relevant to PECs and therefore it can be expected that salts which are strong denaturants would also

be strong dopants for PECs. Figure 4.3 shows that when subjected to increasing concentration of guanidinium bromide (GndmBr) or guanidinium thiocyanate (GndmSCN), PSS:PAH complexes swell significantly, with a corresponding decrease in the modulus, unlike the response observed for KBr. Importantly, the mechanical properties of these complexes are ultimately determined by the amount of water inside the complex as we have reported previously.[1] The rheological response of a highly swollen coacervate phase ($\approx$ 16 wt. % PEC), obtained at an overall GndmBr concentration of 3.25 M is shown in Figure 4.4, where we have used time-temperature superposition to access a broad range of timescales. Here, the typical response of a coacervate is observed, with a liquid-like behavior at high temperatures and low frequencies, and a power-law behavior of ≈ 0.5 at low temperatures and high frequencies.

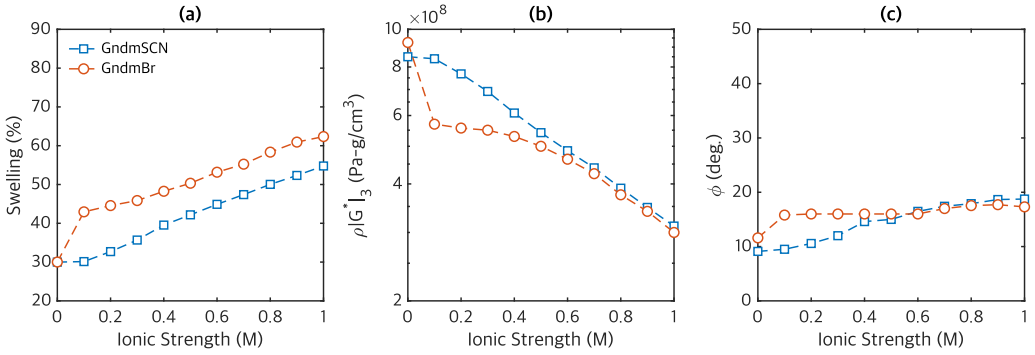

Figure 4.3: (a) Swelling behavior, (b) density-shear modulus product, and (c) viscoelastic phase angle in response to guanidinium salts for spin-coated PSS:PAH films. Both the bromide and thiocyanate salts of guanidinium (Gndm) are effective in swelling PSS:PAH, resulting in lower shear moduli and an increased phase angles, unlike the response for KBr in Figure 4.2. The mechanical properties are primarily a function of the water content.[1]Viscoelastic properties reported at 15 MHz.

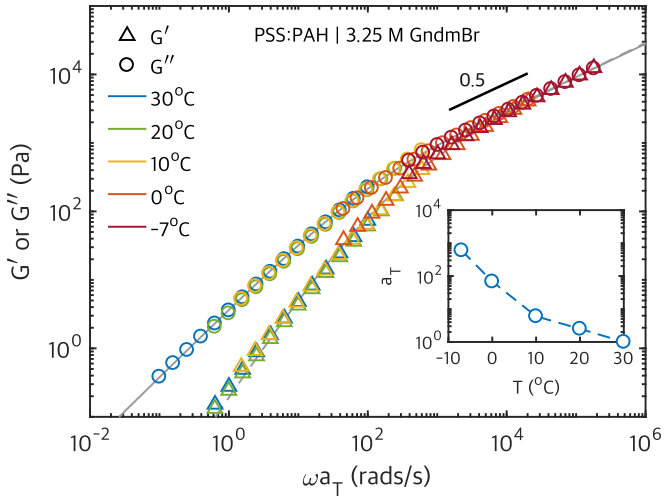

Figure 4.4: Time–temperature superposition of PSS:PAH coacervate formed at a overall GndmBr concentration of 3.25 M. Here, the polymer concentration is ≈16 wt. % in the coacervate phase. A typical polymer solution response is observed even at this high salt concentration. The lowest temperature of −7 °C could be measured before the onset of freezing effects.[1]

Polyanions and polycations associate due to the large entropy gain from counter-ion release. While entropy is the dominant driving force for association, a polyelectrolyte complex's responsiveness and strength are primarily determined by ion and polymer specific interactions. This importance of polymer specific interactions was highlighted in this work by noting that PSS:PAH is stronger and more stable than PSS:QVP-C2, even though the later is quantitatively more hydrophobic. Ion specific interactions allow guanidinium ions to break PSS:PAH complexes when all other common salts fail to do so. Since guanidinium is an organic cation ubiquitous in biology as part of the amino acid arginine, the following question can be posed: how would the complex respond if guanidinium charges were introduced directly into the PAH backbone? Alternatively, what is the role of charge identity in amine versus guanidine in determining the physical properties of the complex? This simple difference can have significant implications in the development of effective antimicrobial agents with low toxicity and low drug resistance.[136, 141, 142] For a polypeptide this would correspond to quantifying the difference in association of lysine versus

arginine with a common polyanion. In the present case it is straightforward to convert PAH into a statistical copolymer with amine and guanidine using the scheme in Figure 4.5a. Due to the molecular simplicity of poly(allylamine) and poly(allylguanidine) this approach is attractive for studying the differences between primary amines (lysine-like) and guanidinium (arginine-like) charges.

The interaction of poly(styrenesulfonate) as the model polyanion with poly(allylamine-*co*-allylguanidine) (PSS:PAH-Gu) can now be studied as a function of the salt concentration by observing whether the resulting complexes remain solid-like or can be dissolved into polymer solutions. Figure 4.5b provides a phase map of the formed complexes as a function of the guanidinium fraction on the polycation. The complex is classified as solid-like if it appears insoluble, a coacervate if a liquid-liquid phase separation occurs, and a polymer solution if it is dissolved completely. We discover that the phase behavior of PSS:PAH-Gu is extremely sensitive to the guanidinium fraction on the backbone. At just 10% guanidnium, the complex forms a cloudy gel instead of a coacervate, indicating the presence of insoluble aggregates. The rheological response of this 'cloudy gel' is atypical of complex coacervate's polymer solution response such as in Figure 4.4, but is characteristic of colloidal gels (Figure 4.6).[143] At higher guanidinium fraction the complex only forms solid-like complexes, suggesting that guanidinium has a higher affinity for poly(styrenesulfonate) than poly(allylamine), consistent with a recent study reporting guanidinium containing polyelectrolyte multilayers to be more rigid.[144] However, it is possible these complexes may be far from their thermodynamic equilibria, and more detailed investigations are needed. Such unique behavior of guanidinium has been observed and utilized in other self-assembling macromolecular systems,[105, 145, 146] and the present work here provides fundamental insights into those observations.

In the current work, we have demonstrated that ion-specific interactions play a key role in determining the stability and responsiveness of charged complexes. These interactions can be exploited to both disassemble complexes, or to increase their stability, depending on the context. In

this particular case, guanidinium was a powerful agent for disassembling the otherwise strongly associating PSS:PAH complex. This ability to break strong ion-pairs likely compliments other proposed mechanisms for guanidinium's denaturing activity.[139, 140, 147, 148, 149] While guanidinium is a strong denaturant as a free salt, it is a strong binding agent when incorporated into the polymer itself, rendering complexes with anionic moieties highly stable, suggesting a mechanism for its interfacial adhesion promoting properties.[150] Therefore, the context in which ion-specific interactions are considered is extremely important for rationalizing observations. Lastly, given guanidinium's biological relevance, its behavior in synthetic macromolecular systems could be better explored because of its technological significance.[142] The present work introduces PAH-Gu polyelectrolytes as a simple and accessible model platform for future investigations.

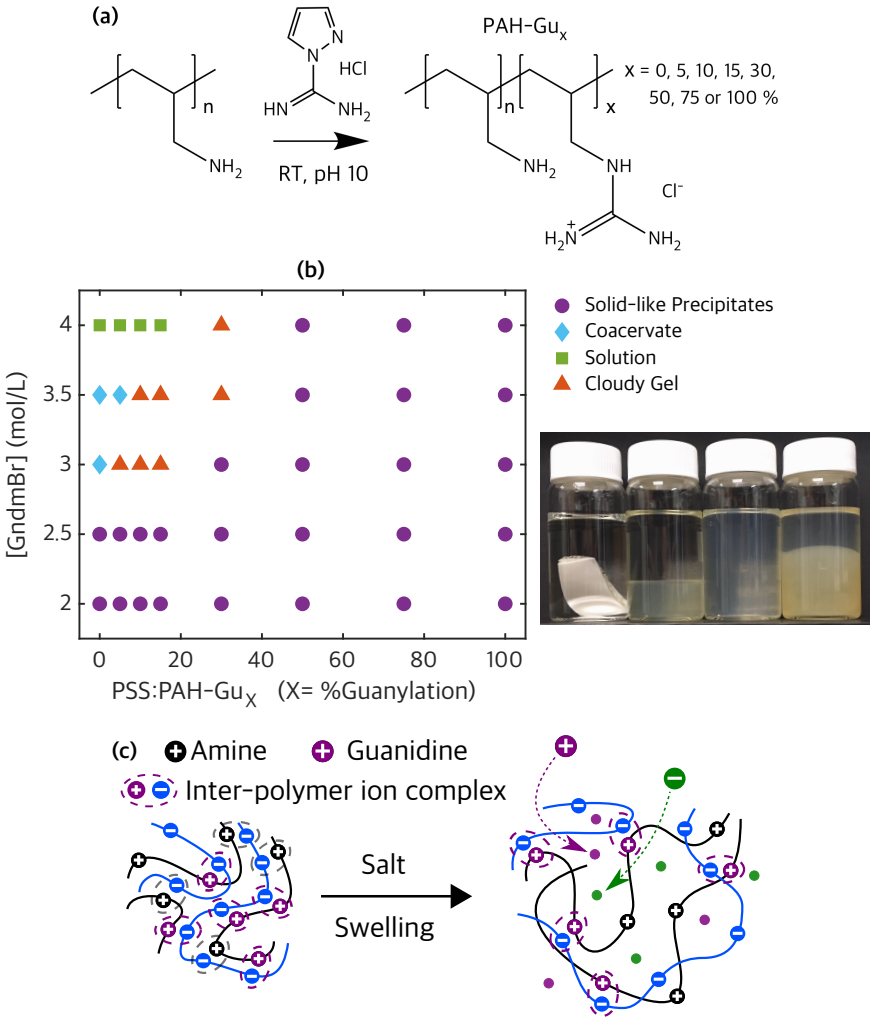

Figure 4.5: (a) Reaction scheme for systematic guanylation of poly(allylamine), (b) phenomenological phase behavior of PSS:PAH-Gu complexes as a function of guanylation percent at pH ≈ 6, and (c) schematic representation of a possible explanation for the observed phase behavior. Guanidinium is able to break the relatively strong ion-complex of styrene sulfonate with allylamine, but not allylguanidine.

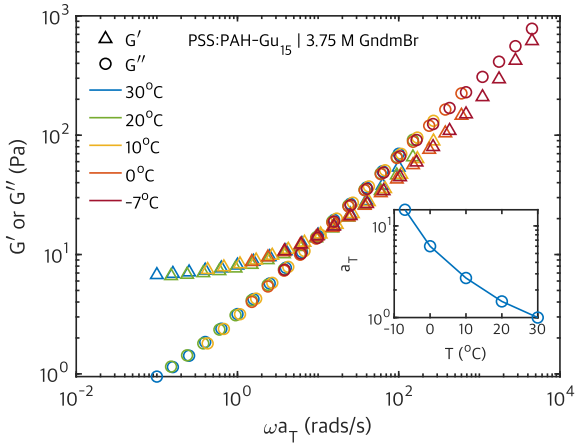

Figure 4.6: Rheological response of a complex of poly(styrenesulfonate) with 15% guanylated poly(allylamine). The typical power-law polymer solution response of coacervates as depicted for PSS:PAH in Figure 4.4 is lost when guanidinium is added directly onto the polyelectrolyte itself. Instead, the rheological response of a colloidal gel is observed, where the storage modulus is nearly independent of frequency at low frequencies. The colloidal gel rheological response supports the hypothesis that insoluble aggregates are forming, which likely also imparts the cloudiness.

4.3 Experimental Methods

Materials: Poly(styrene sulfonate) sodium salt (PSS, MW 200K g mol^{-1}) was purchased from Sigma-Aldrich, poly(4-vinylpyridine) (P4VP, MW 50K g mol^{-1}) from Scientific Polymers, and poly(allylamine) HCl (PAH, 120-200K g mol^{-1}) from Alfa Aesar. 1-bromoethane, potassium bromide, guanidinium bromide, and guanidinium thiocyanate were also purchased from Sigma-Aldrich. 1H-Pyrazole-1-carboxamidine hydrochloride was purchased from Chem-Impex International. Deionized water (conductivity ≈5 μS/cm) was used for making all solutions except when forming coacervates where 18.2 M Ω *cm MilliQ water was used. The pH of water used was observed to be between 5.5-7, as expected from dissolved carbon dioxide, and which is much lower than the pKa of poly(allylamine) at 8.5. Therefore, poly(allylamine) was assumed to be fully ionized.

Quaternization of poly(4-vinylpyridine): In our nomenclature we refer to ethyl substituted

P4VP as QVP-C2. QVP-C2 was synthesized by dissolving 10 wt% P4VP in dimethyl sulfoxide before adding a 30% molar excess of bromoethane. The solution was well stirred for 24 hours at 40^{o}C. This solution was used directly to synthesize the complex with poly(styrenesulfonate) and is discussed below.

Guanylation of poly(allylamine): 5-10 wt% PAH was dissolved in water and the pH was adjusted to ≈10 using sodium hydroxide. Stoichiometric amounts of 1H-Pyrazole-1-carboxamidine hydrochloride was added to the solution and stirred for 4 days at room temperature. Polymer was isolated using dialysis and lyophilization.

Stoichiometric PECs: Once the quaternization reaction was completed (in DMSO), a 1:1 repeat unit molar equivalent of PSS was dissolved in equivalent volume of water separately. This was done by noting the mass was initial P4VP that was quaternized followed by conversion to moles. The two solutions were then simultaneously added to a third beaker of water under stirring. The PECs precipitated out as a white solid that washed with deionized water until the solution conductivity fell to about 50 μS/cm. The precipitates were collected via vacuum filtration and then dried. Since pyridines can have poor thermal stability, the PECs were dried at 60^{o}C and in the presence of drierite for 12 hours to obtain the dry PEC. PSS:PAH complexes were made analogously after the guanylation reaction was completed.

Coacervates: Coacervates were formed from the dry PECs by dissolving them in appropriate salt solutions. In all cases, 1 g of dry PEC was dissolved in 10 ml of the salt solution using MilliQ water (18.2 MΩ cm). The salt concentrations where coacervation was observed was ≈1.5-1.9 M KBr for QVP-C2 and ≈3-3.75 M Guanidinium bromide/thiocyanate for PSS:PAH. The solutions were then well-stirred at room temperature overnight. Once the coacervate phase began to form the solution was annealed at 60^{o}C for 30 min. The solutions were then allowed to equilibrate between 1 week to 1 month, depending on the sample. Coacervates formed at low salt concentrations required longer equilibration times.

Quartz Crystal Rheometry: A custom quartz crystal microbalance (QCM, AWSensors, Valencia, Spain) was used in conjunction with a N2PK impedance analyzer (Thornhill, Canada) for swelling and viscoelastic measurements of spin-coated polyelectrolyte complex films. 1.5 μm polyelectrolyte complex films were directly spin-coated onto 1 inch quartz crystals with Au electrodes (Inficon, East Syracuse, NY) from the polymer-rich coacervate phase. Accurate QCM experiments require highly homogeneous and smooth films. Such high quality films could be obtained by spin-coating coacervates and then annealing them in intermediate ionic strength solutions to smooth the resulting film. Once the coacervate was spin-coated, PSS:QVP-C2 was annealed in 1.0 M KBr solution for 24 hours. PSS:PAH was annealed in 1.25 M GndmSCN for 24 hours. The final film was rinsed with excess deionized water to remove residual salt. The film was then dried over hot drierite to remove all water, and the dry areal mass, $(d\rho)_{dry}$, was recorded using the QCM. Here, d is the film thickness and ρ is the density. The swelling ratio after immersion salt solutions was then computed using Eq. 1.

$$Swelling\% = \frac{Weight_{water+salt}}{Weight_{polymer}} \times 100 = \frac{d\rho - (d\rho)_{dry}}{(d\rho)_{dry}} \times 100 \tag{4.1}$$

The QCM provides changes in the resonance frequency (Δf_n) and dissipation ($\Delta\Gamma_n$) of the piezoelectric quartz crystal at the odd nth harmonic of the fundamental frequency (5 MHz for the crystals used in this work). We monitor Δf_n and $\Delta\Gamma_n$ at n = 3, and 5 by fitting a Lorentzian peak to the conductance and susceptance in the frequency domain. While we prefer to use $\Delta\Gamma_n$, it is equivalent to the widely used QCM-D instrument that operates in the time domain, with $\Delta D_n = 2\Delta\Gamma_n/f_n$ where D is the dissipation factor and f_n is the oscillation frequency. The QCM data was analyzed using the open source *QCMD-Analyze* code to extract accurate viscoelastic properties.[4] More detailed sample preparation procedures and QCM rheometry were reported previously.[1,2]

Interfacial Tension Measurements: The interfacial tension (γ) of the polyelectrolytes used in this work was measured using the pendant drop method. A Kruss DSA100 drop shape analyzer

was used. A 12 μL drop of HPLC grade chloroform was formed in an embedding phase of 18.2 MΩ·cm water. The water/chloroform tension was measured for 10 min to verify that γ was $\approx$32 mN/m (the pristine tension), before polyelectrolyte solutions were injected such that the polymer concentration was 5 mM on a repeat unit basis.

PSS:PAH-Gu Phase behavior: Stock solutions of guanidinium bromide at 2, 2.5, 3, 3.5 and 4 mol/L was prepared. PAH was guanylated at different fractions and using the procedure outlined above and then dialyzed and lyophilized. PSS was lyophilized from the as received solution from the manufacturer. PSS and PAH-Gu were added to a 3 ml vial in a 1:1 ratio, for a total polymer mass $\approx$0.1 g. 1 ml of the stock solutions was added to the vial and the complex allowed to equilibrate for 2 months at room temperature. Visual sample characterization was performed for the solid-like complex, clear liquid-liquid phase separated coacervate, and single phase solutions. In cases where a cloudy gel was observed, larger samples where made and their rheological response recorded.

Rheology: Rheology was performed using an Anton-Paar MCR 302 rheometer with the cone−plate geometry. 50 mm diameter plates with a cone angle of 2° were used to perform frequency sweeps between 0.1 and 300 rads s^{-1}. A 1% strain amplitude was used which was verified to be well within the linear viscoelastic regime using amplitude sweeps. Once the coacervates were loaded, they were allowed to relax for at least 10 min at room temperature. Solvent evaporation was mitigated by placing a small trough of water around the bottom plate of the rheometer and isolating the sample inside a custom chamber.

Chapter 5

Polyelectrolytes at Oil/Water Interfaces

As of the submission of this thesis, this chapter consists of preliminary and unpublished work.

Abstract: Quantifying the behavior of highly charged molecules near hydrophobic interfaces is of paramount importance for many chemical and biological contexts, for example, to inform the design of new polymeric antibiotics to combat drug-resistant bacteria. While the behavior of amphiphilic molecules at interfaces has been well-studied due to their use as surfactants, the affinity of highly charged macromolecules for interfaces is unknown. In the present work, we utilize a set of model cationic polymers in the presence of different electrolytes to elucidate their adsorption behavior to oil/water interfaces. The presence of weakly solvated anions (I^-, SCN^-, ClO_4^-) enables the adsorption of highly cationic polymers, even under dilute conditions. The results suggest that ionic solvation of both the polyelectrolyte and the counterions plays a synergistic role in mediating adsorption to hydrophobic interfaces. These results also provide physical insight into how cationic molecules physically disrupt the bacterial cell membrane, providing an effective antimicrobial approach, and may inform the design of new future antibiotics.

5.1 Introduction

Elucidating the self-assembly mechanisms of highly charged molecules at hydrophobic interfaces is critical for understanding the transport of charge-containing molecules through biological membranes, and in the design of new polymeric antibiotics to combat drug resistant bacteria. Cationic macromolecules may preferentially interact with hydrophobic interfaces– such as the bacterial cell membrane– to physically disrupt its integrity, providing a powerful antimicrobial approach.[142, 151] Transport of biomolecular cargo can also be facilitated by highly charged macromolecules[152], however, the dominating non-covalent interactions that enable these phenomena are not yet well understood. Traditionally, small or large molecules with well-defined hydrocarbon segments are utilized to control adsorption, and consequently many commercial products such as paints, detergents and personal care paraphernalia rely on controlling molecular amphiphilicity to control stability or function. Due to these large commercial applications, hydrophobicity driven self-assembly of molecules to hard or soft interfaces has been well-studied.[153, 154, 155, 156] However, quantifying the behavior of highly charged macromolecules lacking any distinguishable hydrophobic segments at interfaces is of fundamental chemical and biological importance, and it requires consideration of the dielectric mismatch across the interface, ionic correlations, solvation effects, and polymer and counterion entropy.[7]

Interfacial tension, as measured by Drop Shape Apparatus, is a very useful method for determining the interfacial behavior of block ionomers. Interfacial tension can be measured by extracting the drop profile in time increments and fitting it to the Laplace equation (Eq. 5.1) as described in Figure 5.1. It is to be noted that the Laplace equation describes a balance between the surface tension γ, which tries to keep the spherical shape of the drop, and the density difference, which tries to pull the drop in an upward direction. A deformation of the drop, as shown in Figure 5.1, is indicative of changes in the interfacial tension, and is tracked by extracting the drop profile and fitting R_0, the radius of curvature at the apex, and B_0, the shape parameter, to calculate the inter-

facial tension γ.[157] In Eq. 5.1, $\Delta\rho$ is the difference in densities of the two liquids, and g is the acceleration due to gravity.

$$B_o = \frac{\Delta\rho g R_o^2}{\gamma} \tag{5.1}$$

5.2 Results and Discussion

We first consider a model experiment to build intuition behind the interfacial assembly of amphiphilic molecules. Figure 5.1b shows the synthesis of a block copolymer whose degree of amphiphilicity can be modulated by varying the charge fraction (f_q) on the P2VP block. Larger f_q result in a greater discrepancy in the solvophilic characters. Therefore, with increasing f_q the interfacial affinity is expected to increase, and interfacial tension measurements show that an increase in charge fraction is correlated with a significant drop in the interfacial tension at the chloroform-water interface (see Figure 5.2). This is due to increased adsorption of the block copolymers at the water-chloroform interface with increasing charge. The difference is largely insignificant from 0% to 4% charge, but is non-monotonic and larger in magnitude with subsequent increases in copolymer's charge fraction.

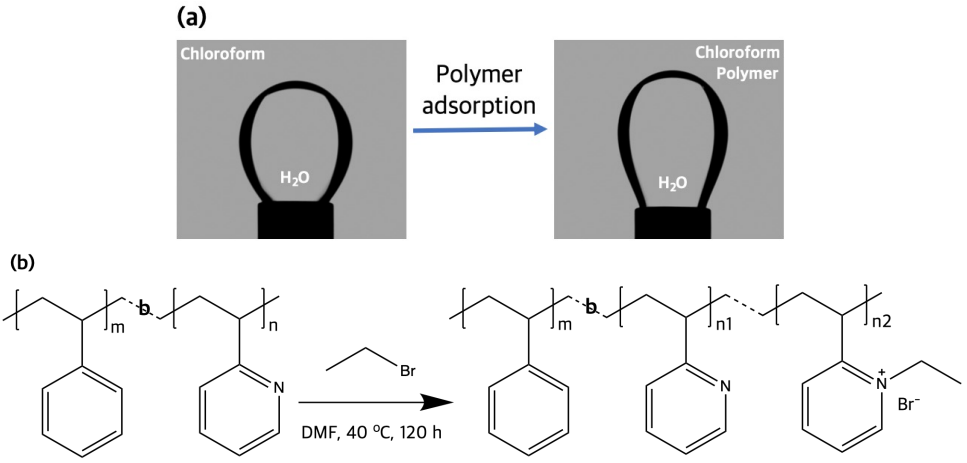

Figure 5.1: (a) Schematic for calculating the interfacial tension. Drop deformation is indicative of changes in the surface tension. The surface tension is calculated by fitting the drop profile and determining the shape parameter B_0 and radius of curvature R_0, which are related to the tension, γ, via Eq. 5.1. (b) Reaction scheme for quaternizing the poly(2-vinylpyridine) block of PS-b-P2VP with bromoethane. Here, poly(styrene) (PS) block remains hydrophobic, the unquaternized P2VP units are polar hydrophobic, and the quaternized units are ionizable and therefore hydrophilic.

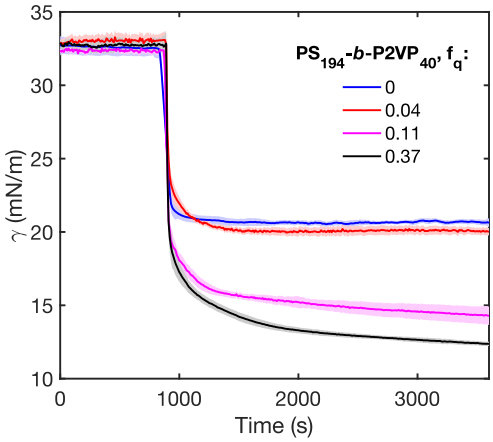

Figure 5.2: Interfacial tension of the diblock copolymer PS-*b*-P2VP at chloroform-water interface and at different charge fractions, f_q (degree of quaternization), for the P2VP block. The pristine water/chloroform tension is measured for 900 s to ensure absence of contaminants, before polymer injection into the chloroform phase resulting in adsorption. A substantial drop in interfacial tension is seen for all samples. Error bars are reported as the standard deviation of three measurements. Solution pH was mildly acidic due to carbonic acid buildup under ambient conditions, therefore the P2VP units were assumed to be partially charged (pK_a P2VP ≈ 5). These data were collected in collaboration with Ha-Kyung Kwon.

Let us now consider the interfacial behavior of a set of highly cationic polyelectrolytes that lack any significant hydrophobic segments in their molecular architecture. In the absence of well-defined hydrophobic moieties and the presence of ionizable charges, it is unclear whether the molecules would be interfacially active or not. The molecules shown in Figure 5.3a are polymer salts that gains considerable entropy by dissociating the ion-pars. Confining these molecules to any interface would result in significant loss of counterion configurational and polymer conformational entropy. The absence of anchoring hydrophobic segments here fails provide the usual driving force for adsorption. To gain physical insight about the behavior of highly charged polyelectrolytes, we measured the interfacial tension of a water/chloroform interface in the presence of poly(N-ethyl-4-vinylpyridinium) (QVP-C2). As shown in Figure 5.3b, we find that QVP-C2 has no discernible interfacial activity in the presence of sodium chloride, but that in the presence of sodium thiocyanate it is readily sequestered to the interface. The drop in tension with increasing thiocyanate concentration corresponds to an increasing equilibrium concentration of the adsorbates. This simple result implies that the nature of the (counter)ions present in solution can dictate the adsorption fate of highly charged macromolecules.

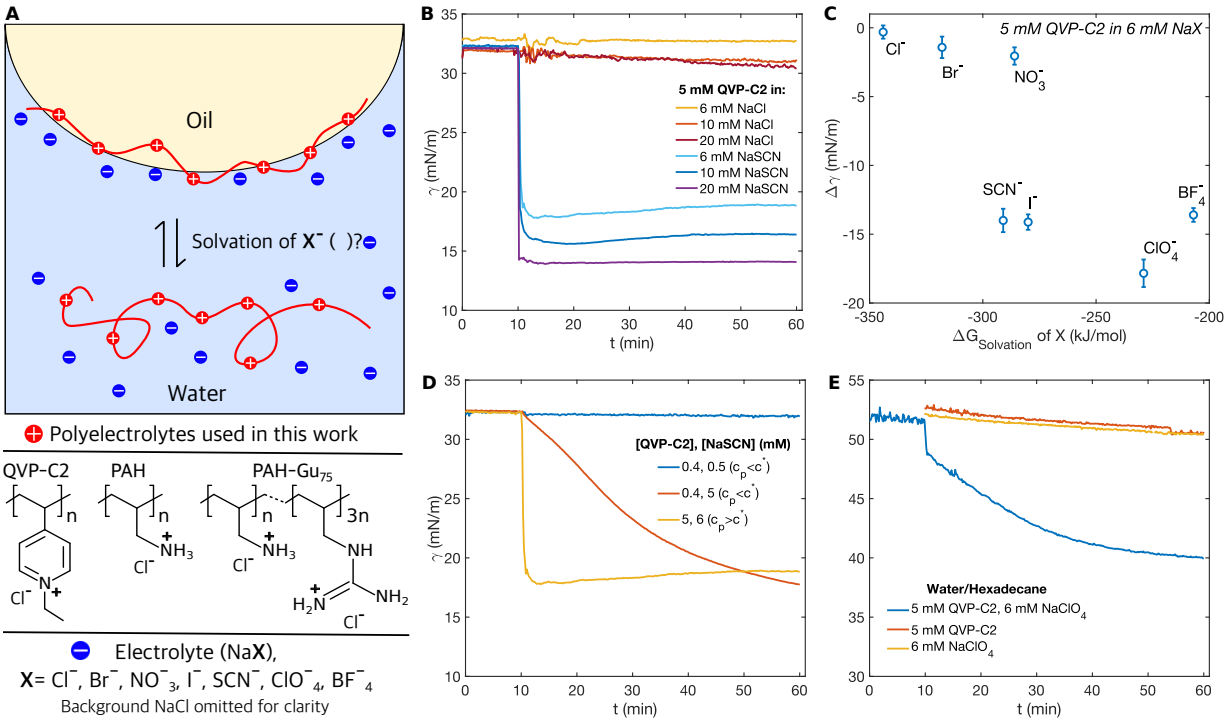

Figure 5.3: (a) Schematic representation of ion mediated adsorption of polyelectrolytes to hydrophobic interfaces. The chemical structures of the polymers used in the study are also shown. (b) Adsorption of QVP-C2 in the presence of NaCl and NaSCN to a chloroform interface. (c) Drop in chloroform interfacial tension ($\Delta\gamma$) as a function of the ions present in solution. Solvation of the anion controls the degree of association to the polyelectrolyte and the ultimate adsorption, which is seen as a drop in the interfacial tension. (d) Concentration effects on the adsorption process. (e) Universality of the adsorption is shown by the tendency of polyelectrolytes to adsorb to hexadecane interface in the presence of perchlorate.

The difference between the chloride and thiocyanate anions lies in their relative solvation states in water. Chlorine is considered to be a well solvated anion, while thiocyanate is the more poorly solvated specie. Ionic solvation can be quantified in terms of the solvation free energy, $\Delta G_{Solvation}$, where a more negative value represents a more well solvated ion.[158] To probe ionic solvation effects on the adsorption of QVP-C2, we utilized a series of anions as the supporting electrolyte, and measured the drop in interfacial tension relative to the pristine interface ($\Delta\gamma$) as a function of the $\Delta G_{Solvation}$ of the anion. Figure 5.3c shows that relatively well solvated anions such as Cl^-, Br^- and NO_3^- fail to sequester QVP-C2 to the interface. A transition in the adsoprtion behavior occurs

when the anion solvation reaches ≈-290 kJ/mol, where anions with $\Delta G_{Solvation}$ below this number (I^-, SCN^-, ClO_4^-, BF_4^-) all confine the polyelectrolyte to the interface. This suggests that depending on the solvation of the anions present in solution, the cationic polyelectrolyte may or may not be interfacially stable. While the trend in Figure 5.3c may entice one to invoke the Hofmeister series, it must be noted that this series is phenomenological (and reversed for cations), and that arguments directly employing solvation free energies are more robust. Table 1 reports that individually neither the electrolytes nor the polyelectrolytes have any interfacial activity in this concentration regime, confirming that both must be present simultaneously for adsorption to proceed synergistically.

It is now evident that the nature of the counter-ions or co-ions present in solution along with the polyelectrolyte mediates the adsorption behavior. Further thermodynamic insight can be gleaned by considering QVP-C2 adsorption at different concentrations. The relevant concentration benchmark for polyelectrolytes is the overlap concentration, c^*.[159] c^* depends on the ionic strength of the solution, and can be approximated by Eq 5.2.

$$c^* = \frac{3M_w}{4\pi N_A R_g^3} \tag{5.2}$$

Literature values of R_g for quaternized poly(viylpyridines) [159] can be used to estimate c^*, which we calculate to be 0.6-3.5 mM for QVP-C2 in salt-free conditions. Therefore, we now study the adsorption of QVP-C2 in the dilute ($c_p < c^*$) and semi-dilute ($c_p > c^*$) regimes as shown in Figure 5.3d. When the polymer and electrolyte are both dilute, entropy of mixing appears to prevent adsorption of QVP-C2 even when the electrolyte anion is the poorly solvated thiocyanate. However, when thiocyanate is present in significant excess of QVP-C2, the polyelectrolyte is consigned to the interface even under this dilute condition. In the semi-dilute regime, the polymer also adsorbs as long as the concentration of the of supporting electrolyte exceeds the polyelectrolyte concentration (Figure 5.3d). These results indicate that the concentration and the identity of the supporting electrolyte is the key determinant of polyelectrolyte adsorption. To explore the generality of solva-

tion mediated adsorption, we performed the same experiment with the water/hexadecane interface (Figure 5.3e), and find that the same phenomenon is observed as in water/chloroform.

Water/Chloroform Interface	
Solution	γ (mN/m)
Water/Chloroform	32.30 $\pm$0.05
5 mM QVP-C2	32.25 $\pm$0.20
6 mM NaCl	32.13 $\pm$0.10
6 mM NaBr	32.12 $\pm$0.10
6 mM $NaNO_3$	32.10 $\pm$0.07
6 mM NaI	32.42 $\pm$0.12
6 mM NaSCN	31.90 $\pm$0.10
6 mM $NaClO_4$	32.30 $\pm$0.07
6 mM $NaBF_4$	32.16 $\pm$0.10
5 mM PAH	32.30 $\pm$0.13
5 mm PAH-Gu_{75}	32.20 $\pm$0.11

Table 5.1: Individual polyelectrolyte solutions or salt solutions do not display any significant interfacial activity in this concentration regime. The tension remains close to the pristine value of $\approx$ 32.8 mN/m.

Understanding the behavior of charges near hydrophobic interfaces is significant for the design of cell-membrane disrupting antimicrobial macromolecules. In biology, the two prevalent cationic groups come from lysine and arginine. The most important difference between these two amino acids is their cationic charge identity, where lysine is a primary amine and arginine contains a guanidinium group. Despite this simple difference, it is arginine that is a recurrent motif in several interfacial contexts over lysine, such as in the RGD sequence involved in cell adhesion, cell-penetrating peptides, and antimicrobial molecules. Recently, we demonstrated that guanidinium possesses the ability to form strongly associating ion-complexes, which is possibly a contributing factor for its adhesion promoting properties, and here we seek to investigate it's behavior near hydrophobic interfaces. We hypothesize that guanidinium may potentially be a more interfacially active charge than amines, explaining it's enhanced presence in biological interfacial contexts. We use poly(allylamine) (PAH) and guanylated poly(allylamine) (PAH-Gu) as model approximations

for lysine-like and arginine-like macromolecules. Both PAH and PAH-Gu are highly cationic, and their simple architecture that is devoid of any secondary functionality (such as hydrogen bonding amide groups or hydrophobic domains) enables an unambiguous comparison of guanidines relative to amines in macromolecular constructs.

To study the interfacial activity of PAH and PAH-Gu, the interfacial tension of a semi-dilute solution of these polyelectrolytes with chloroform was measured, as listed in Table 5.1. The addition of guanidinium functionality to polly(allylamine) appears to endow no interfacial propensity under salt-free conditions. However, in the presence of poorly solvated electrolytes, PAH-Gu polyelectrolytes exhibit interfacial activity, while PAH remains agnostic, as shown in Figure 5.4. This suggests that the guanidinium groups inherently possess the capacity to interact with hydrophobic surfaces, but that this interaction must be facilitated by the accompanying counterions. Without counterion assistance, it appears that entropic losses from interfacial assembly remain too great. The combined polyelectrolyte and ion solvation effects can overcome this thermodynamic barrier and drive interfacial assembly.

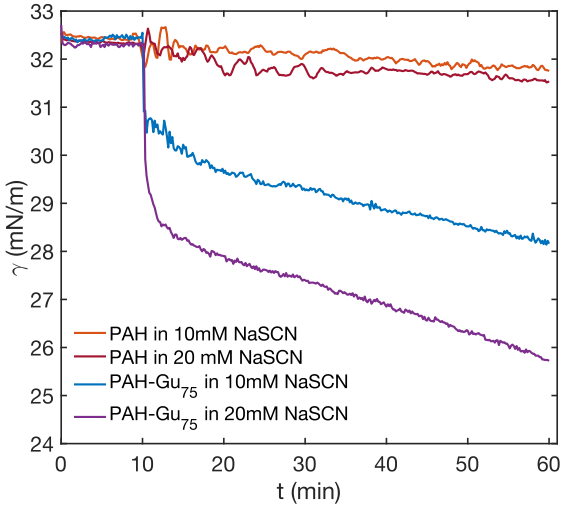

Figure 5.4: Adsorption of poly(allylamine) versus guanylated poly(allylamine). Guanidinium containing polyelectrolytes are interfacially active in the presence of weakly solvated anions, while their primary amine counterparts do not display any interfacial activity.

We now turn to MD simulations of our QVP-C2 polyelectrolyte to shed light on the interfacial segregation. A coarse-graining scheme as reported previously and again detailed in Figure 5.5 was used to model a 100 unit polyelectrolyte.[7] This length is assumed to be large enough such that the polymer is in the high molecular weight limit. The initial configuration of the polymer at t=0 was set near the interface in the presence of NaCl (Figure 5.6a) and NaI (Figure 5.6c). At t>0, the polymer is repelled from the interface for NaCl, while it strongly adsorbs for the NaI. Here, Figure 5.6d shows that iodine preferentially partitions to the interface with the help of the polymer. Figure 5.8 plots the iodine density as a function of distance from the interface for varying bulk iodine concentrations. A sharp peak in the density profile near the interface is observed in all cases, suggesting accumulation of the polymer and iodine in the interfacial region.

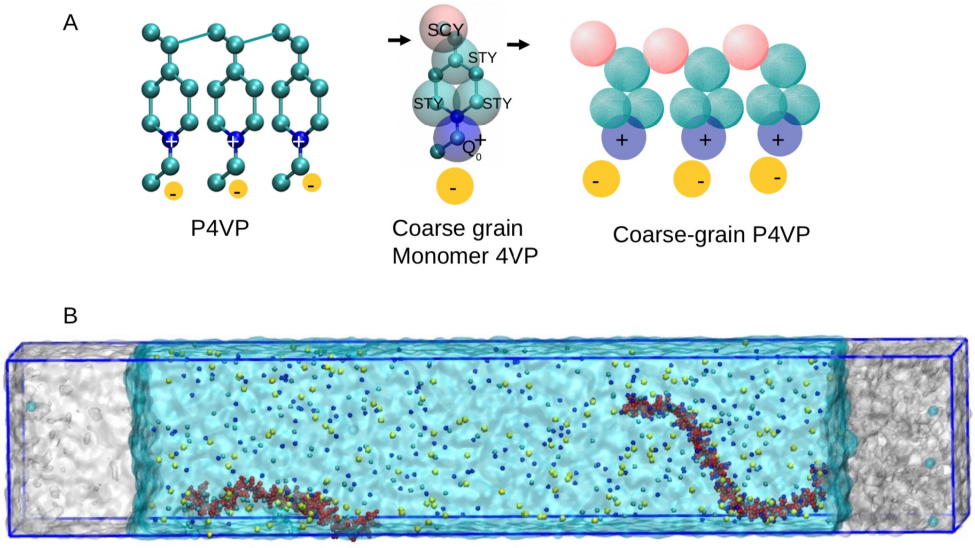

Figure 5.5: Models and simulation setup. A) Chemical structure of quaternized poly-4-vinylpiridine (QVP-C2); monomer coarse-grain model represented by five beads, and P4VP coarse-grain model. The beads color code is as follows: The polymer backbone groups are colored in pink (SCY); the hydrophobic ring groups are colored in cyan (STY); the quaternized group is colored in dark-blue (Q_0); the counterion is in yellow. B) The simulation cell is built by placing an aqueous phase between two liquid chloroform slabs. The total number of chloroform molecules is 12800. The aqueous phase is made of N_w=40000 water beads and N_s pairs of salt ions, N_c polymer counterions, and 2 polymer molecules. A water bead represents 4 water molecules. We varied the type of salt ions. The interaction between the particles is taken into account by means of the Martini force field parameters. MD simulations were performed by Felipe Jiménez-Ángeles.

The electrolyte composition is given in Table 1. The first two simulations are designed to study the adsorption of a single molecule on each interface; the box dimensions in the systems 1 and 2 are 10.5 nm x 10.5 nm x 56.5 nm in *x*, *y*, and *z* directions, respectively. In systems 3 to 6, 24 polymer molecules are distributed between the two interfaces; the box dimensions in the systems 3 to 6 are 20 nm x 20 nm x 71 nm in *x*, *y*, and *z* directions, respectively. Our simulation protocol consists of a 10 ns run to thermalize the system at P_z= 1 atm and T= 298 K; in this step we use the Berendsen thermostat (τ_T= 0.1 ps) and barostat (τ_P= 0.5 ps). The equilibration−production run is performed at P_z= 1 atm and T= 298 K for at least 160 ns. The integration of the Newton's equation of motion is performed using a time steps of 10 fs. The simulations are performed using 3-dimensional periodic boundary conditions are using the open source code GROMACS.

System	Electrolyte	N_{clf}	N_w	N_s	N_c	Chain length	$N_{QVP\text{-}C2}$
1	NaCl	12800	40000	200	100	100	2
2	NaI	12800	40000	100	100	100	2
3	NaCl	48000	176000	360	1440	60	24
4	NaI	48000	176000	360	1200 Cl^-+ 240 I^-	60	24
5	NaI	48000	176000	360	600 Cl^-+ 840 I^-	60	24
6	NaI	48000	176000	720	600 Cl^-+ 840 I^-	60	24

Table 5.2: System compositions used in MD simulations. The aqueous phase is made of N_w=40000 water beads and N_s pairs of salt ions, N_c polymer counterions.

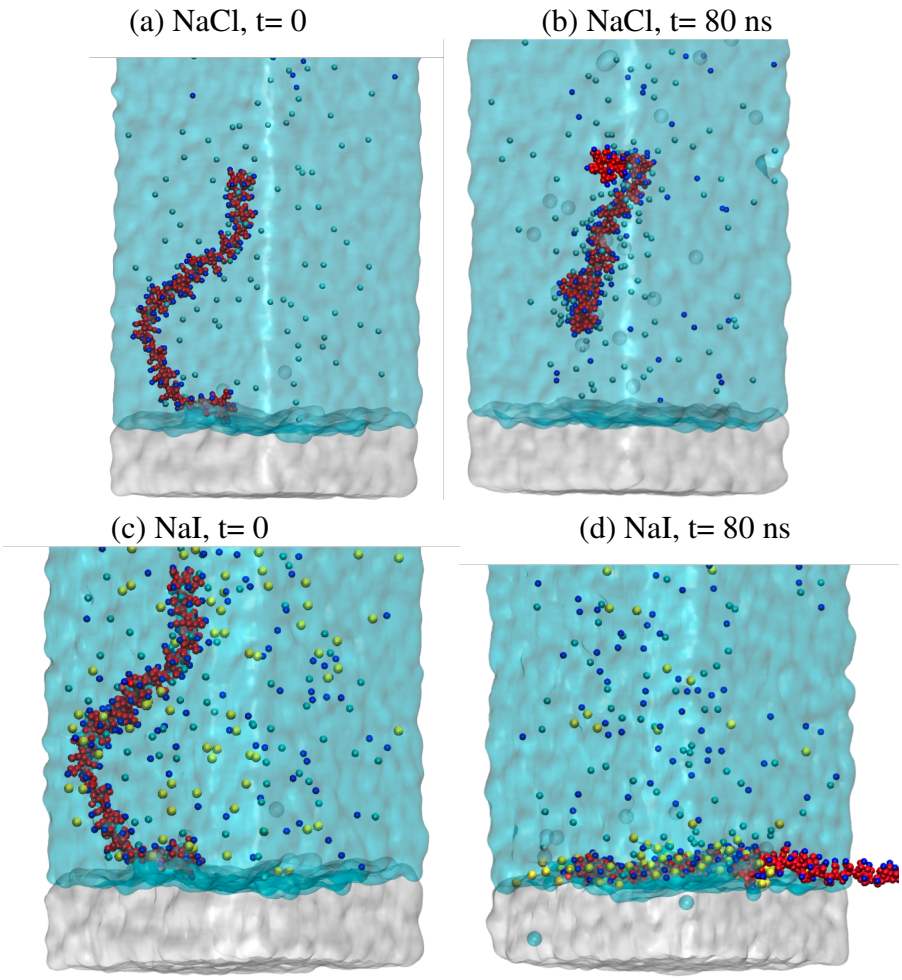

Figure 5.6: Molecular Dynamics (MD) simulations of QVP-C2 adsorbing to a chloroform/water interface. The coarse-grained model was used as previously described.[7] (a) and (b) describe the adsorption in the presence of NaCl, while (c) and (d) describes the adsorption in the presence of NaI for a 100 unit polymer. Note that in this case the polymer is 100% charged. The simulation conditions correspond to the systems 1 and 2 in Table 5.2. In both systems the simulations are started from very similar conditions by placing the polymer close to the liquid-liquid interface. This condition is selected to save computational time. The main difference between the two simulation is the composition of the electrolyte. In the NaCl system we observe that the polymers detach from the interface and move away from it into the aqueous solution. On the contrary, in the NaI system, the polymer is adsorbed and stays completely flat on the interface. MD simulations were performed by Felipe Jiménez-Ángeles.

Systems 3 to 6 in Table 5.2 are designed to study the collective adsorption of the polymer at the interface. We observe a significant difference in the polymer adsorption by changing the type

of electrolyte. Figure 5.7a shows the polymer desorbing from the interface when the electrolyte is NaCl and it moves into the aqueous phase. The calculated interfacial tension in system 3 is about 28.5 mN/m. When the electrolyte is NaI the polymer is completely adsorbed at the interface (Figure 5.7b). We observe that the polymer stays completely flat on the interface. The interfacial tension from the simulations of systems 4 to 6 is 26.6, 24.6, 24 mN/m.

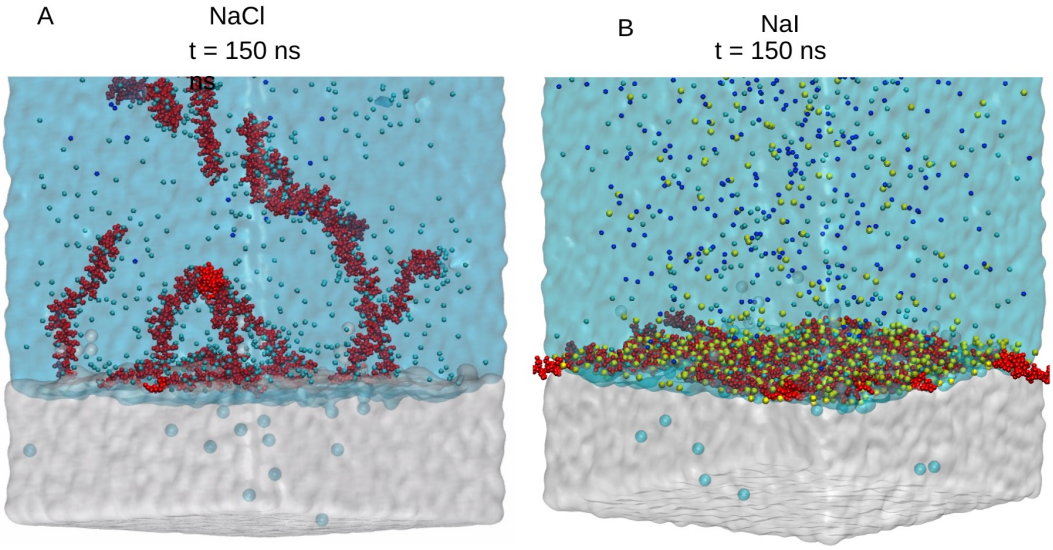

Figure 5.7: The collective adsorption of QVP-C2 in the presence and absence of NaI. The system compositions are 3 and 4 from table 5.2.

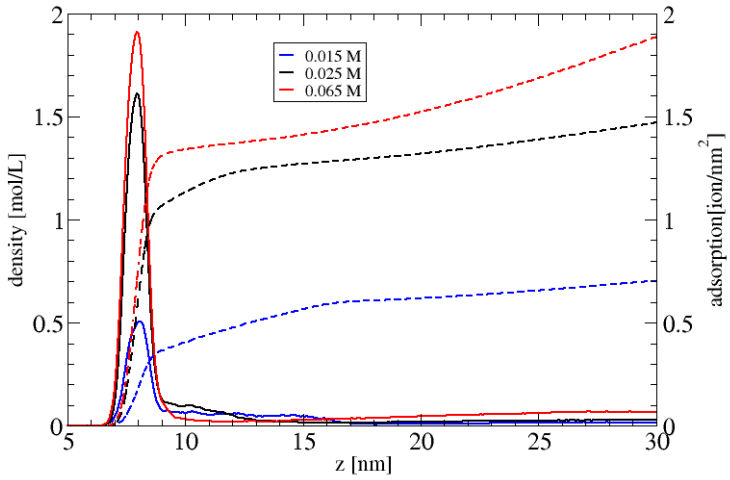

Figure 5.8: Density of iodine (solid lines) as a function of distance from the interface for the polymer model in Figure 5.6. The effect of increasing the bulk iodine concentration from 0.015 M to 0.065 M corresponding to systems 4-6 is shown. In all cases, a concentration peak is observed near the interface. The dashed lines correspond to the integral of the density peak, giving the adsorption in ions per area.

Figure 5.8 shows the I^- density profile from the simulation of systems 4 to 6 and the cumulative adsorption of I^-. The cumulative adsorption is calculated by integrating the density profile of I^-. The I^- bulk concentration is 0.015, 0.025, and 0.065 mol/L for systems 4, 5, and 6, respectively. A clear peak of adsorption of the I^- ion is observed at the interface. The height of the peak increases significantly by increasing the bulk concentration from 0.015 to 0.025 mol/L but it does not increases proportionally from 0.025 to 0.065 mol/L. This indicates that the interface is reaching a saturation point. The I^- adsorption including only the ions in the adsorption peak is about 0.35, 1.2 and 1.4 ions/nm^2 in the systems 4, 5, and 6, respectively.

Finally, we investigated the behavior of the ions at the interface without the polymer to gain insight into the adsorption mechanisms. The density profiles of pure NaCl and NaI are shown in Figure 5.9. In Figure 5.9a, the density profiles show that both, Na^+ and Cl^- ions, are desorbed from the interface. The ions are uniformly distributed away from both interface. Figure 5.9b shows that

the I^- ions are mildly adsorbed at the interface (see the adsorption peak) and in consequence the Na^+ ions form a diffuse distribution into the aqueous phase as a function of the separation distance to the interface. We hypothesize that the polymer adsorption is driven by the electrostatic attraction created by the ions adsorbed at the interface. In addition, the hydrophobic interaction between the polymer backbone and the chloroform contribute to stabilize the polymer adsorbed at the interface.

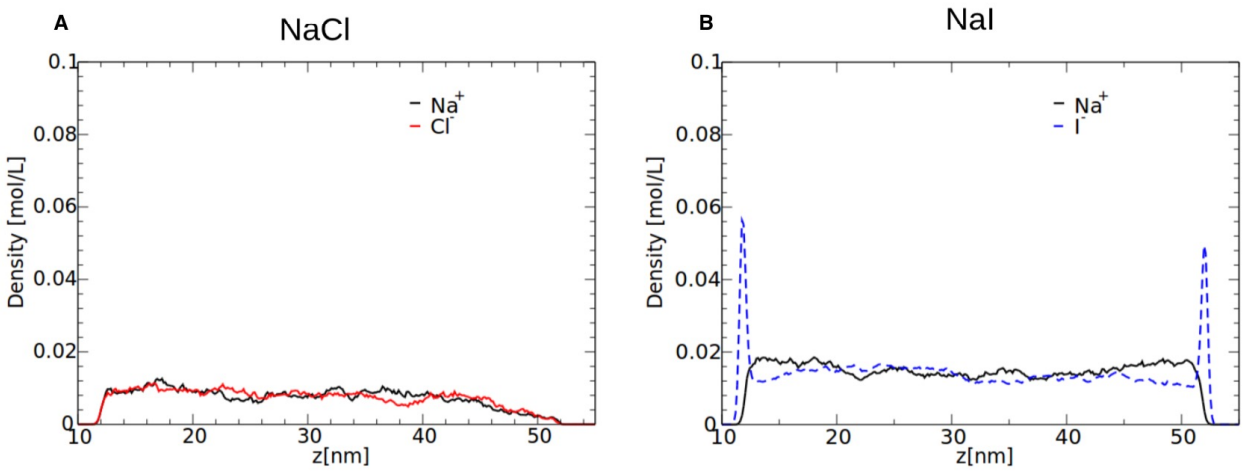

Figure 5.9: Interfacial behavior of pure salt solutions.

Chapter 6

Future Work, Outlook, and Summary

The work presented in this thesis has added to understanding the physical behavior of polyelectrolyte complexes and polyelectrolytes in general. The implications for future work from the context of this thesis is split into two sections. The first section discusses the more immediate work which can be performed to further extend the physical understanding of charged complexes. The second section identifies critical areas of study needed to significantly advance the field of complexes and polyelectrolytes from both an application and fundamental science standpoint.

6.1 Future Work

This thesis studied in detail the salt responsiveness, hydrophobicity, and ion-pairing affinity between oppositely charged polyelectrolytes. A simple yet fairly robust way to think about polyelectrolyte complexes is in terms of a Salt Resistance (Eq. 6.1), defined as the critical salt concentration needed to fully disassociate the complex by charge screening. The Salt Resistance of a complex comprising a particular polycation and a polyanion can be thought of as a function where different non-covalent interactions and physical parameters such as hydrophobicity, molecular weight, chain topology/architecture, ion-pairing strength, hydrogen-bonding, and salt identity can all contribute to the observed stability. Weakly associating complexes have a low salt resistance, while

on the other end of the spectrum, strongly associating complexes have a very high salt resistance and are frequently insoluble. Here, the salt used to dissolve the complex is very important, as we and others have demonstrated.[1, 40, 66, 127] Recently, the roles of hydrophobicity, salt identity, molecular weight, and even ion-pairing strength, has been studied in terms of the rheology, responsiveness, and phase behavior of PECs. The emerging picture from these studies, along with the results from Chapter 3 and 4, suggest that the water content of the complexes determines the rheological properties of the system.[1, 3, 40, 67, 68, 160, 161] However, investigations related to the chain topology/architecture[108] and hydrogen-bonding contributions[162] are much more rare. Of all the non-covalent interactions which affect the properties of PECs, hydrogen bonding contributions are the most poorly understood. Therefore, a significant effort must be dedicated to quantifying the role of this interaction in the context of PECs.

$$Salt\,Resistance = f(Hydrophobicity, Steric\,Effects, Molecular\,Weight, Molecular\,Architecture,$$

$$Ion-pairing\,Affinity, Hydrogen\,Bonding, Salt\,Identity) \tag{6.1}$$

This thesis has shown that the Salt Resistance function is non-trivial, and that individual non-covalent interactions are not coupled linearly. For example, in Chapter 3 we found that systematically increasing the hydrophobicity increased the salt resistance. This is perhaps intuitive, as a more hydrophobic complex is expected to swell less in response to salt. While we did not discuss steric hindrance effects directly in Chapter 3, we showed that increasing steric hindrance by adding longer carbon side chains (which should lower the salt resistance since individual ions may presumably penetrate the complex with better efficiency) did not appear to have an important effect, and that hydrophobic interactions were dominant. More investigations are needed on the role of steric hindrance in charged complexes. We also showed in Chapter 3 that marginally changing the hydrophobicity nearly modulated out the capability of better solvated salts to swell the complex,

meaning that hydrophobic effects manifest themselves with greater potency against better solvated ions. However, in Chapter 4 we showed that the more hydrophobic complex (PSS:QVP-C2) was actually *less* salt resistant compared to a complex which was more hydrophilic, but appears to have had a higher ion-pairing affinity (PSS:PAH).[40] These simple comparisons are deeply insightful, as it shows the importance of developing well thought out model systems where the effect of individual non-covalent interactions may be assessed unambiguously to effectively deconvolute the salt resistance function, because the individual interactions may be non-linearly coupled. To this end, it is hoped that the model systems of QVP molecules introduced in Chapter 3 and the guanylated poly(allylamine) introduced in Chapter 4 will find more prominent roles in future investigations.

Another important aspect of complexes that needs greater attention from the research community is their thermomechanical properties. Few investigations have tackled this problem adequately, and there is much room for more rigorous studies. Here, the QCM is uniquely suited to shed light on the temperature responsiveness, since it directly correlates the swelling behavior with mechanical properties.

The QCM in itself is a powerful instrument for characterizing the properties of thin soft materials, and it has been largely underutilized in soft materials research. While the availability of the QCM-D instrument would suggest that it should be a more mainstream analytical tool for polymer science, but the analysis usually provided with commercially available instruments has much need for improvement. Equally important is to educate potential users on its capabilities and limitations. To this end Chapter 1 demonstrated how the QCM can be used as an analytical tool, and importantly provided the thickness limitations for accurate viscoelastic modeling of polymer materials (Figure 1.8). This work has also made available a powerful MATLAB data analysis program that can directly analyze data from the popular QCM-D instrument (link here). It is hoped this thesis will act as a lighthouse for users of this instrument. Yet, much work needs to be done to further advertise and advocate the versatility and uniqueness of QCM rheology.

Finally, the preliminary results presented in Chapter 5 can easily be extended to study phase behavior of polyelectrolyte solutions as a function of the background electrolyte, since weakly solvated salts can precipitate some polycations. Mapping out this phase behavior where homogeneous solutions exist and where precipitates form using the three model polyelectrolytes introduced in Figure 5.3 will yield a physical picture of the competitive association behavior of counterions with the polymer. The concentration dependence of these behavior can be correlated with the observed oil/water interfacial tension drop. Taken together, this approach can inform a better understanding of the thermodynamics of polyelectrolyte solutions.

6.2 Outlook

The idea of salt induced dissolution of a PEC into a polymer solution, termed saloplasticity, is a powerful processing concept which needs to be investigated more deeply.[6, 66, 114] Our own recent work used this concept to control the porosity of water and solvent purification membranes.[4] The saloplastic concept is still in its infancy, and there is an immense opportunity for using this approach to solve both new and old problems. The stability of PECs in both organic and most aqueous environments, and their high temperature tolerance can easily be foreseen to be industrially useful. While it is difficult to speculate where PECs may find commercial use, we attempted to use saloplastic processing to create versatile membranes, and can offer another glimpse of a potential application. Methods of passive cooling of buildings and roofings by heat reflection are foreseen to be an important strategy for reducing heating costs. A recent advancement showed the use of hierarchically porous coatings which may be used to reflect a large spectrum of light, thereby reducing energy absorption.[163] There is a desire to make these coatings from aqueous solutions, due to fire and environmental safety concerns. We recently showed how hierarchically porous coatings/membranes may be synthesized from a coacervating solution.[4] Therefore, one use of these porous PEC coatings could be in the area of passive cooling, for which the optical

properties of porous complexes need to be studied.

A significant effort for PECs has always focused on biomedical applications (coatings, drug delivery, etc) from the days of polyelectrolyte multilayering. An emerging research thrust is now in the area of complexing proteins and biomolecules with synthetic polyelectrolytes to control their stability, delivery, or release.[164, 165] Analogously, polypeptides are being considered as biocompatible or biodegradable macromolecules instead of synthetic polyelectrolytes.[108, 110] Both of these efforts require rigorous investigations of phase behavior and salt responsiveness. Another important biologically relevant research area, especially for delivery applications, is in designing new block copolyelectrolyte approaches to self assembly.[166] These structures may assemble by association of two complexing polyelectrolyte blocks, which preserves a hydrophilic character where cargo may be loaded. Understanding the self-assembly pathways[167] and connecting the physical behavior of homopolyelectrolytes to the response of their block copolymer counterparts remains an important challenge. To this end, in Chapter 4 we made a comparison between the poly(allylamines) and poly(allylguanidines).[40] These molecules are Lysine-like and Arginine-like, respectively, which allow an unambiguous comparison of the effect of these two biologically relevant cationic charges in complexation. It is paramount to understand the differences of primary amines and guanidines in macromolecular contexts since this would enhance the knowledge of how cationic polymers interact with cell-membranes. Another important outstanding challenge is that currently there is very little work reported on complexes of polyphosphates. Since the charge on DNA helix is a phosphate, fundamental investigations are needed to show how polyphosphates associate with cationic polymers.

The bulk of this thesis has revolved around quantifying the physical behavior of complexes of oppositely charged polymers. Yet the responsiveness of these materials are a reflection of the individual ion-polyelectrolyte interactions. It is a much more difficult matter to quantitatively study the dynamics of polyelectrolyte solutions, but the in Chapter 5 we introduced interfacial ten-

sion measurements as an elegant method to study the competitive association between individual ions and polyelectrolytes. The dynamics of polyelectrolyte solutions are of significant chemical and biological importance, and in Chapter 5 we demonstrated how ion-specific interactions can mediate the adsorption of highly charged molecules to hydrophobic interfaces. Quantifying the behavior of highly cationic molecules with hydrophobic surfaces is of paramount importance in the development of new polymeric antibiotics, and here we again utilized the partially guanylated poly(allylamines) to show the difference in adsorption between primary amines and guanidines. Currently, there is a need to develop a more predictive theory of polyelectrolyte solutions, but in a series of insightful work Douglas et al. have shown how the polyelectrolyte-solvent or solvent-ion interactions may govern the thermodynamic properties of polyelectrolyte solutions.[168, 169, 170] These simulations ultimately may be adopted to elucidate how ion-mediated adsorption of polyelectrolytes to interfaces occur. This combined effort of the experimental interfacial data presented in this work along with Molecular Dynamics simulations may ultimately lead to a greater physical understanding of polyelectrolyte solutions. Furthermore, sophisticated experimental techniques such as X-ray reflectivity of Liquid-Liquid interfaces and X-ray Fluorescence Near Total Internal Reflection (XFNTR) may be utilized to directly probe the specific ion concentrations at oil/water interfaces.[171, 172, 173] These combined efforts can inform a new theory of polyelectrolyte solutions, heralding a significant advance in the field of polymer science.

6.3 Summary

This thesis attempted to paint a holistic mechanical picture of polyelectrolyte complexes (PECs) from solid-like materials to liquid-like coacervates. While the main thrust of the present work focused on PECs, an underlying theme here was the use of the quartz crystal microbalance (QCM) as an advanced fixed frequency rheometer. Chapter 1 provided the theoretical background and experimental suggestions needed to accurately extract viscoelastic properties of polymer thin films

using the QCM. The QCM proved to be a very useful tool for studying PECs because it enabled simultaneous measurement of the swelling ratio and the mechanical properties of the complex, resulting in the swelling-modulus and swelling-phase angle master curves shown in Figure 3.5. These master curves suggest that it is the water content of the complex which dictates properties. Another important aspect of PEC mechanical behavior is that they span the entire range of properties from glassy materials to polymer solutions. This mechanical spectrum was quantified using the QCM in Figure 3.3, which shows the continuous transition from rubbery solids to coacervate to single phase solution as a function of the KBr salt concentration. We identified the transition to the coacervate phase occurs around 1.0 M KBr and to a single phase solution around 1.8 M KBr for the model system of PSS:PDADMA. The swelling-modulus and the swelling-phase angle master curves along with the mechanical spectrum adds to the emergent picture for the mechanical behavior of PECs.

While PECs composed of strong polyelectrolytes proved to be excellent model systems to study non-covalent and ion-specific interactions in Chapters 3 and 4, it is desirable to understand the individual ion-polyelectrolyte interactions. It was demonstrated in Chapter 5 that interfacial tension measurement of polyelectrolyte solutions is a brilliant approach to study their dynamics. Preliminary results from Chapter 5 showed that the solvation of both the polymer and the accompanying counter or co-ions can play a synergistic role in enhancing hydrophobic effects. In the limit of highly charged molecules, hydrophobic effects manifest themselves in terms of solvation, which was elegantly demonstrated in Figure 5.3c. Figure 5.3c is deeply insightful as it shows that highly charged polyelectrolytes can self-assemble to hydrophobic interfaces against strong entropic penalties. Furthermore, the difference in adsorption between poly(allylamine) and poly(allylguanidine) in Figure 5.4 showed that guanidine is a more interfacially active charge than primary amines. This is the difference between Lysine and Arginine among amino acids, and it is Arginine which is a more recurrent theme in interfacial contexts such as in the RGD sequence of

cell-adhesion, cell-penetrating peptides, and antimicrobial macromolecules. However, the adsorption of poly(allylguanidine) had to be mediated by the counter or co-ions present in solution– again highlighting the synergistic role of ion-polyelectrolyte interactions in determining their behavior.

Returning to the QCM, it is hoped this body of work will act as a guide for new users of the instrument interested in viscoelastic analysis. The QCM's potential has largely not been realized by the polymer science community, and therefore there exists a significant opportunity to exploit its utility in soft matter research. One limitation the instrument has faced is that the viscoelastic analysis which can be performed using the popular QCM-D instrument is not adequately intuitive. Furthermore, there exists quantitative thickness limits which must be obeyed for accurate mechanical characterization. To these ends, the present work made two important contributions to the field of QCM rheometery. First, the thickness limits which need to be met for a polymer material with a certain complex shear modulus ($\rho|G_n^*|$) and or phase angle (ϕ) for accurate viscoelastic analysis was shown in Figure 1.8. For the best response, harmonic 3, 5 and 7 are recommended, and at these harmonics films $\approx$1-7 microns can be analyzed. Stiffer or glassier films require thicknesses on order of 5 microns, while softer films require thicknesses of about 1 microns. Second, the power-law frequency assumption was introduced as a much more realistic and robust approach for modeling viscoelastic data. A data analysis program (found here) was provided to directly analyze data from the popular QCM-D instrument.

Bibliography

[1] Kazi Sadman, Qifeng Wang, Yaoyao Chen, Bavand Keshavarz, Zhang Jiang, and Kenneth R. Shull. Influence of Hydrophobicity on Polyelectrolyte Complexation. *Macromolecules*, 50(23):9417–9426, December 2017.

[2] Kristopher D. Kelly and Joseph B. Schlenoff. Spin-Coated Polyelectrolyte Coacervate Films. *ACS Appl Mater Interfaces*, 7(25):13980–13986, July 2015.

[3] Yalin Liu, Brian Momani, H. Henning Winter, and Sarah L. Perry. Rheological characterization of liquid-to-solid transitions in bulk polyelectrolyte complexes. *Soft Matter*, 13(40):7332–7340, October 2017.

[4] Kazi Sadman, David E. Delgado, Yechan Won, Qifeng Wang, Kimberly A. Gray, and Kenneth R. Shull. Versatile and High-Throughput Polyelectrolyte Complex Membranes via Phase Inversion. *ACS Appl. Mater. Interfaces*, 11(17):16018–16026, May 2019.

[5] Kazi Sadman, Clinton G. Wiener, R. A. Weiss, Christopher C. White, Kenneth R. Shull, and Bryan D. Vogt. Quantitative Rheometry of Thin Soft Materials Using the Quartz Crystal Microbalance with Dissipation. *Anal. Chem.*, 90(6):4079–4088, March 2018.

[6] Qifeng Wang and Joseph B. Schlenoff. The Polyelectrolyte Complex/Coacervate Continuum. *Macromolecules*, 47(9):3108–3116, May 2014.

[7] Felipe Jiménez-Ángeles, Ha-Kyung Kwon, Kazi Sadman, Thomas Wu, Kenneth R. Shull, and Monica Olvera de la Cruz. Self-Assembly of Charge-Containing Copolymers at the

Liquid–Liquid Interface. *ACS Cent. Sci.*, 5(4):688–699, April 2019.

[8] David M. H. Kern. The Polarography and Standard Potential of the Oxygen-Hydrogen Peroxide Couple. *J Am Chem Soc*, 76(16):4208–4214, August 1954.

[9] Günter Sauerbrey. Verwendung von Schwingquarzen zur Wägung dünner Schichten und zur Mikrowägung. *Z. Für Phys. Hadrons Nucl.*, 155(2):206–222, April 1959.

[10] Markku Leskelä and Mikko Ritala. Atomic layer deposition (ALD): From precursors to thin film structures. *Thin Solid Films*, 409(1):138–146, April 2002.

[11] Steven M. George. Atomic Layer Deposition: An Overview. *Chem. Rev.*, 110(1):111–131, January 2010.

[12] K. Keiji. Kanazawa and Joseph G. Gordon. Frequency of a quartz microbalance in contact with liquid. *Anal. Chem.*, 57(8):1770–1771, July 1985.

[13] Kazi Sadman, Qifeng Wang, Shawn H. Chen, David E. Delgado, and Kenneth R. Shull. pH-Controlled Electrochemical Deposition of Polyelectrolyte Complex Films. *Langmuir*, 33(8):1834–1844, February 2017.

[14] Vadim Dargel, Netanel Shpigel, Sergey Sigalov, Prasant Nayak, Mikhael D. Levi, Leonid Daikhin, and Doron Aurbach. In situ real-time gravimetric and viscoelastic probing of surface films formation on lithium batteries electrodes. *Nat. Commun.*, 8(1):1389, November 2017.

[15] Nicolas Jäckel, Vadim Dargel, Netanel Shpigel, Sergey Sigalov, Mikhael D. Levi, Leonid Daikhin, Doron Aurbach, and Volker Presser. In situ multi-length scale approach to understand the mechanics of soft and rigid binder in composite lithium ion battery electrodes. *Journal of Power Sources*, 371:162–166, December 2017.

[16] Nico B. Eisele, Fredrik I. Andersson, Steffen Frey, and Ralf P. Richter. Viscoelasticity of Thin Biomolecular Films: A Case Study on Nucleoporin Phenylalanine-Glycine Repeats Grafted to a Histidine-Tag Capturing QCM-D Sensor. *Biomacromolecules*, 13(8):2322–

2332, August 2012.

[17] Elizabeth J. Martin, Robin Pourzal, Mathew T. Mathew, and Kenneth R. Shull. Dominant Role of Molybdenum in the Electrochemical Deposition of Biological Macromolecules on Metallic Surfaces. *Langmuir*, 29(15):4813–4822, April 2013.

[18] Pegah N. Abadian, Pranali J. Buch, Edgar D. Goluch, Jun Li, and Zheng Zhang. Real-Time Monitoring of Urinary Encrustation Using a Quartz Crystal Microbalance. *Anal. Chem.*, 90(3):1531–1535, February 2018.

[19] C. E. Reed, K. Keiji Kanazawa, and J. H. Kaufman. Physical description of a viscoelastically loaded AT-cut quartz resonator. *J. Appl. Phys.*, 68(5):1993–2001, September 1990.

[20] F. Nelson Nunalee, Kenneth R. Shull, Bruce P. Lee, and Phillip B. Messersmith. Quartz Crystal Microbalance Studies of Polymer Gels and Solutions in Liquid Environments. *Anal. Chem.*, 78(4):1158–1166, February 2006.

[21] D. Johannsmann, K. Mathauer, G. Wegner, and W. Knoll. Viscoelastic properties of thin films probed with a quartz-crystal resonator. *Phys. Rev. B*, 46(12):7808, 1992.

[22] Diethelm Johannsmann. Viscoelastic, mechanical, and dielectric measurements on complex samples with the quartz crystal microbalance. *Phys Chem Chem Phys*, 10(31):4516–4534, July 2008.

[23] Ilya Reviakine, Diethelm Johannsmann, and Ralf P. Richter. Hearing What You Cannot See and Visualizing What You Hear: Interpreting Quartz Crystal Microbalance Data from Solvated Interfaces. *Anal. Chem.*, 83(23):8838–8848, December 2011.

[24] Elizabeth J. Martin, Mathew T. Mathew, and Kenneth R. Shull. Viscoelastic Properties of Electrochemically Deposited Protein/Metal Complexes. *Langmuir*, 31(13):4008–4017, April 2015.

[25] Jingjing Wei, David A. Hoagland, Guangyu Zhang, and Zhaohui Su. Effect of Divalent Counterions on Polyelectrolyte Multilayer Properties. *Macromolecules*, 49(5):1790–1797,

March 2016.

[26] Hirokazu Tanoue, Norifumi L. Yamada, Kohzo Ito, and Hideaki Yokoyama. Quantitative Analysis of Polymer Brush Formation Kinetics Using Quartz Crystal Microbalance: Viscoelasticity of Polymer Brush. *Langmuir*, 33(21):5166–5172, May 2017.

[27] Stefan Adam, Meike Koenig, Keith Brian Rodenhausen, Klaus-Jochen Eichhorn, Ulrich Oertel, Mathias Schubert, Manfred Stamm, and Petra Uhlmann. Quartz crystal microbalance with coupled spectroscopic ellipsometry-study of temperature-responsive polymer brush systems. *Applied Surface Science*, 421:843–851, November 2017.

[28] Dehui Lin, Patricia Lopez-Sanchez, Nichola Selway, and Michael J. Gidley. Viscoelastic properties of pectin/cellulose composites studied by QCM-D and oscillatory shear rheology. *Food Hydrocolloids*, 79:13–19, June 2018.

[29] Judith Petri and Diethelm Johannsmann. Determination of the Shear Modulus of Thin Polymer Films with a Quartz Crystal Microbalance: Application to UV-Curing. *Anal. Chem.*, 91(2):1595–1602, January 2019.

[30] Connor R. Bilchak, Yucheng Huang, Brian C. Benicewicz, Christopher J Durning, and Sanat K. Kumar. High-Frequency Mechanical Behavior of Pure Polymer-Grafted Nanoparticle Constructs. *ACS Macro Lett.*, 8(3):294–298, March 2019.

[31] Michael Rodahl, Fredrik Höök, Anatol Krozer, Peter Brzezinski, and Bengt Kasemo. Quartz crystal microbalance setup for frequency and Q-factor measurements in gaseous and liquid environments. *Rev. Sci. Instrum*, 66(7):3924–3930, July 1995.

[32] Maria Claesson, Nam-Joon Cho, Curtis W. Frank, and Martin Andersson. Vesicle Adsorption on Mesoporous Silica and Titania. *Langmuir*, 26(22):16630–16633, November 2010.

[33] Maria Claesson, Akbar Ahmadi, Hoda M. Fathali, and Martin Andersson. Improved QCM-D signal-to-noise ratio using mesoporous silica and titania. *Sens. Actuators B Chem.*, 2012.

[34] J. A. Forrest, C. Svanberg, K. Révész, M. Rodahl, L. M. Torell, and B. Kasemo. Relaxation

dynamics in ultrathin polymer films. *Phys. Rev. E*, 58(2):R1226–R1229, August 1998.

[35] Sang-Wook Lee and Daeyeon Lee. Integrated Study of Water Sorption/Desorption Behavior of Weak Polyelectrolyte Layer-by-Layer Films. *Macromolecules*, 46(7):2793–2799, April 2013.

[36] Lauren F. Sturdy, Alexander Yee, Francesca Casadio, and Kenneth R. Shull. Quantitative characterization of alkyd cure kinetics with the quartz crystal microbalance. *Polymer*, 103:387–396, October 2016.

[37] M V Voinova, M Rodahl, M Jonson, and B Kasemo. Viscoelastic Acoustic Response of Layered Polymer Films at Fluid-Solid Interfaces: Continuum Mechanics Approach. *Phys. Scr.*, 59(5):391–396, May 1999.

[38] Francois Chambon and H. Henning Winter. Linear Viscoelasticity at the Gel Point of a Crosslinking PDMS with Imbalanced Stoichiometry. *Journal of Rheology*, 31(8):683–697, November 1987.

[39] Garret C. DeNolf, Lauren F. Sturdy, and Kenneth R. Shull. High-Frequency Rheological Characterization of Homogeneous Polymer Films with the Quartz Crystal Microbalance. *Langmuir*, 30(32):9731–9740, August 2014.

[40] Kazi Sadman, Qifeng Wang, and Kenneth R. Shull. Guanidinium Can Break and Form Strongly Associating Ion Complexes. *ACS Macro Lett.*, 8(2):117–122, February 2019.

[41] C. Joshua Yeh, Michael Hu, and Kenneth R. Shull. Oxygen Inhibition of Radical Polymerizations Investigated with the Rheometric Quartz Crystal Microbalance. *Macromolecules*, 51(15):5511–5518, August 2018.

[42] S. S. Bae, K. Chakrabarty, T. A. P. seery, and R. A. Weiss. Thermoprocessible Hydrogels. I. Synthesis and Properties of Polyacrylamides with Perfluoroalkyl Side Chains. *J. Macromol. Sci. A*, 36(7-8):931–948, January 1999.

[43] Jun Tian, Thomas A. P. Seery, and R. A. Weiss. Physically Cross-Linked Alkylacrylamide

Hydrogels: Phase Behavior and Microstructure. *Macromolecules*, 37(26):9994–10000, December 2004.

[44] Clinton G. Wiener, R. A. Weiss, and Bryan D. Vogt. Overcoming confinement limited swelling in hydrogel thin films using supramolecular interactions. *Soft Matter*, 10(35):6705–6712, August 2014.

[45] Jagoba J. Iturri Ramos, Stefan Stahl, Ralf P. Richter, and Sergio E. Moya. Water Content and Buildup of Poly(diallyldimethylammonium chloride)/Poly(sodium 4-styrenesulfonate) and Poly(allylamine hydrochloride)/Poly(sodium 4-styrenesulfonate) Polyelectrolyte Multilayers Studied by an in Situ Combination of a Quartz Crystal Microbalance with Dissipation Monitoring and Spectroscopic Ellipsometry. *Macromolecules*, 43(21):9063–9070, November 2010.

[46] Bryan D. Vogt, Eric K. Lin, Wen-li Wu, and Christopher C. White. Effect of Film Thickness on the Validity of the Sauerbrey Equation for Hydrated Polyelectrolyte Films. *J. Phys. Chem. B*, 108(34):12685–12690, August 2004.

[47] Christopher C. White and John L. Schrag. Theoretical predictions for the mechanical response of a model quartz crystal microbalance to two viscoelastic media: A thin sample layer and surrounding bath medium. *J. Chem. Phys.*, 111(24):11192–11206, December 1999.

[48] Michael C. Koetting and Nicholas A. Peppas. pH-Responsive poly(itaconic acid-co-N-vinylpyrrolidone) hydrogels with reduced ionic strength loading solutions offer improved oral delivery potential for high isoelectric point-exhibiting therapeutic proteins. *Int. J. Pharm.*, 471(1):83–91, August 2014.

[49] Eric Verploegen, Johannes Soulages, Mariel Kozberg, Tejia Zhang, Gareth McKinley, and Paula Hammond. Reversible Switching of the Shear Modulus of Photoresponsive Liquid-Crystalline Polymers. *Angewandte Chemie International Edition*, 48(19):3494–3498, April

2009.

[50] Daniel J. Schmidt, Fevzi Ç. Cebeci, Z. Ilke Kalcioglu, Samantha G. Wyman, Christine Ortiz, Krystyn J. Van Vliet, and Paula T. Hammond. Electrochemically Controlled Swelling and Mechanical Properties of a Polymer Nanocomposite. *ACS Nano*, 3(8):2207–2216, August 2009.

[51] Daniel J. Schmidt, Joshua S. Moskowitz, and Paula T. Hammond. Electrically Triggered Release of a Small Molecule Drug from a Polyelectrolyte Multilayer Coating. *Chem. Mater.*, 22(23):6416–6425, December 2010.

[52] David A. Brass and Kenneth R. Shull. Membrane-enhanced surface acoustic wave analysis of grafted polymer brushes. *J. Appl. Phys.*, 103(7):073517, 2008.

[53] David E. Delgado, Lauren F. Sturdy, Craig W. Burkhart, and Kenneth R. Shull. Validation of quartz crystal rheometry in the megahertz frequency regime. *J. Polym. Sci. Part B Polym. Phys.*, 0(0).

[54] Xuefeng Tang, Jiajie Fang, Xianbin Du, and Da-Ming Zhu. Probing the viscoelastic moduli of thin, soft films with a quartz crystal resonator. *J. Appl. Polym. Sci.*, 134(10):n/a–n/a, March 2017.

[55] Diethelm Johannsmann. *The Quartz Crystal Microbalance in Soft Matter Research*. Soft and Biological Matter. Springer International Publishing, Cham, 2015.

[56] Kris C. Wood, James Q. Boedicker, David M. Lynn, and Paula T. Hammond. Tunable Drug Release from Hydrolytically Degradable Layer-by-Layer Thin Films. *Langmuir*, 21(4):1603–1609, February 2005.

[57] Amy M Peterson, Christine Pilz-Allen, Tatiana Kolesnikova, Helmuth Möhwald, and Dmitry Shchukin. Growth Factor Release from Polyelectrolyte-Coated Titanium for Implant Applications. *ACS Appl Mater Interfaces*, 6(3):1866–1871, February 2014.

[58] Daria V. Andreeva, Dmitri Fix, Helmuth Möhwald, and Dmitry G. Shchukin. Self-

Healing Anticorrosion Coatings Based on pH-Sensitive Polyelectrolyte/Inhibitor Sandwich-like Nanostructures. *Adv Mater*, 20(14):2789–2794, July 2008.

[59] Qiang Zhao, Quanfu F. An, Yanli Ji, Jinwen Qian, and Congjie Gao. Polyelectrolyte complex membranes for pervaporation, nanofiltration and fuel cell applications. *J Membr Sci*, 379(1–2):19–45, September 2011.

[60] Sangsik Kim, Jun Huang, Yongjin Lee, Sandipan Dutta, Hee Young Yoo, Young Mee Jung, YongSeok Jho, Hongbo Zeng, and Dong Soo Hwang. Complexation and coacervation of like-charged polyelectrolytes inspired by mussels. *PNAS*, 113(7):E847–E853, February 2016.

[61] Marco Dompé, Francisco J. Cedano-Serrano, Olaf Heckert, Nicoline van den Heuvel, Jasper van der Gucht, Yvette Tran, Dominique Hourdet, Costantino Creton, and Marleen Kamperman. Thermoresponsive Complex Coacervate-Based Underwater Adhesive. *Adv. Mater.*, page 1808179, March 2019.

[62] S. S. Shiratori and M. F. Rubner. pH-Dependent Thickness Behavior of Sequentially Adsorbed Layers of Weak Polyelectrolytes. *Macromolecules*, 33(11):4213–4219, 2000.

[63] Tarek R. Farhat and Joseph B. Schlenoff. Corrosion Control Using Polyelectrolyte Multilayers. *Electrochem. Solid-State Lett.*, 5(4):B13–B15, January 2002.

[64] Koji Itano, Jeeyoung Choi, and Michael F. Rubner. Mechanism of the pH-Induced Discontinuous Swelling/Deswelling Transitions of Poly(allylamine hydrochloride)-Containing Polyelectrolyte Multilayer Films. *Macromolecules*, 38(8):3450–3460, April 2005.

[65] Adam J. Nolte, Robert E. Cohen, and Michael F. Rubner. A Two-Plate Buckling Technique for Thin Film Modulus Measurements: Applications to Polyelectrolyte Multilayers. *Macromolecules*, 39(14):4841–4847, July 2006.

[66] Ramy A. Ghostine, Rabih F. Shamoun, and Joseph B. Schlenoff. Doping and Diffusion in an Extruded Saloplastic Polyelectrolyte Complex. *Macromolecules*, 46(10):4089–4094,

May 2013.

[67] Lu Li, Samanvaya Srivastava, Marat Andreev, Amanda B. Marciel, Juan J. de Pablo, and Matthew V. Tirrell. Phase Behavior and Salt Partitioning in Polyelectrolyte Complex Coacervates. *Macromolecules*, 51(8):2988–2995, April 2018.

[68] Mo Yang, Jianbing Shi, and Joseph B. Schlenoff. Control of Dynamics in Polyelectrolyte Complexes by Temperature and Salt. *Macromolecules*, 52(5):1930–1941, March 2019.

[69] Paula T. Hammond. Engineering materials layer-by-layer: Challenges and opportunities in multilayer assembly. *AIChE J.*, 57(11):2928–2940, November 2011.

[70] Peter Bieker and Monika Schönhoff. Linear and Exponential Growth Regimes of Multilayers of Weak Polyelectrolytes in Dependence on pH. *Macromolecules*, 43(11):5052–5059, June 2010.

[71] Pierre Schaaf, Jean-Claude Voegel, Loïc Jierry, and Fouzia Boulmedais. Spray-Assisted Polyelectrolyte Multilayer Buildup: From Step-by-Step to Single-Step Polyelectrolyte Film Constructions. *Adv Mater*, 24(8):1001–1016, February 2012.

[72] Li Xu, Denis Pristinski, Aliaksandr Zhuk, Chris Stoddart, John F. Ankner, and Svetlana A. Sukhishvili. Linear versus Exponential Growth of Weak Polyelectrolyte Multilayers: Correlation with Polyelectrolyte Complexes. *Macromolecules*, 45(9):3892–3901, May 2012.

[73] Chungyeon Cho, Ju-Won Jeon, Jodie Lutkenhaus, and Nicole S. Zacharia. Electric Field Induced Morphological Transitions in Polyelectrolyte Multilayers. *ACS Appl. Mater. Interfaces*, 5(11):4930–4936, June 2013.

[74] I Krylova. Painting by electrodeposition on the eve of the 21st century. *Prog Org Coat*, 42(3–4):119–131, September 2001.

[75] Kevin C. Krogman, Joseph L. Lowery, Nicole S. Zacharia, Gregory C. Rutledge, and Paula T. Hammond. Spraying asymmetry into functional membranes layer-by-layer. *Nat Mater*, 8(6):512–518, June 2009.

[76] T. Garnier, A. Dochter, N. T. T. Chau, P. Schaaf, L. Jierry, and F. Boulmedais. Surface confined self-assembly of polyampholytes generated from charge-shifting polymers. *Chem. Commun.*, 51(74):14092–14095, 2015.

[77] Alexandre Dochter, Tony Garnier, Elodie Pardieu, Nguyet Trang Thanh Chau, Clément Maerten, Bernard Senger, Pierre Schaaf, Loïc Jierry, and Fouzia Boulmedais. Film Self-Assembly of Oppositely Charged Macromolecules Triggered by Electrochemistry through a Morphogenic Approach. *Langmuir*, 31(37):10208–10214, September 2015.

[78] A. Pascal Ngankam and Paul R. Van Tassel. Continuous polyelectrolyte adsorption under an applied electric potential. *PNAS*, 104(4):1140–1145, January 2007.

[79] Young Hoon Ko, Young Hun Kim, Juhyun Park, Ki Tae Nam, Jong Hyeok Park, and Pil J. Yoo. Electric-Field-Assisted Layer-by-Layer Assembly of Weakly Charged Polyelectrolyte Multilayers. *Macromolecules*, 44(8):2866–2872, April 2011.

[80] Paul R. Van Tassel. Polyelectrolyte adsorption and layer-by-layer assembly: Electrochemical control. *Curr Opin Colloid Interface Sci*, 17(2):106–113, April 2012.

[81] Gaulthier Rydzek, Qingmin Ji, Mao Li, Pierre Schaaf, Jonathan P. Hill, Fouzia Boulmedais, and Katsuhiko Ariga. Electrochemical nanoarchitectonics and layer-by-layer assembly: From basics to future. *Nano Today*, 10(2):138–167, 2015.

[82] Sara Nilsson, Fredrik Björefors, and Nathaniel D. Robinson. Electrochemical quartz crystal microbalance study of polyelectrolyte film growth under anodic conditions. *Applied Surface Science*, 280:783–790, September 2013.

[83] Elizabeth J. Martin, Kazi Sadman, and Kenneth R. Shull. Anodic Electrodeposition of a Cationic Polyelectrolyte in the Presence of Multivalent Anions. *Langmuir*, 32(31):7747–7756, August 2016.

[84] W.M. Haynes. *CRC Handbook of Chemistry and Physics*. CRC Press, 95 edition, 2014.

[85] Comsol Multiphysics 5.2 Corrosion Module Users Guide. November 2015.

[86] Xi-Liang Luo, Jing-Juan Xu, Ying Du, and Hong-Yuan Chen. A glucose biosensor based on chitosan–glucose oxidase–gold nanoparticles biocomposite formed by one-step electrodeposition. *Anal Biochem*, 334(2):284–289, November 2004.

[87] Xin Pang and Igor Zhitomirsky. Electrophoretic deposition of composite hydroxyapatite-chitosan coatings. *Mater. Charact.*, 58(4):339–348, April 2007.

[88] Yangshuai Liu, Dan Luo, Mustafa S. Ata, Tianshi Zhang, Cameron J. Wallar, and Igor Zhitomirsky. Universal dispersing agent for electrophoretic deposition of inorganic materials with improved adsorption, triggered by chelating monomers. *J. Colloid Interface Sci.*, 462:1–8, January 2016.

[89] Karen L. Stewart and Andrew A. Gewirth. Mechanism of Electrochemical Reduction of Hydrogen Peroxide on Copper in Acidic Sulfate Solutions. *Langmuir*, 23(19):9911–9918, September 2007.

[90] Marc Gerlache, ZÜHre Senturk, Guy Quarin, and Jean-Michel Kauffmann. Electrochemical behavior of H2O2 on gold. *Electroanalysis*, 9(14):1088–1092, October 1997.

[91] Rungsima Chollakup, Wirasak Smitthipong, Claus D. Eisenbach, and Matthew Tirrell. Phase Behavior and Coacervation of Aqueous Poly(acrylic acid)-Poly(allylamine) Solutions. *Macromolecules*, 43(5):2518–2528, March 2010.

[92] Mikko Salomäki and Jouko Kankare. Modeling the Growth Processes of Polyelectrolyte Multilayers Using a Quartz Crystal Resonator. *J Phys Chem B*, 111(29):8509–8519, July 2007.

[93] Bin Sun, Christopher M. Jewell, Nathaniel J. Fredin, and David M. Lynn. Assembly of Multilayered Films Using Well-Defined, End-Labeled Poly(acrylic acid): Influence of Molecular Weight on Exponential Growth in a Synthetic Weak Polyelectrolyte System. *Langmuir*, 23(16):8452–8459, July 2007.

[94] Biao Han, Daphney R. Chery, Jie Yin, X. Lucas Lu, Daeyeon Lee, and Lin Han. Nanome-

chanics of layer-by-layer polyelectrolyte complexes: A manifestation of ionic cross-links and fixed charges. *Soft Matter*, 12(4):1158–1169, January 2016.

[95] Jad A. Jaber and Joseph B. Schlenoff. Mechanical Properties of Reversibly Cross-Linked Ultrathin Polyelectrolyte Complexes. *J Am Chem Soc*, 128(9):2940–2947, March 2006.

[96] Jad A. Jaber and Joseph B. Schlenoff. Dynamic Viscoelasticity in Polyelectrolyte Multilayers: Nanodamping. *Chem. Mater.*, 18(24):5768–5773, November 2006.

[97] Evan Spruijt, Martien A. Cohen Stuart, and Jasper van der Gucht. Linear Viscoelasticity of Polyelectrolyte Complex Coacervates. *Macromolecules*, 46(4):1633–1641, February 2013.

[98] Shannon M. Notley, Simon Biggs, Vincent S. J. Craig, and Lars W˚agberg. Adsorbed layer structure of a weak polyelectrolyte studied by colloidal probe microscopy and QCM-D as a function of pH and ionic strength. *Phys Chem Chem Phys*, 6(9):2379–2386, 2004.

[99] Shannon M. Notley, Malin Eriksson, and Lars W˚agberg. Visco-elastic and adhesive properties of adsorbed polyelectrolyte multilayers determined in situ with QCM-D and AFM measurements. *J. Colloid Interface Sci.*, 292(1):29–37, December 2005.

[100] J. D. Mendelsohn, C. J. Barrett, V. V. Chan, A. J. Pal, A. M. Mayes, and M. F. Rubner. Fabrication of Microporous Thin Films from Polyelectrolyte Multilayers. *Langmuir*, 16(11):5017–5023, May 2000.

[101] Olga E. Philippova, Dominique Hourdet, Roland Audebert, and Alexei R. Khokhlov. pH-Responsive Gels of Hydrophobically Modified Poly(acrylic acid). *Macromolecules*, 30(26):8278–8285, December 1997.

[102] Lev Bromberg. Properties of Aqueous Solutions and Gels of Poly(ethylene oxide)-b-poly(propylene oxide)-b-poly(ethylene oxide)-g-poly(acrylic acid). *J Phys Chem B*, 102(52):10736–10744, December 1998.

[103] C. Tanford. The hydrophobic effect and the organization of living matter. *Science*, 200(4345):1012–1018, June 1978.

[104] L. Lins and R. Brasseur. The hydrophobic effect in protein folding. *FASEB J*, 9(7):535–540, January 1995.

[105] Tae-Young Heo, Inhye Kim, Liwen Chen, Eunji Lee, Sangwoo Lee, and Soo-Hyung Choi. Effect of Ionic Group on the Complex Coacervate Core Micelle Structure. *Polymers*, 11(3):455, March 2019.

[106] Yaoyao Chen and Kenneth R. Shull. High-Toughness Polycation Cross-Linked Triblock Copolymer Hydrogels. *Macromolecules*, 50(9):3637–3646, May 2017.

[107] Ran Shi, Tao Lin Sun, Feng Luo, Tasuku Nakajima, Takayuki Kurokawa, Yue Zhen Bin, Michael Rubinstein, and Jian Ping Gong. Elastic–Plastic Transformation of Polyelectrolyte Complex Hydrogels from Chitosan and Sodium Hyaluronate. *Macromolecules*, 51(21):8887–8898, November 2018.

[108] Brandon M. Johnston, Cameron W. Johnston, Rachel A. Letteri, Tyler K. Lytle, Charles E. Sing, Todd Emrick, and Sarah L. Perry. The effect of comb architecture on complex coacervation. *Org. Biomol. Chem.*, 15(36):7630–7642, 2017.

[109] Joseph B. Schlenoff, Amir H. Rmaile, and Claudiu B. Bucur. Hydration Contributions to Association in Polyelectrolyte Multilayers and Complexes: Visualizing Hydrophobicity. *J. Am. Chem. Soc.*, 130(41):13589–13597, October 2008.

[110] Sara Tabandeh and Lorraine Leon. Engineering Peptide-Based Polyelectrolyte Complexes with Increased Hydrophobicity. *Molecules*, 24(5):868, January 2019.

[111] M. Tekaat, D. Bütergerds, M. Schönhoff, A. Fery, and C. Cramer. Scaling properties of the shear modulus of polyelectrolyte complex coacervates: A time-pH superposition principle. *Phys. Chem. Chem. Phys.*, 17(35):22552–22556, August 2015.

[112] Jingcheng Fu and Joseph B. Schlenoff. Driving Forces for Oppositely Charged Polyion Association in Aqueous Solutions: Enthalpic, Entropic, but Not Electrostatic. *J Am Chem Soc*, 138(3):980–990, January 2016.

[113] Evan Spruijt. Relaxation Dynamics at Different Time Scales in Electrostatic Complexes: Time-Salt Superposition. *Phys. Rev. Lett.*, 105(20), 2010.

[114] Pierre Schaaf and Joseph B. Schlenoff. Saloplastics: Processing Compact Polyelectrolyte Complexes. *Adv. Mater.*, 27(15):2420–2432, April 2015.

[115] Samim Ali, Markus Bleuel, and Vivek M. Prabhu. Lower Critical Solution Temperature in Polyelectrolyte Complex Coacervates. *ACS Macro Lett.*, 8(3):289–293, March 2019.

[116] Johan Mähler and Ingmar Persson. A Study of the Hydration of the Alkali Metal Ions in Aqueous Solution. *Inorg Chem*, 51(1):425–438, January 2012.

[117] Yun Wang, Veronika Kozlovskaya, Imee G. Arcibal, Donald M. Cropek, and Eugenia Kharlampieva. Highly swellable ultrathin poly(4-vinylpyridine) multilayer hydrogels with pH-triggered surface wettability. *Soft Matter*, 9(39):9420–9429, 2013.

[118] Eugenia Kharlampieva and Svetlana A. Sukhishvili. Ionization and pH Stability of Multilayers Formed by Self-Assembly of Weak Polyelectrolytes. *Langmuir*, 19(4):1235–1243, February 2003.

[119] Aditya Jaishankar and Gareth H. McKinley. Power-law rheology in the bulk and at the interface: Quasi-properties and fractional constitutive equations. *Proc. R. Soc. A*, 469(2149):20120284, January 2013.

[120] Damian Craiem and Richard L Magin. Fractional order models of viscoelasticity as an alternative in the analysis of red blood cell (RBC) membrane mechanics. *Phys Biol*, 7(1):13001, January 2010.

[121] R. L. Bagley and P. J. Torvik. A Theoretical Basis for the Application of Fractional Calculus to Viscoelasticity. *Journal of Rheology*, 27(3):201–210, June 1983.

[122] Liviu-Iulian Palade, Vicent Verney, and Pierre Attané. A modified fractional model to describe the entire viscoelastic behavior of polybutadienes from flow to glassy regime. *Rheola Acta*, 35(3):265–273, May 1996.

[123] Z. Tang, Y. Wang, P. Podsiadlo, and N. A. Kotov. Biomedical Applications of Layer-by-Layer Assembly: From Biomimetics to Tissue Engineering. *Adv. Mater.*, 18(24):3203–3224, December 2006.

[124] Xiangxi Meng, Jessica D. Schiffman, and Sarah L. Perry. Electrospinning Cargo-Containing Polyelectrolyte Complex Fibers: Correlating Molecular Interactions to Complex Coacervate Phase Behavior and Fiber Formation. *Macromolecules*, 51(21):8821–8832, November 2018.

[125] Jingcheng Fu, Hadi M. Fares, and Joseph B. Schlenoff. Ion-Pairing Strength in Polyelectrolyte Complexes. *Macromolecules*, 50(3):1066–1074, February 2017.

[126] Alessandro Borgia, Madeleine B. Borgia, Katrine Bugge, Vera M. Kissling, Pétur O. Heidarsson, Catarina B. Fernandes, Andrea Sottini, Andrea Soranno, Karin J. Buholzer, Daniel Nettels, Birthe B. Kragelund, Robert B. Best, and Benjamin Schuler. Extreme disorder in an ultrahigh-affinity protein complex. *Nature*, 555(7694):61–66, March 2018.

[127] Samim Ali and Vivek M. Prabhu. Relaxation Behavior by Time-Salt and Time-Temperature Superpositions of Polyelectrolyte Complexes from Coacervate to Precipitate. *Gels*, 4(1):11, January 2018.

[128] Brian W. Stanton, Jeremy J. Harris, Matthew D. Miller, and Merlin L. Bruening. Ultrathin, Multilayered Polyelectrolyte Films as Nanofiltration Membranes. *Langmuir*, 19(17):7038–7042, August 2003.

[129] Gleb B. Sukhorukov, Johannes Schmitt, and Gero Decher. Reversible swelling of polyanion/polycation multilayer films in solutions of different ionic strength. *Berichte Bunsenges. Für Phys. Chem.*, 100(6):948–953, June 1996.

[130] Zsombor Feldötö, Imre Varga, and Eva Blomberg. Influence of Salt and Rinsing Protocol on the Structure of PAH/PSS Polyelectrolyte Multilayers. *Langmuir*, 26(22):17048–17057, November 2010.

[131] Stephan T. Dubas and Joseph B. Schlenoff. Swelling and Smoothing of Polyelectrolyte Multilayers by Salt. *Langmuir*, 17(25):7725–7727, December 2001.

[132] Jad A. Jaber and Joseph B. Schlenoff. Counterions and Water in Polyelectrolyte Multilayers: A Tale of Two Polycations. *Langmuir*, 23(2):896–901, January 2007.

[133] Hadi M. Fares, Qifeng Wang, Mo Yang, and Joseph B. Schlenoff. Swelling and Inflation in Polyelectrolyte Complexes. *Macromolecules*, 52(2):610–619, January 2019.

[134] Adam J. Nolte, Michael F. Rubner, and Robert E. Cohen. Determining the Young's Modulus of Polyelectrolyte Multilayer Films via Stress-Induced Mechanical Buckling Instabilities. *Macromolecules*, 38(13):5367–5370, June 2005.

[135] Valentin V. Lulevich and Olga I. Vinogradova. Effect of pH and Salt on the Stiffness of Polyelectrolyte Multilayer Microcapsules. *Langmuir*, 20(7):2874–2878, March 2004.

[136] Gregory J. Gabriel, Ahmad E. Madkour, Jeffrey M. Dabkowski, Christopher F. Nelson, Klaus Nüsslein, and Gregory N. Tew. Synthetic Mimic of Antimicrobial Peptide with Nonmembrane-Disrupting Antibacterial Properties. *Biomacromolecules*, 9(11):2980–2983, November 2008.

[137] Mikko Salomäki and Jouko Kankare. Specific Anion Effect in Swelling of Polyelectrolyte Multilayers. *Macromolecules*, 41(12):4423–4428, June 2008.

[138] Yang Li, Yiguang Wang, Gang Huang, Xinpeng Ma, Kejin Zhou, and Jinming Gao. Chaotropic-Anion-Induced Supramolecular Self-Assembly of Ionic Polymeric Micelles. *Angew. Chem. Int. Ed.*, 53(31):8074–8078, July 2014.

[139] P. E. Mason, G. W. Neilson, C. E. Dempsey, A. C. Barnes, and J. M. Cruickshank. The hydration structure of guanidinium and thiocyanate ions: Implications for protein stability in aqueous solution. *PNAS*, 100(8):4557–4561, April 2003.

[140] Jan Heyda, Halil I. Okur, Jana Hladílková, Kelvin B. Rembert, William Hunn, Tinglu Yang, Joachim Dzubiella, Pavel Jungwirth, and Paul S. Cremer. Guanidinium can both Cause and

Prevent the Hydrophobic Collapse of Biomacromolecules. *J. Am. Chem. Soc.*, 139(2):863–870, January 2017.

[141] Katherine E. S. Locock, Thomas D. Michl, Jules D. P. Valentin, Krasimir Vasilev, John D. Hayball, Yue Qu, Ana Traven, Hans J. Griesser, Laurence Meagher, and Matthias Haeussler. Guanylated Polymethacrylates: A Class of Potent Antimicrobial Polymers with Low Hemolytic Activity. *Biomacromolecules*, 14(11):4021–4031, November 2013.

[142] Willy Chin, Guansheng Zhong, Qinqin Pu, Chuan Yang, Weiyang Lou, Paola Florez De Sessions, Balamurugan Periaswamy, Ashlynn Lee, Zhen Chang Liang, Xin Ding, Shujun Gao, Collins Wenhan Chu, Simone Bianco, Chang Bao, Yen Wah Tong, Weimin Fan, Min Wu, James L. Hedrick, and Yi Yan Yang. A macromolecular approach to eradicate multidrug resistant bacterial infections while mitigating drug resistance onset. *Nat. Commun.*, 9(1):917, March 2018.

[143] You-Yeon Won, Steve P. Meeker, Veronique Trappe, David A. Weitz, Nancy Z. Diggs, and Jacob I. Emert. Effect of Temperature on Carbon-Black Agglomeration in Hydrocarbon Liquid with Adsorbed Dispersant. *Langmuir*, 21(3):924–932, February 2005.

[144] Zheng Cao, Pavlo I. Gordiichuk, Katja Loos, Ernst J. R. Sudhölter, and Louis C. P. M. de Smet. The effect of guanidinium functionalization on the structural properties and anion affinity of polyelectrolyte multilayers. *Soft Matter*, 12(5):1496–1505, January 2016.

[145] Aaron D. Robison, Simou Sun, Matthew F. Poyton, Gregory A. Johnson, Jean-Philippe Pellois, Pavel Jungwirth, Mario Vazdar, and Paul S. Cremer. Polyarginine Interacts More Strongly and Cooperatively than Polylysine with Phospholipid Bilayers. *J. Phys. Chem. B*, 120(35):9287–9296, September 2016.

[146] Mao Hori, Horacio Cabral, Kazuko Toh, Akihiro Kishimura, and Kazunori Kataoka. Robust Polyion Complex Vesicles (PICsomes) under Physiological Conditions Reinforced by Multiple Hydrogen Bond Formation Derived by Guanidinium Groups. *Biomacromolecules*,

August 2018.

[147] C. Derek Ma, Chenxuan Wang, Claribel Acevedo-Vélez, Samuel H. Gellman, and Nicholas L. Abbott. Modulation of hydrophobic interactions by proximally immobilized ions. *Nature*, 517(7534):347, January 2015.

[148] Chenxuan Wang, Chi-Kuen Derek Ma, Hongseung Yeon, Xiaoguang Wang, Samuel H. Gellman, and Nicholas L. Abbott. Nonadditive Interactions Mediated by Water at Chemically Heterogeneous Surfaces: Nonionic Polar Groups and Hydrophobic Interactions. *J. Am. Chem. Soc.*, 139(51):18536–18544, December 2017.

[149] Mario Vazdar, Jan Heyda, Philip E. Mason, Giulio Tesei, Christoph Allolio, Mikael Lund, and Pavel Jungwirth. Arginine "Magic": Guanidinium Like-Charge Ion Pairing from Aqueous Salts to Cell Penetrating Peptides. *Acc. Chem. Res.*, 51(6):1455–1464, June 2018.

[150] Erika Geihe Stanzl, Brian M. Trantow, Jessica R. Vargas, and Paul A. Wender. Fifteen Years of Cell-Penetrating, Guanidinium-Rich Molecular Transporters: Basic Science, Research Tools, and Clinical Applications. *Acc. Chem. Res.*, 46(12):2944–2954, December 2013.

[151] Shu J. Lam, Neil M. O'Brien-Simpson, Namfon Pantarat, Adrian Sulistio, Edgar H. H. Wong, Yu-Yen Chen, Jason C. Lenzo, James A. Holden, Anton Blencowe, Eric C. Reynolds, and Greg G. Qiao. Combating multidrug-resistant Gram-negative bacteria with structurally nanoengineered antimicrobial peptide polymers. *Nat. Microbiol.*, 1(11):nmicrobiol2016162, September 2016.

[152] Colin J. McKinlay, Robert M. Waymouth, and Paul A. Wender. Cell-Penetrating, Guanidinium-Rich Oligophosphoesters: Effective and Versatile Molecular Transporters for Drug and Probe Delivery. *J Am Chem Soc*, 138(10):3510–3517, March 2016.

[153] Jaemyung Kim, Laura J. Cote, Franklin Kim, Wa Yuan, Kenneth R. Shull, and Jiaxing Huang. Graphene Oxide Sheets at Interfaces. *J. Am. Chem. Soc.*, 132(23):8180–8186, June 2010.

[154] Matthew D. Reichert and Lynn M. Walker. Interfacial Tension Dynamics, Interfacial Mechanics, and Response to Rapid Dilution of Bulk Surfactant of a Model Oil–Water-Dispersant System. *Langmuir*, 29(6):1857–1867, February 2013.

[155] Muhammad Shahzad Kamal, Ibnelwaleed A. Hussein, and Abdullah S. Sultan. Review on Surfactant Flooding: Phase Behavior, Retention, IFT, and Field Applications. *Energy Fuels*, 31(8):7701–7720, August 2017.

[156] Stephanie M. Kirby, Shelley L. Anna, and Lynn M. Walker. Effect of Surfactant Tail Length and Ionic Strength on the Interfacial Properties of Nanoparticle–Surfactant Complexes. *Soft Matter*, 14(1):112–123, 2018.

[157] Daniel Carvajal, Evan J. Laprade, Kevin J. Henderson, and Kenneth R. Shull. Mechanics of pendant drops and axisymmetric membranes. *Soft Matter*, 7(22):10508–10519, November 2011.

[158] Yizhak Marcus. *Ions in Solution and Their Solvation*. John Wiley & Sons, June 2015.

[159] M. Beer, M. Schmidt, and M. Muthukumar. The Electrostatic Expansion of Linear Polyelectrolytes: Effects of Gegenions, Co-ions, and Hydrophobicity. *Macromolecules*, 30(26):8375–8385, December 1997.

[160] Xuejian Lyu and Amy M. Peterson. Humidity Tempering of Polyelectrolyte Complexes. *Macromolecules*, 51(23):10003–10010, December 2018.

[161] Joshua T. O'Neal, Kathryn G. Wilcox, Yanpu Zhang, Ian M. George, and Jodie L. Lutkenhaus. Comparison of KBr and NaCl effects on the glass transition temperature of hydrated layer-by-layer assemblies. *J. Chem. Phys.*, 149(16):163317, July 2018.

[162] Lele Mathis, Yaoyao Chen, and Kenneth R. Shull. Tuning the Viscoelasticity of Hydrogen-Bonded Polymeric Materials through Solvent Composition. *Macromolecules*, 51(11):3975–3982, June 2018.

[163] Jyotirmoy Mandal, Yanke Fu, Adam C. Overvig, Mingxin Jia, Kerui Sun, Norman N. Shi,

Hua Zhou, Xianghui Xiao, Nanfang Yu, and Yuan Yang. Hierarchically porous polymer coatings for highly efficient passive daytime radiative cooling. *Science*, 362(6412):315–319, October 2018.

[164] Allie C. Obermeyer, Carolyn E. Mills, Xue-Hui Dong, Romeo J. Flores, and Bradley D. Olsen. Complex coacervation of supercharged proteins with polyelectrolytes. *Soft Matter*, 12(15):3570–3581, April 2016.

[165] Alexander E. Marras, Jeffrey R. Vieregg, Jeffrey M. Ting, Jack D. Rubien, and Matthew V. Tirrell. Polyelectrolyte Complexation of Oligonucleotides by Charged Hydrophobic—Neutral Hydrophilic Block Copolymers. *Polymers*, 11(1):83, January 2019.

[166] Jeffrey M. Ting, Hao Wu, Abraham Herzog-Arbeitman, Samanvaya Srivastava, and Matthew V. Tirrell. Synthesis and Assembly of Designer Styrenic Diblock Polyelectrolytes. *ACS Macro Lett.*, 7(6):726–733, June 2018.

[167] Hao Wu, Jeffrey M. Ting, Olivia Werba, Siqi Meng, and Matthew V. Tirrell. Non-equilibrium phenomena and kinetic pathways in self-assembled polyelectrolyte complexes. *J. Chem. Phys.*, 149(16):163330, July 2018.

[168] Marat Andreev, Alexandros Chremos, Juan de Pablo, and Jack F. Douglas. Coarse-Grained Model of the Dynamics of Electrolyte Solutions. *J. Phys. Chem. B*, 121(34):8195–8202, August 2017.

[169] Alexandros Chremos and Jack F. Douglas. The Influence of Polymer and Ion Solvation on the Conformational Properties of Flexible Polyelectrolytes. *Gels*, 4(1):20, March 2018.

[170] Alexandros Chremos and Jack F. Douglas. Polyelectrolyte association and solvation. *J. Chem. Phys.*, 149(16):163305, July 2018.

[171] Wei Bu, Binyang Hou, Miroslav Mihaylov, Ivan Kuzmenko, Binhua Lin, Mati Meron, L. Soderholm, Guangming Luo, and Mark L. Schlossman. X-ray fluorescence from a model liquid/liquid solvent extraction system. *Journal of Applied Physics*, 110(10):102214,

November 2011.

[172] Wei Bu, Miroslav Mihaylov, Daniel Amoanu, Binhua Lin, Mati Meron, Ivan Kuzmenko, L. Soderholm, and Mark L. Schlossman. X-ray Studies of Interfacial Strontium–Extractant Complexes in a Model Solvent Extraction System. *J. Phys. Chem. B*, 118(43):12486–12500, October 2014.

[173] Zhu Liang, Wei Bu, Karl J. Schweighofer, David J. Walwark, Jeffrey S. Harvey, Glenn R. Hanlon, Daniel Amoanu, Cem Erol, Ilan Benjamin, and Mark L. Schlossman. Nanoscale view of assisted ion transport across the liquid–liquid interface. *PNAS*, page 201701389, March 2018.